U.S. Department of
Transportation

**Federal Railroad
Administration**

Steel Alloys with Lower Bainite Microstructures for Use in Railroad Cars and Track

Office of Research and
Development
Washington, DC 20590

DOT/FRA/ORD-01/15

Final Report
January 2002

REPORT DOCUMENTATION PAGE

Form Approved
OMB No. 0704-0188

1. AGENCY USE ONLY (Leave blank)	2. REPORT DATE	3. REPORT TYPE AND DATES COVERED
	January 2002	Final Report

4. TITLE AND SUBTITLE
Steel Alloys with Lower Bainite Microstructures for Use in Railroad Cars and Track

5. FUNDING NUMBERS
R-8009/RR-819

6. AUTHOR(S)
Roger K. Steele *

7. PERFORMING ORGANIZATION NAME(S) AND ADDRESS(ES)
U.S. Department of Transportation
Research and Special Programs Administration
John A. Volpe National Transportation Systems Center
Cambridge, MA 02142-1093

8. PERFORMING ORGANIZATION REPORT NUMBER
DOT-VNTSC-FRA-98-11

9. SPONSORING/MONITORING AGENCY NAME(S) AND ADDRESS(ES)
U.S. Department of Transportation
Federal Railroad Administration
Office of Research and Development
1120 Vermont Avenue, NW
Mail Stop 20
Washington, D.C. 20590

10. SPONSORING/MONITORING AGENCY REPORT NUMBER
DOT/FRA/ORD-01/15

11. SUPPLEMENTARY NOTES
*Metallurgical Consulting Services, Inc.
487 Bolton Road
Vernon, CT 06066

12a. DISTRIBUTION/AVAILABILITY STATEMENT
This document is available to the public through the National Technical Information Service, Springfield, VA 22161. This document is also available on the FRA web site at www.fra.dot.gov.

12b. DISTRIBUTION CODE

13. ABSTRACT (Maximum 200 words)

In-line hardening of railroad rails to produce a very fine pearlite microstructure has become a commercial reality. A question that this report seeks to answer is whether or not it is possible to find an alloy composition that will permit the development of lower bainite microstructures by in-line hardening in rails, wheels, and tank car plate. The application of the in-line hardening process becomes more difficult in the production of lower bainite microstructures because of the need to quench in a controlled fashion to lower "isothermal" transformation temperatures. Use of the computer program SteCal™ has suggested that the addition of molybdenum with boron will achieve the needed development of a bainite nose accompanied by suppression of the pearlite transformation. This approach appears to be applicable to rails and tank car plates. It is not clear, however, that wheels, which can undergo rapid heating and quenching during extreme service braking, would benefit from the same approach.

14. SUBJECT TERMS
Alloy, bainite, bainite nose, hardenability, in-line hardening, isothermal, martensite, microstructures, pearlite, quench and transformation temperature

15. NUMBER OF PAGES
96

16. PRICE CODE

17. SECURITY CLASSIFICATION OF REPORT	18. SECURITY CLASSIFICATION OF THIS PAGE	19. SECURITY CLASSIFICATION OF ABSTRACT	20. LIMITATION OF ABSTRACT
Unclassified	Unclassified	Unclassified	Unlimited

PREFACE

This report was sponsored by the U.S. Department of Transportation (US DOT), and the Federal Railroad Administration's (FRA) Office of Research and Development. Metallurgical Consulting Services, Inc., of Vernon, Connecticut, prepared this study for the Volpe National Transportation Systems Center (Volpe Center), which administered the project for the FRA.

This study focuses on the question of whether or not it is possible to find an alloy composition that will permit the development of lower bainite microstructures by in-line hardening in rails, wheels, and tank car plate. The computer model SteCal™ is used to show, semiquantitatively, the effect of alloy element variations upon key transformation parameters and on the time-temperature and continuous-cooling transformation diagrams. The study has suggested that the addition of molybdenum with boron will encourage the development of a bainite nose accompanied by suppression of the pearlite transformation. This approach appears to be applicable to rails and tank car plates. It is not clear, however, that wheels, which can undergo rapid heating and quenching during extreme service braking, would benefit from the same approach.

METRIC/ENGLISH CONVERSION FACTORS

ENGLISH TO METRIC

LENGTH (APPROXIMATE)

1 inch (in) = 2.5 centimeters (cm)
1 foot (ft) = 30 centimeters (cm)
1 yard (yd) = 0.9 meter (m)
1 mile (mi) = 1.6 kilometers (km)

AREA (APPROXIMATE)

1 square inch (sq in, in^2) = 6.5 square centimeters (cm^2)
1 square foot (sq ft, ft^2) = 0.09 square meter (m^2)
1 square yard (sq yd, yd^2) = 0.8 square meter (m^2)
1 square mile (sq mi, mi^2) = 2.6 square kilometers (km^2)
1 acre = 0.4 hectare (he) = 4,000 square meters (m^2)

MASS - WEIGHT (APPROXIMATE)

1 ounce (oz) = 28 grams (gm)
1 pound (lb) = 0.45 kilogram (kg)
1 short ton = 2,000 pounds (lb) = 0.9 tonne (t)

VOLUME (APPROXIMATE)

1 teaspoon (tsp) = 5 milliliters (ml)
1 tablespoon (tbsp) = 15 milliliters (ml)
1 fluid ounce (fl oz) = 30 milliliters (ml)
1 cup (c) = 0.24 liter (l)
1 pint (pt) = 0.47 liter (l)
1 quart (qt) = 0.96 liter (l)
1 gallon (gal) = 3.8 liters (l)
1 cubic foot (cu ft, ft^3) = 0.03 cubic meter (m^3)
1 cubic yard (cu yd, yd^3) = 0.76 cubic meter (m^3)

TEMPERATURE (EXACT)

[(x-32)(5/9)] °F = y °C

METRIC TO ENGLISH

LENGTH (APPROXIMATE)

1 millimeter (mm) = 0.04 inch (in)
1 centimeter (cm) = 0.4 inch (in)
1 meter (m) = 3.3 feet (ft)
1 meter (m) = 1.1 yards (yd)
1 kilometer (km) = 0.6 mile (mi)

AREA (APPROXIMATE)

1 square centimeter (cm^2) = 0.16 square inch (sq in, in^2)
1 square meter (m^2) = 1.2 square yards (sq yd, yd^2)
1 square kilometer (km^2) = 0.4 square mile (sq mi, mi^2)
10,000 square meters (m^2) = 1 hectare (ha) = 2.5 acres

MASS - WEIGHT (APPROXIMATE)

1 gram (gm) = 0.036 ounce (oz)
1 kilogram (kg) = 2.2 pounds (lb)
1 tonne (t) = 1,000 kilograms (kg) = 1.1 short tons

VOLUME (APPROXIMATE)

1 milliliter (ml) = 0.03 fluid ounce (fl oz)
1 liter (l) = 2.1 pints (pt)
1 liter (l) = 1.06 quarts (qt)
1 liter (l) = 0.26 gallon (gal)
1 cubic meter (m^3) = 36 cubic feet (cu ft, ft^3)
1 cubic meter (m^3) = 1.3 cubic yards (cu yd, yd^3)

TEMPERATURE (EXACT)

[(9/5) y + 32] °C = x °F

QUICK INCH - CENTIMETER LENGTH CONVERSION

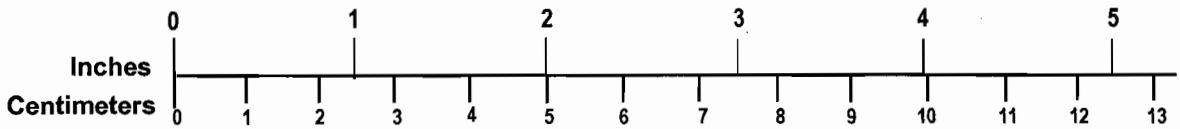

QUICK FAHRENHEIT - CELSIUS TEMPERATURE CONVERSION

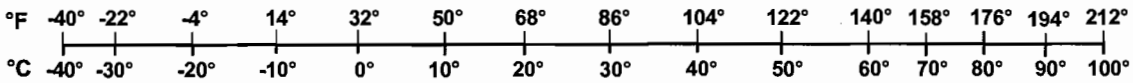

For more exact and or other conversion factors, see NIST Miscellaneous Publication 286, Units of Weights and Measures. Price $2.50 SD Catalog No. C13 10286

Updated 6/17/98

TABLE OF CONTENTS

LIST OF FIGURES

LIST OF FIGURES (Cont.)

LIST OF FIGURES (Cont.)

LIST OF FIGURES (Cont.)

LIST OF TABLES

Übersetzungen (Translations)

Figure No.	German	English Translation
9	Chemische Zusammensetzung	Chemical Composition
	Umwandlungstemperatur	Conversion Temperature
	Kühlbettabkühlung	Cooling Bed Cooldown
	Fuß	Base
	Kopf	Top
	Abkühlungzeit	Cooling Time
	Mechanistic Eigenschaften	Mechanical Properties
	Wärmebehandlung	Heat Treatment
	Walzzustand	Rolled State
	Angelassen	Tempered
10	Prüfbahn	Test Track
	Härte	Hardness
	Abstand von der Fahrkante in mm	Distance from the Running Surface in mm
11	DVMF – Proben	Impact Toughness Test
	Probenlänge: längs	Test Direction: Longitudinal
	Bainitischer Schienenstahl	Bainitic Rail Steel
	Perlitische Schienenstähle	Pearlitic Rail Steels
	Kerbschlagarbeit in J	Impact Energy in Joules
	Güte	Grade
	Temperatur	Temperature
12	Maximaler Verschleiß bei Ausbau	Maximum Track Wear upon Completion
	Verschleiß in mm^2	Track Wear in Square Millimeters
	Verschleiß	Track Wear
	Gesamtbelastung in Mill. T	Total (Track) Loading in Millions of Tons
47	Wärmeeinflußzone	Heat Affected Zone
	Fußaußenkante	Base Outside Edge
	3 mm unter der Fahrfläche	3 mm beneath the Running Surface
	Härte	Hardness
	WEZ	HAZ
	Zwischenguss	Cast Filler Metal
	2 mm unter der Fahrfläche	2 mm beneath the Running Surface
	Abstand von der Schweissnahtmitte in mm	Distance from the middle of the weldment in mm

DEFINITIONS

A_1 or A_e .....Temperature of eutectoid transformation
Ac_1.....Austenite start temperature (during heating)
Ac_3.....Austenite finish temperature (during heating)
A_5 .....Percent elongation in a 5 cm gage length
B_s.....Bainite start temperature
B_f.....Bainite finish temperature
CCT.....Continuous-Cooling Transformation diagram
DPN.....Obsolete symbol for Vickers Hardness (HV)
F .....Ferrite
HV10.....Vickers Hardness (10 scale)
M_s.....Martensite start temperature
M_f.....Martensite finish temperature
P_s .....Pearlite start temperature
P_f.....Pearlite finish temperature
R_B .....Rockwell hardness (B scale)
R_C .....Rockwell hardness (C scale)
R_e.....Yield strength
R_m.....Ultimate tensile strength
S/R .....Slip/roll ratio (wear testing)
TS.....Tensile strength
tsi.....tons per square inch
TTT .....Time-Temperature Transformation diagram
w/o.....weight percent
YS .....Yield strength
Z .....Percent reduction in area

EXECUTIVE SUMMARY

Laboratory experiments have shown that eutectoid carbon steel heat treated to a bainitic microstructure can have remarkably superior wear resistance over that of the best pearlitic microstructure railroad steel. The toughness of lower baintic steel is superior to upper bainitic steel of the same strength. A commercial bainitic rail steel has been developed in Europe which does exhibit better toughness and wear resistance than pearlitic head hardened rail steel, but it has an upper bainite microstructure. In-line hardening, which is currently being used commercially to produce very high strength pearlitic rail steel, offers the potential to produce a lower bainite rail steel of great toughness, strength, and wear resistance. The composition(s) of such steel has not yet been established.

The computer model SteCal™ has been used to show, semiquantitatively, the effect of alloy element variations upon key transformation parameters and on the time-temperature and continuous-cooling transformation diagrams. The results of the analysis suggest that the commercial rail steel composition could be modified by reduction in the molybdenum content and by the addition of boron (0.003 weight percent (w/o)) to produce an alloy which could work with an in-line hardening process to yield lower bainite microstructures. In rail, hardnesses over 500 BHN would appear to be possible. Some questions exist about how well such an alloy would roller straighten.

The application of this alloy to wheels has been examined. The chill quenching of the wheel rim from above 1,292°F (700°C), which is possible in some extreme braking situations, appears to make the rail alloy potentially unsatisfactory because the increased time to the start of the bainite transformation designed into the alloy (for in-line hardening) increases the likelihood of martensite formation. Instead, the use of lower carbon but more highly alloyed steel currently being developed for switch and turnout frogs by the Oregon Graduate Institute seems more likely to meet the challenge of avoiding martensite formation under rim chill quenching conditions.

The basic TC 128 steel composition used in some tank car shell applications can be modified. This could be done by increasing the molybdenum content slightly, and adding boron (0.003 w/o) to produce a steel which can be in-line hardened to achieve strength properties about 50 percent greater than those currently achieved with the alloy. Toughness also is likely to increase significantly. However, questions remain about how easily a stronger plate can be cold roll-formed and what cooling rates develop upon fabrication welding.

1. INTRODUCTION

In-line heat treatment of hot-formed steel mill products potentially offers the opportunity to achieve superior strength, ductility, and toughness at modest cost. The approach has been applied to the manufacture of railroad rail in an extremely refined pearlitic microstructure. With appropriate adjustments to chemical composition to control the transformation behavior, the approach provides a means to achieve close-to-isothermally produced bainitic microstructures of better strength, ductility, and toughness over the current pearlitic microstructure hot-formed mill products. In the railroad field, the approach appears to be applicable to the manufacture of rails, wheels, and tank car plate.

This report reviews (a) the essential features of the in-line heat treatment process as it is currently applied to rails in the United States, (b) studies that have shown the value of bainitic microstructures, and (c) the characteristics of bainitic microstructures. A widely available computer code, SteCal™, has been used to assess the effect of alloying additions on transformation behavior in a semiquantitative fashion. Finally, the applicability of the in-line heat treating approach for achieving bainitic microstructures in rails, wheels, and tank car plate is discussed.

2. BACKGROUND

2.1 THE IN-LINE HARDENING PROCESS

The essential feature of the in-line heat treating process is the ability to transform the high temperature austenitic structure that exists immediately following the hot rolling process to the desired room temperature structure without the normal intermediate steps of cooling to room temperature and then reheating (resolutionizing) prior to accelerated cooling. Although the commercial application of this idea is recent (since 1990), the concept originated at Bethlehem Steel in the late 1960s [1]. A great part of the background to be described below has been drawn from work published by B. L. Bramfitt and his colleagues at the Bethlehem Steel Corporation and Pennsylvania Steel Technologies, Inc. [2,3,4]. The in-line hardening developments undertaken by Pennsylvania Steel Technologies have been based on technology pioneered by Aciere Rodange Esch Schifflange and its predecessors [5,6].

Figure 1 illustrates the continuous cooling transformation of rail steel as portrayed by Bramfitt [2] based on the work of Kennon [7]. Air-cooling of conventional (non-hardened) rail steel corresponds to path 1; the iron carbide interlamellar spacing of pearlite produced along this path is about 2000 to 4000 angstroms. Cooling along path 2 will produce a much finer pearlite (about 1000 angstroms), but below point (d) on path 2, bainite and then untempered martensite will be produced instead of pearlite. The bainite and untempered martensite are not preferred transformation products when formed with pearlite. Ideally, cooling along path 3 would be preferred because only a very fine pearlite would be produced. The dashed line on path 3 is nearly isothermal indicating that the pearlite will be of uniform interlamellar spacing as opposed to the varying spacing achieved between points (a) and (b) on path 1. The key issue will be to produce such an isothermal type of transformation in a bainitic region of the transformation diagram. The question is whether or not it is possible to have a transformation diagram where such an isothermal transformation can be made to occur.

To achieve the isothermal transformation (to pearlite) by in-line hardening, initially a rapid quench must bring the surface temperature (of the rail head locally) close to that of the pearlite nose in the time interval prior to the start of the pearlite transformation. This is illustrated on Figure 2. Continuous cooling rates (in the temperature range from 1,472° - 932°F (800° - 500°C) up to about 464°F (240°C) per minute would cause fully pearlitic microstructures only. Higher continuous rates would cause mixed microstructures. But were rates in the vicinity of 752° to about 1,202°F (400° to approximately 650°C) per minute to be applied only until the pearlite start boundary was reached and then interrupted, an approximation of isothermal conditions could be achieved in the rail as a whole. The interruption of cooling would allow heat from the interior of the rail to rewarm the surface to a higher temperature so that little or no transformation to pearlite would occur. Repetition of this quench/interrupt sequence through many cycles in the course of rail passage (about one minute) through the hardening unit will yield a cooling history at the interior close, to that shown in Figure 3. Because heat must be extracted from the rail surface, the interior-cooling rate will be less than that achievable at the surface. Typical surface and interior cooling paths are shown in Figure 4. Note that the cooling curves become

isothermal at about 1,112°F (600°C) after about 1 minute. Even very near the surface (1 mm) the temperature does not drop below 932°F (500°C) so bainite will not start to form. Since the pearlite transformation requires about 1 minute before it starts and the rail travel time through the quenching unit takes about 1 minute, the majority of the pearlite transformation will occur outside the quenching unit.

The intermittent quenching action is achieved with water sprays applied to the head, web, and base (discretionary) of the rail as portrayed in Figure 5. The web and base sprays control rail distortion while the head sprays achieve the head hardening. Quenching is divided into four independently controlled zones (Figure 6), each just under 25 m long. The speed of the rail at entry to the quench unit is controlled on the basis of the rail temperature measured in close proximity to entry to the quenching unit. Inside the quench unit, the rail speed is adjusted for section size and chemical composition (i.e., transformation characteristics).

It may be worthwhile at this point to recall that after each spray quench is interrupted, the surface temperature rises so that pearlite transformation is avoided and the hot metal at the surface remains austenitic. Were bainite the desired structure from an alloy with the same transformation characteristics (Figure 1), the increase in surface temperature after quench interruption could leave the metal in the midst of the pearlite transformation region. Thus, for the in-line process to be applied for a bainite structure, it appears that the region above the bainite nose on the transformation diagram should be austenite, not pearlite. This is illustrated in Figure 7.

2.2 THE VALUE OF BAINITIC MICROSTRUCTURES

Laboratory experiments by Kalousek, et al. [8] and subsequently by Clayton and Devanathan [9] have shown that up to hardnesses near Rc 39–40, the wear resistance of pearlitic rail steel, under conditions simulating dry curve wear, is several times better than that of the same rail steel in the bainitic condition at the same hardness. However, when the hardness of bainite is increased significantly above the maximum pearlite hardness (Rc 39–40)[1] to Rc 49 and 54 by isothermal transformation at temperatures below the pearlite nose, Clayton and Devanathan [9] have shown that wear resistance increases remarkably. This is illustrated in Figure 8, where even at contact pressures and slip/roll ratios well in excess of those considered representative of today's heavy wheel load conditions, the wear resistance of the bainitic structure is outstanding. This behavior suggests that both rails and wheels made of eutectoid carbon steel may benefit from having a bainitic microstructure.

[1] At hardnesses above Rc 40, pearlite can exist only in combination with other structures such as bainite or martensite.

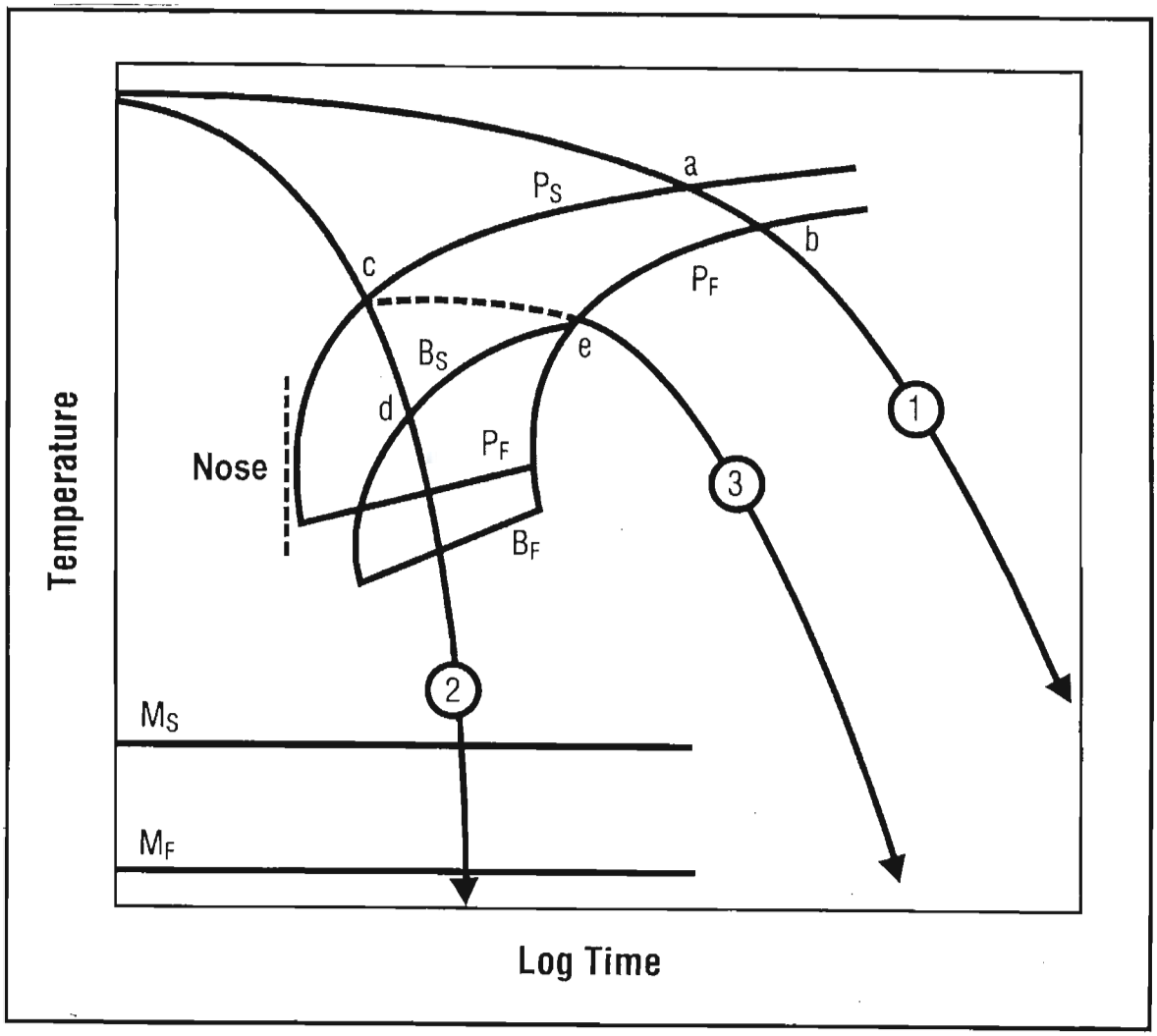

Figure 1. Schematic Representation of a Continuous Cooling Transformation Diagram of an Eutectoid Steel (Source: Kennon, Ref. 7)

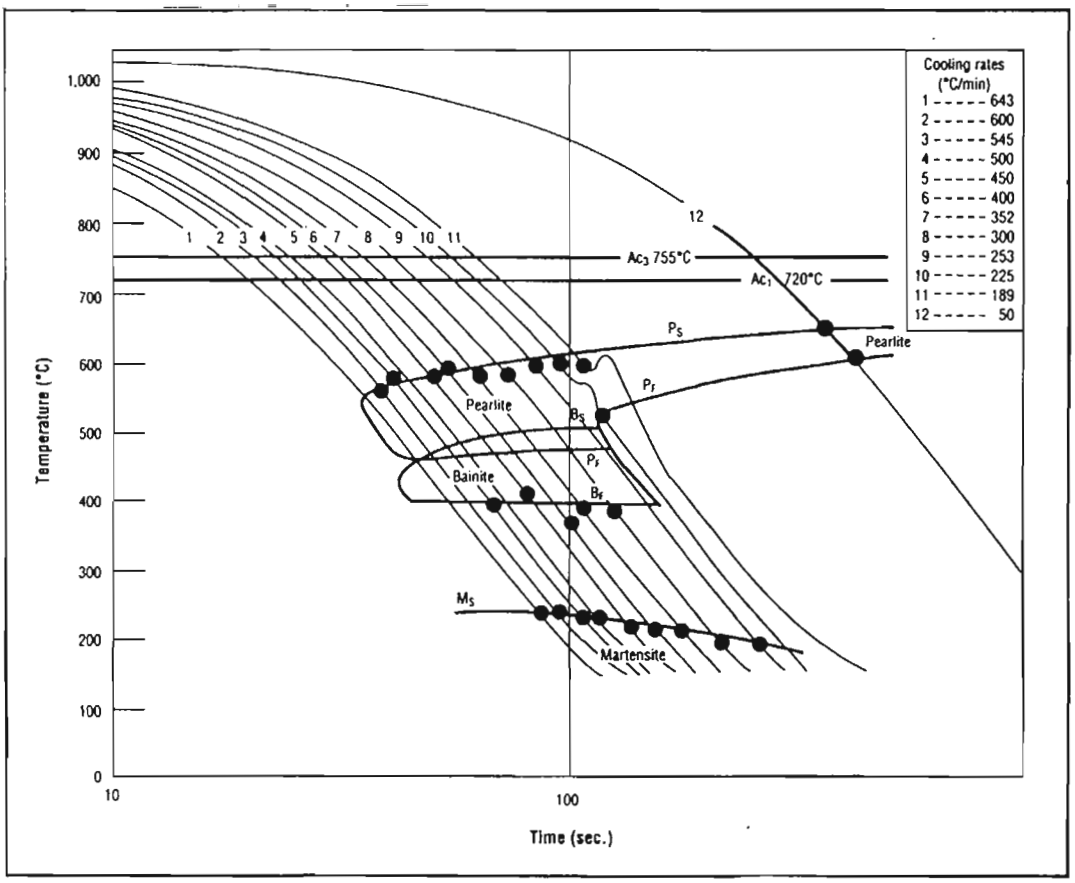

Figure 2. Continuous Cooling Transformation Diagram of a Rail Steel (Source: Bramfitt, Ref. 2)

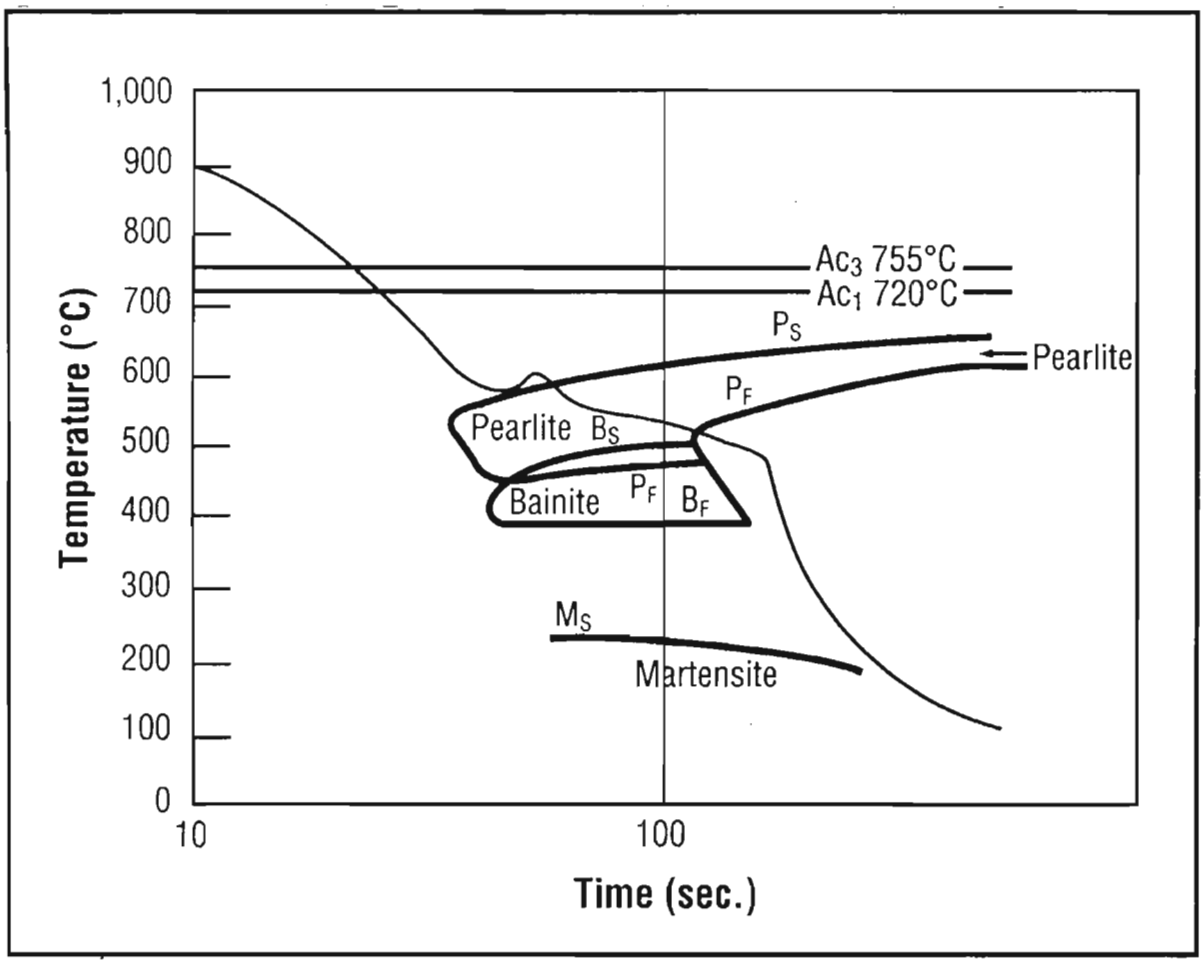

Figure 3. Continuous Cooling Transformation Diagram Showing Cooling Path for In-Line Process (Source: Bramfitt, Ref. 2)

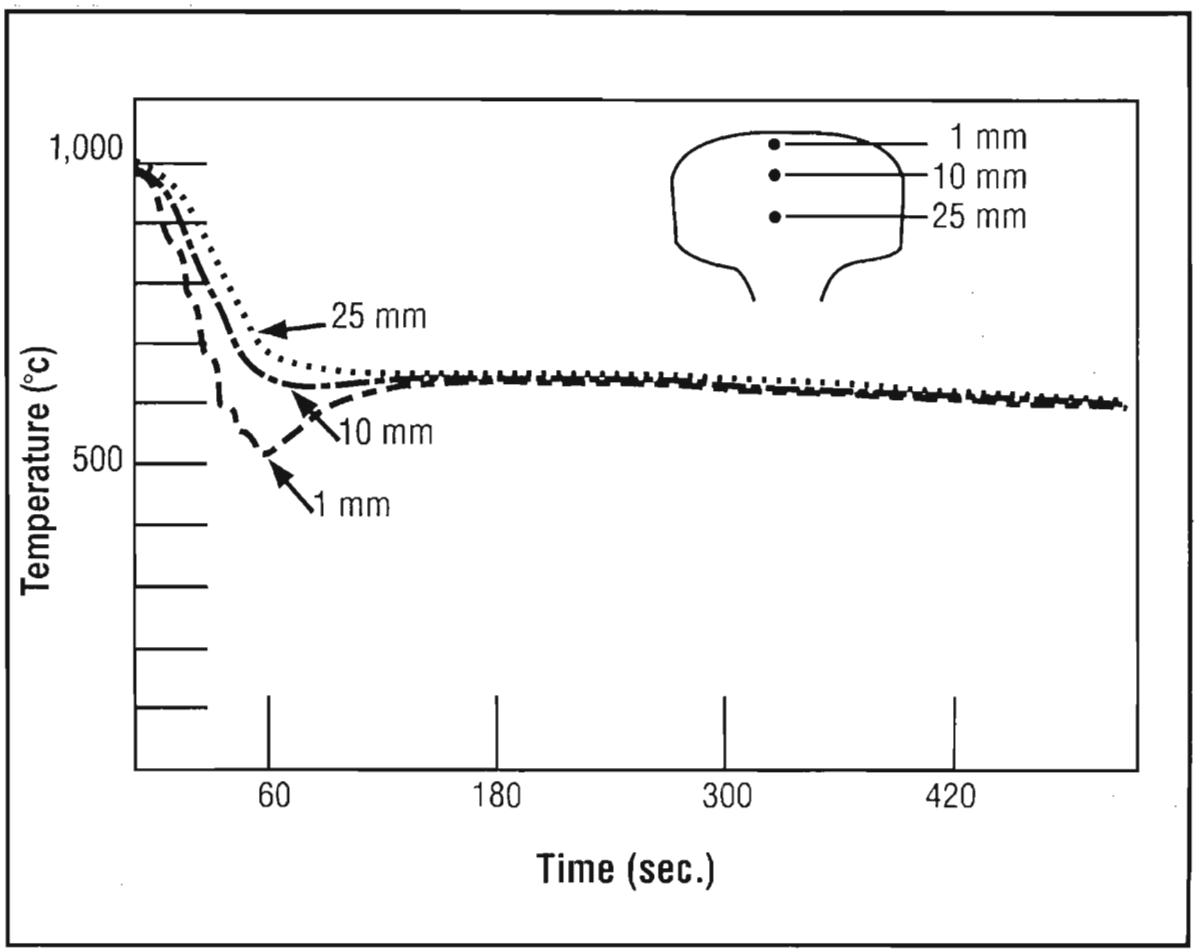

Figure 4. Cooling Curves of Rail at Three Locations (Source: Bramfitt, Ref. 2)

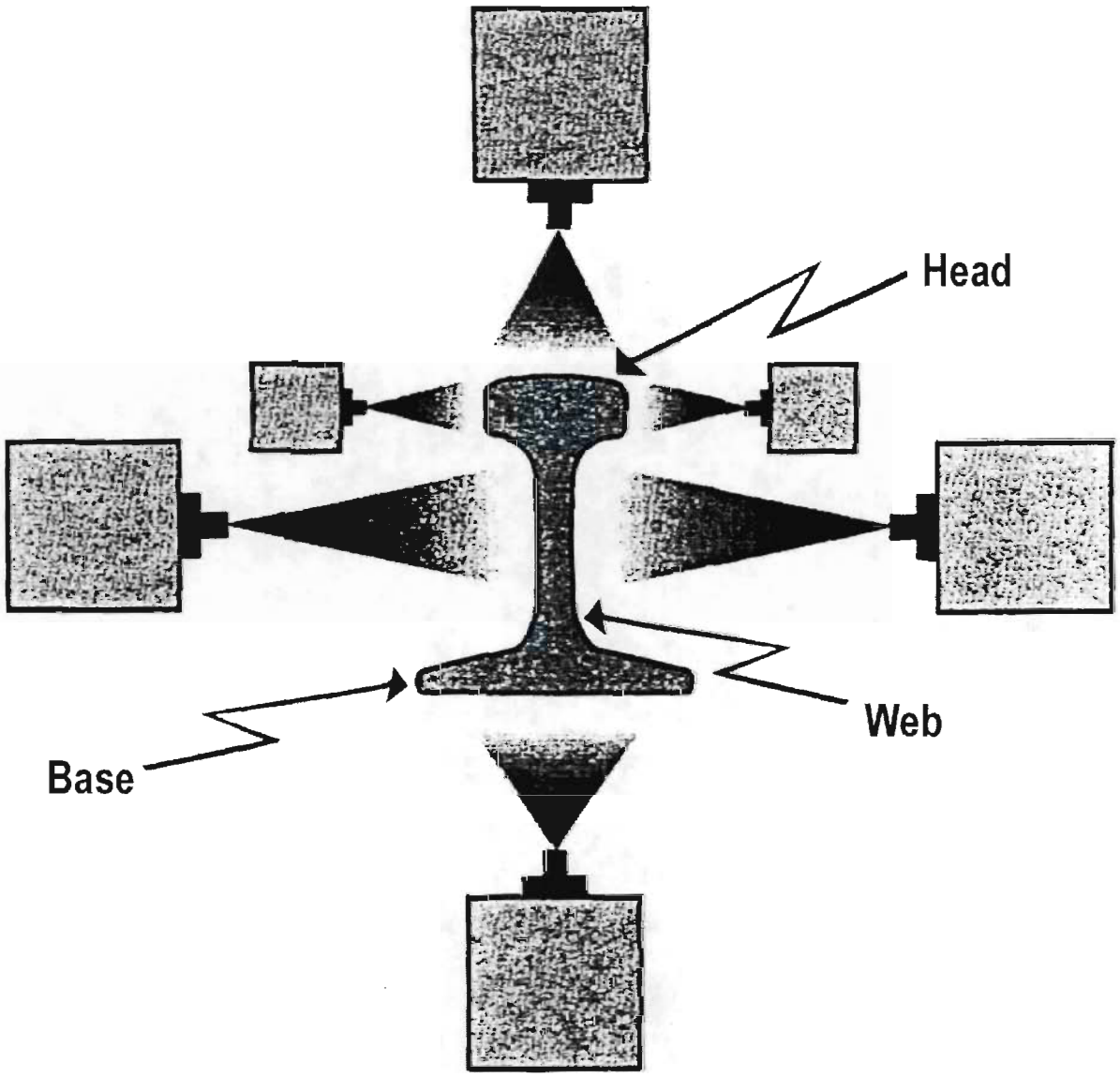

Figure 5. Schematic Representation of Spray Configuration for In-Line Hardener (Source: Bramfitt et al., Ref. 4)

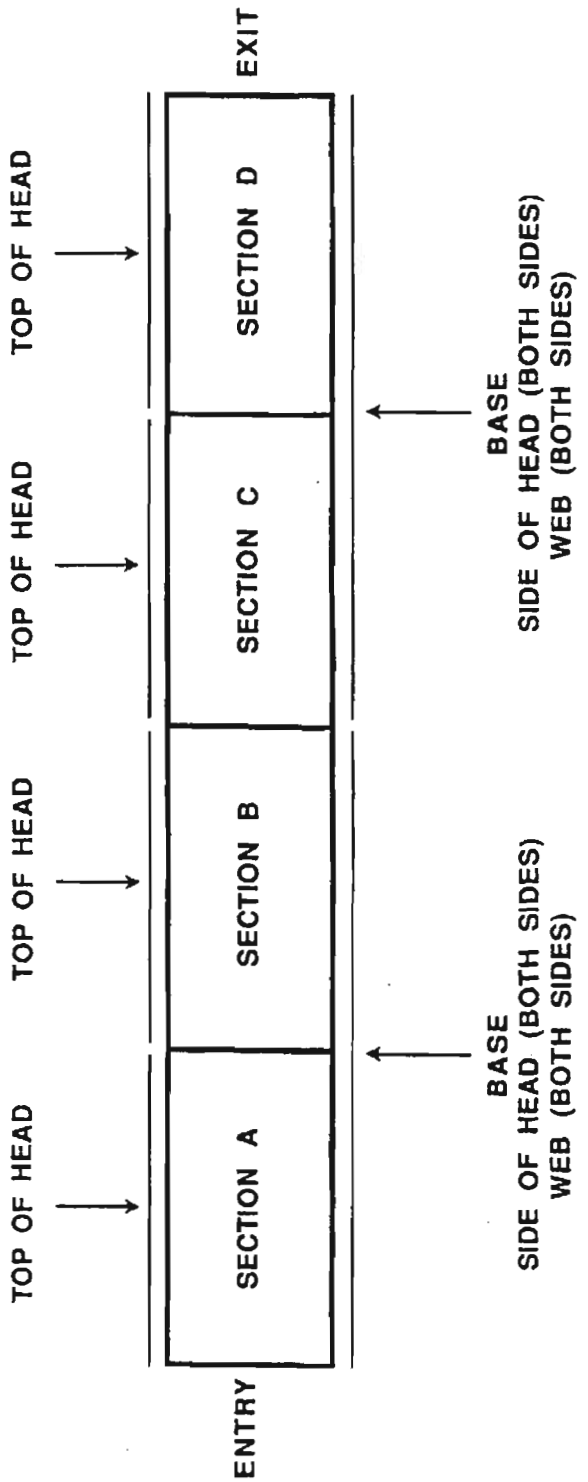

Figure 6. Illustration of Quenching Zones in In-Line Hardener (Source: Bramfitt et al., Ref. 4)

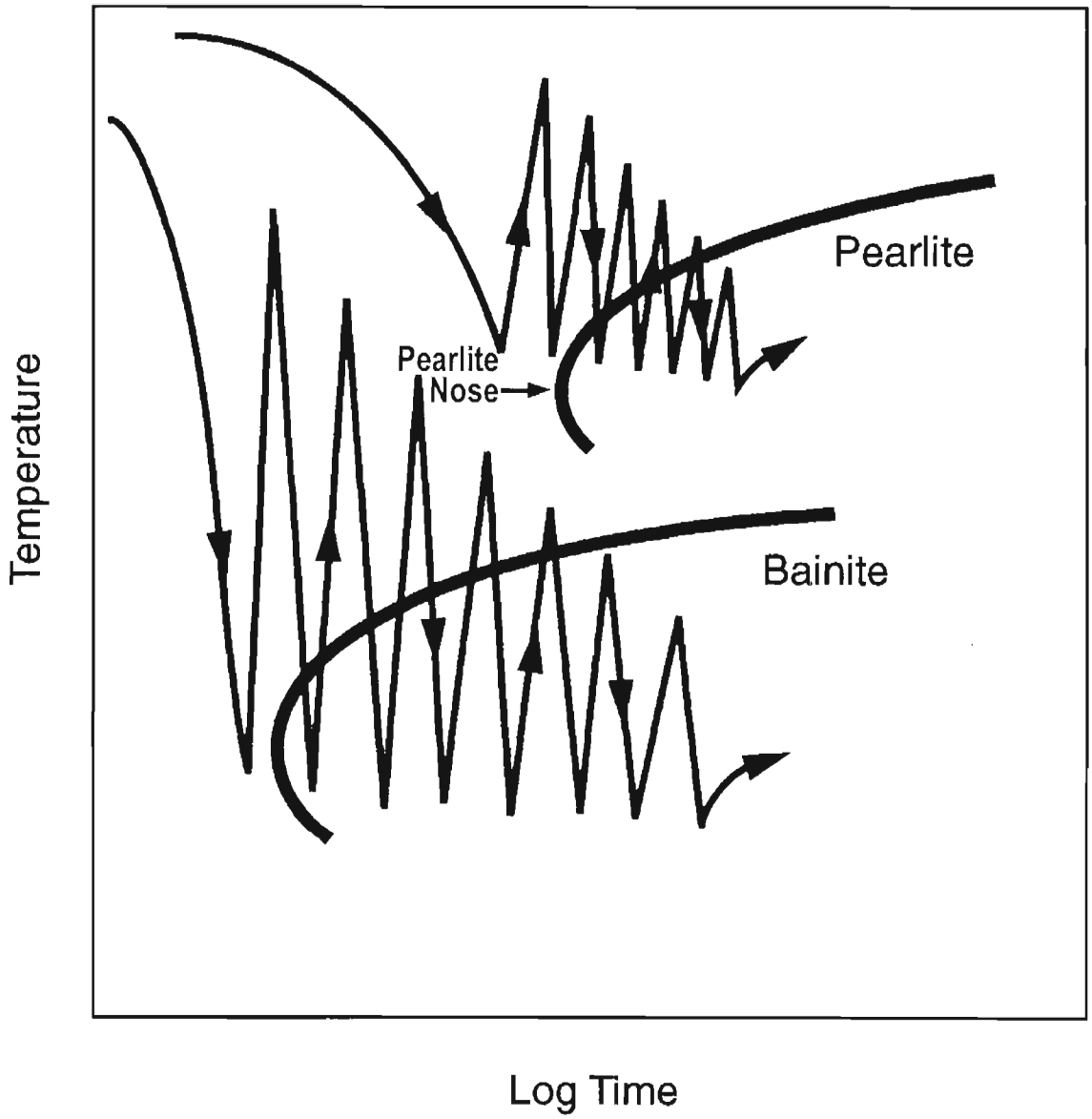

Figure 7. Conceptual Illustration of Bainite Compared to Pearlite Surface Cooling Paths

Recently published work by de Boer et al. [10] shows that bainitic rails can be produced just above the maximum hardness for a pearlitic structure with considerable improvement in wear performance. The chemical composition, mechanical properties achieved, the transformation diagram, and an illustration of the metallographic structure are illustrated in Figure 9. The composition is noteworthy for its modest carbon level and the relatively high levels of silicon and molybdenum. More will be said about the significance of this later. The as-rolled (Walzzustand) mechanical properties appear to be achieved by continuous cooling on the rail cooling bed (Khlbettabkhlung). The entire rail appears to be bainitic. A subsequent thermal treatment at 1,022°F (550°C) for 1 hour appears to increase the mechanical properties significantly. The 1,022°F is substantially above the bainite start temperature, which appears to be near 878°F (470°C); this suggests that the 1,022°F treatment may have an aging effect, precipitating carbide from retained austenite trapped between bainite needles. The ultimate tensile strength of 1455 MPa translates to a Brinell hardness of about 420. The hardness distribution with depth in the rail-head is quite uniform, consistent with other rails which normally cool on cooling beds[2] as shown in Figure 10. Figure 11 illustrates that the impact toughness of the bainitic steel is considerably above that of pearlitic rail steels and that the ductile to brittle transition occurs at lower temperatures. Both flash butt and thermite welds have been made; however, in the case of the flash butt welds, the hardness of the region just inside the boundaries of the heat affected zone increased to nearly 500 BHN; the microstructure there was indicated to be entirely bainitic and free of martensite. The wear performance of the rail is approximately 50 percent better than that of head-hardened rail (Figure 12).

The work of de Boer et al. points to the advantage that bainitic microstructures have over pearlitic ones with regard to impact toughness. As a general rule, the impact toughness of pearlitic steels is inferior to that of bainitic steels of the same composition. Usually, impact toughness itself is not used in comparisons; instead the temperature at which fracture turns from ductile to brittle is most often the parameter of interest (Figure 13). Low temperatures of transition are desired. Figure 11 shows that the bainitic steel has a lower transition temperature than do any of the pearlitic steels with which it is compared. However, bainitic microstructures do not always yield lower transition temperatures when compared with tempered martensitic microstructures. This is illustrated for a manganese-molybdenum-boron steel in Figure 14. This being so, one may ask why tempered martensitic microstructures are not used. The answer is not entirely obvious. There is a cost to the post-quench tempering that would be necessary. Figure 15 illustrates the time needed at different temperatures to lower the hardness. But perhaps the greatest problem would be the likelihood of quench cracking and distortion (in complicated shapes such as rails and wheels) that could result from the non-time-dependent nature of the martensite transformation.

[2] The 900A, 1100, 1200 rails are not quenched rails whereas the HH 1200 rail is a quenched head-hardened rail.

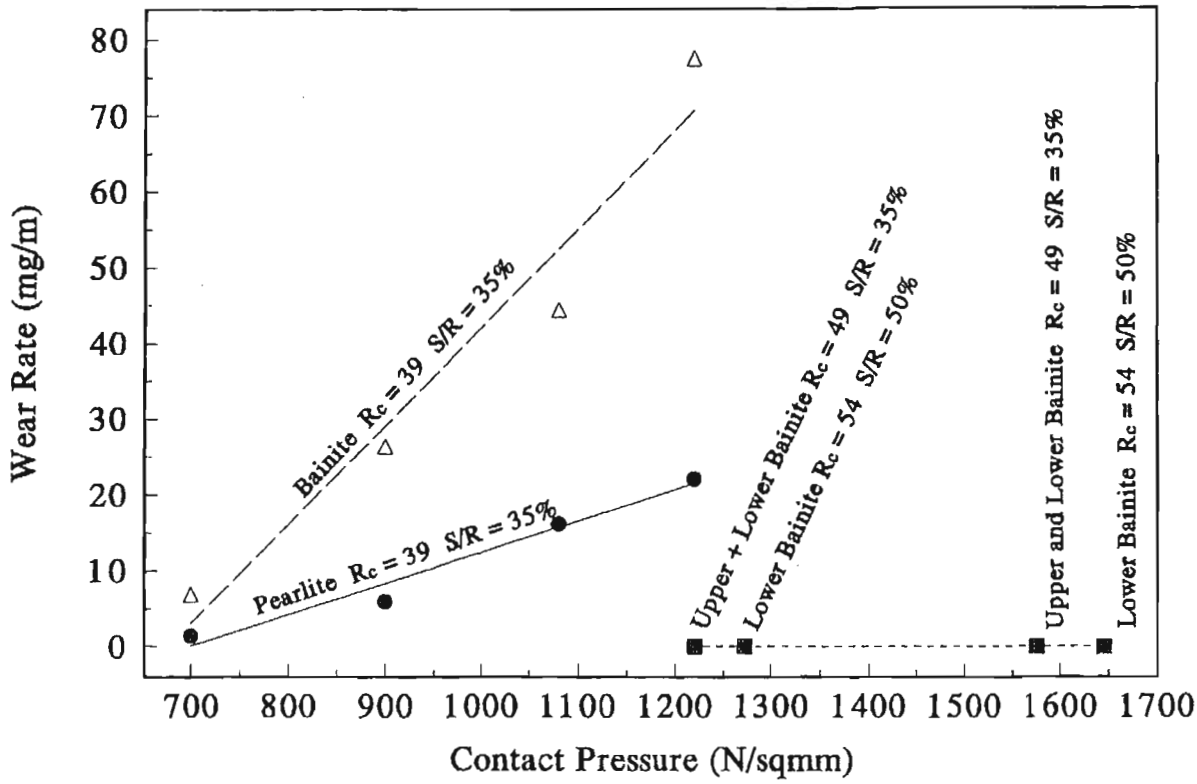

Figure 8. Wear Rates at Increasing Contact Pressures for Pearlitic and Bainitic Microstructures (Source: Clayton/Devanathan, Ref. 9)

Chemische Zusammensetzung [%]					
C	Si	Mn	Cr	Mo	V
0,4	1,5	0,7	1,1	0,8	0,1

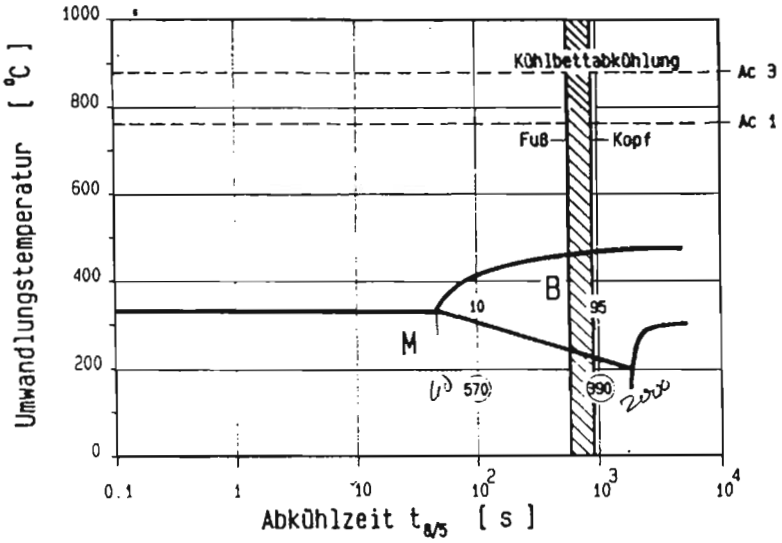

Wärmebehandlung	Mechanische Eigenschaften			
	R_e	R_m	A_5	Z
	N/mm²	N/mm²	%	%
Walzzustand	815	1326	9	15
Angelassen (550°C/60' L)	1037	1455	13	38

Figure 9. Characteristics of a Bainitic Rail Steel (Source: de Boer et al., Ref. 10)

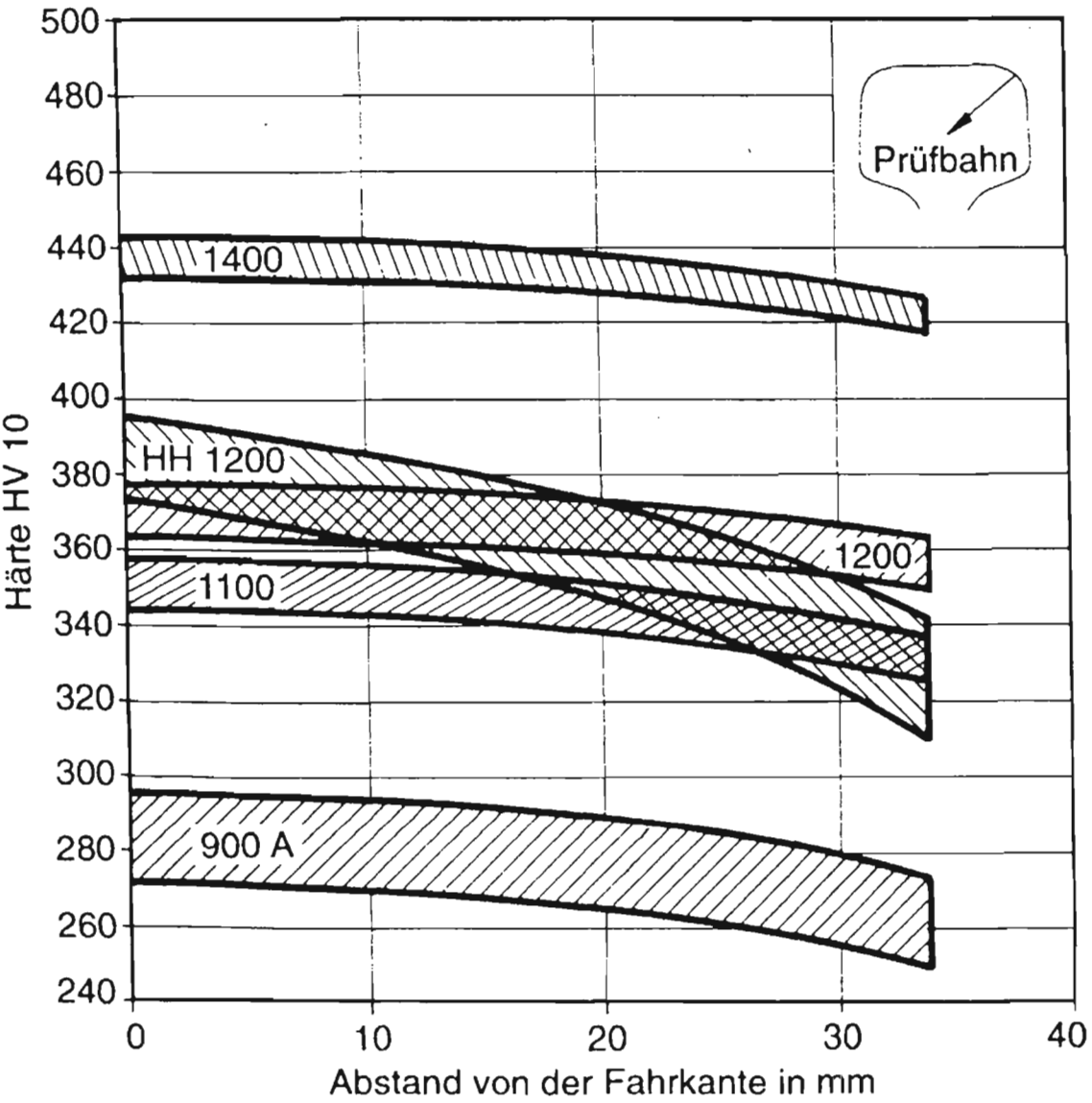

Figure 10. Hardness Traverses from Rail Head Corners (Source: de Boer et al., Ref. 10)

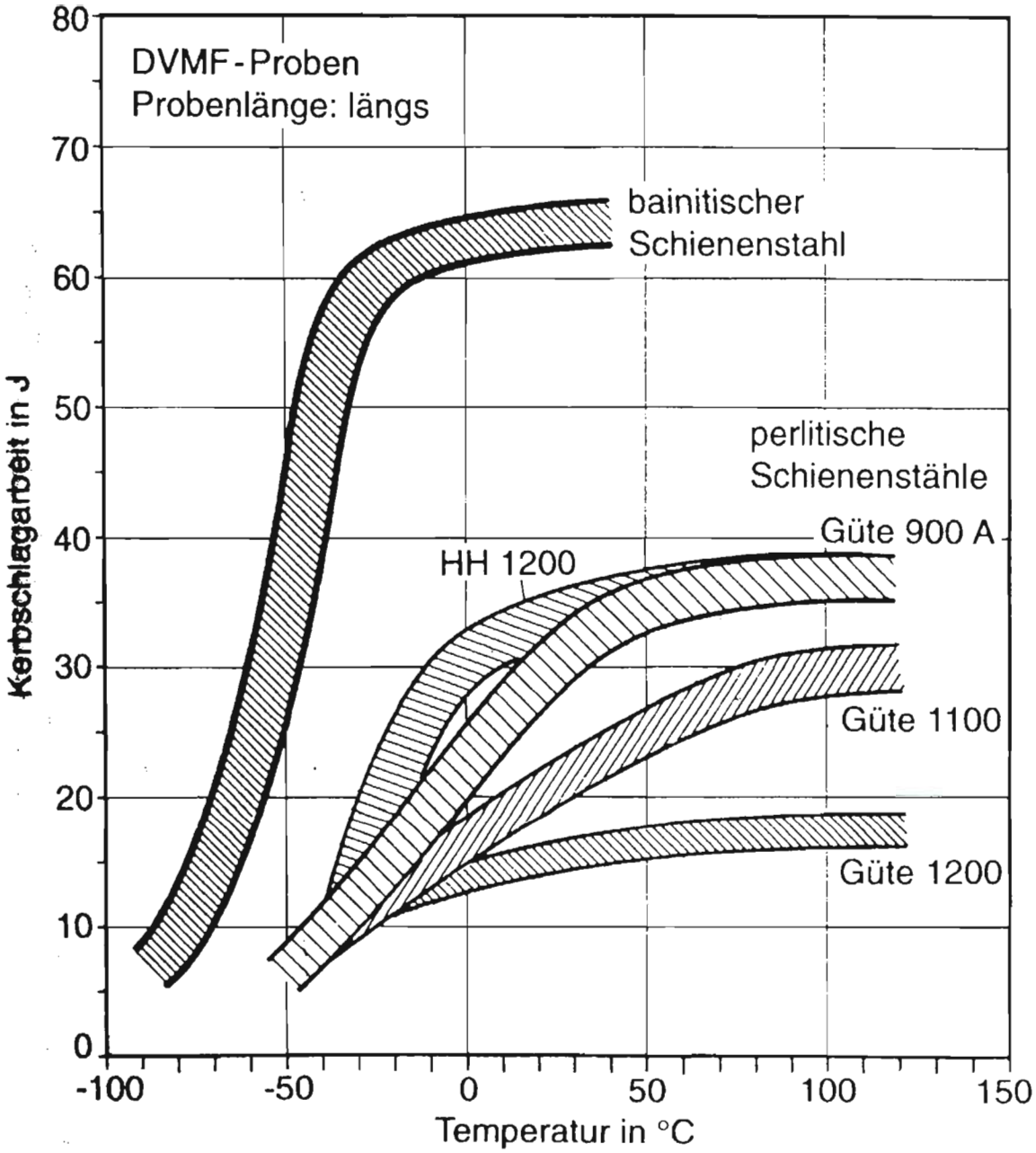

Figure 11. Impact Energy as a Function of Test Temperature (Source: de Boer et al., Ref. 10)

2.3 THE CHARACTER OF BAINITE AND ITS TRANSFORMATION

Bainite is the transformation product which forms below the nose of the pearlite transformation curves but above the martensite start temperature. This is illustrated in Figure 16. If the isothermal transformation diagram (TTT) does not exhibit a distinct bainite nose (left), the formation of bainite will be accompanied by the formation of pearlite at temperatures just below the pearlite nose. At much lower temperatures, but above the martensite start (M_s), bainite will be the sole product. If a distinct bainite nose exists (right), the transformation product will be entirely bainite if the temperature is below the bainite start (B_s), the highest temperature at which bainite can form.

Since it is located between the higher temperature pearlite transformation region and the lower temperature martensite region, the character of bainite is intermediate between those of pearlite and martensite. Pearlite is a product, the amount of which is controlled by the diffusion of carbon (i.e., the reaction is time dependent). Martensite, on the other hand, is formed by a shearing transformation, the extent of which depends upon temperature but not time. Therefore, bainite has some of the characteristics of each.

Where a distinct bainite nose does exist, there is a difference in the bainite morphology approximately above and below the nose position. Above the nose, upper bainite develops, while below the nose, lower bainite develops. The differences in the morphology are illustrated in Figure 17 taken from reference 11.

Pickering [13] notes that in low carbon upper bainite, lath ferrite forms first from austentite by a shear process. Carbon enrichment occurs within the matrix austenite. This enrichment can lead to retention of untransformed austenite. As continued formation of ferrite laths occurs, regions of carbon-enriched austenite become entrapped between the ferrite laths. Eventually carbides form in the austenite. At higher carbon contents (perhaps 0.5 weight percent (w/o) carbon), iron carbide appears to be the initial nucleating phase. Increasing the silicon content tended to increase the amount of retained austenite [14].

In lower bainite, the ferrite lath appears to become supersaturated in carbon and the iron carbide precipitates within the ferrite, rather than in the austentite [13]. The carbide precipitate occurs on planes oriented across the length of the ferrite lath. The precipitate appears to be in the form of rods or small plates. Retained austenite generally is not observed in lower bainite; the carbides that form in the ferrite laths have been observed to be epsilon carbides [14].

Pickering observed that the temperature above which lower bainite would not form increased with carbon content up to about 0.5 w/o, above which that temperature dropped quickly and leveled off at 662°F (350°C) at and above 0.7 w/o carbon [13]. This is illustrated in Figure 18. The data, however, come from steels containing a relatively restricted alloy content[3]. Working with other steels having different combinations of Ni, Cr, and Mo, Parker [15] found that the "transition from lower to upper bainite depends upon the eutectoid composition, which shifts to lower carbon contents with higher concentrations of alloying elements that increase hardenability."

[3] 0.5 percent Mo and boron and 1 percent Cr, 0.5 percent Mo and boron.

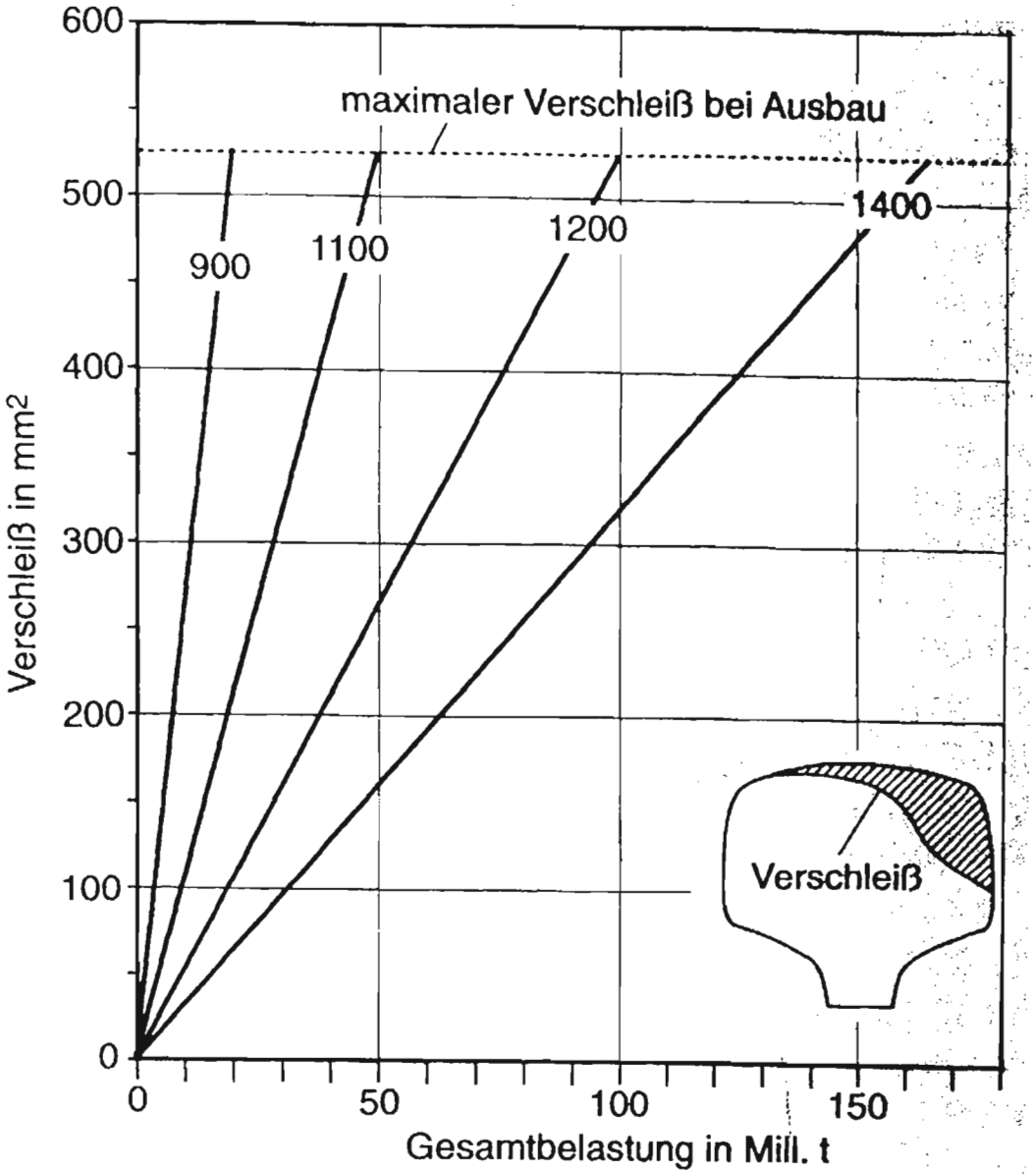

Figure 12. Wear Loss of Rail Steels in 300-Meter Radius Test Curves (Source: de Boer et al., Ref. 10)

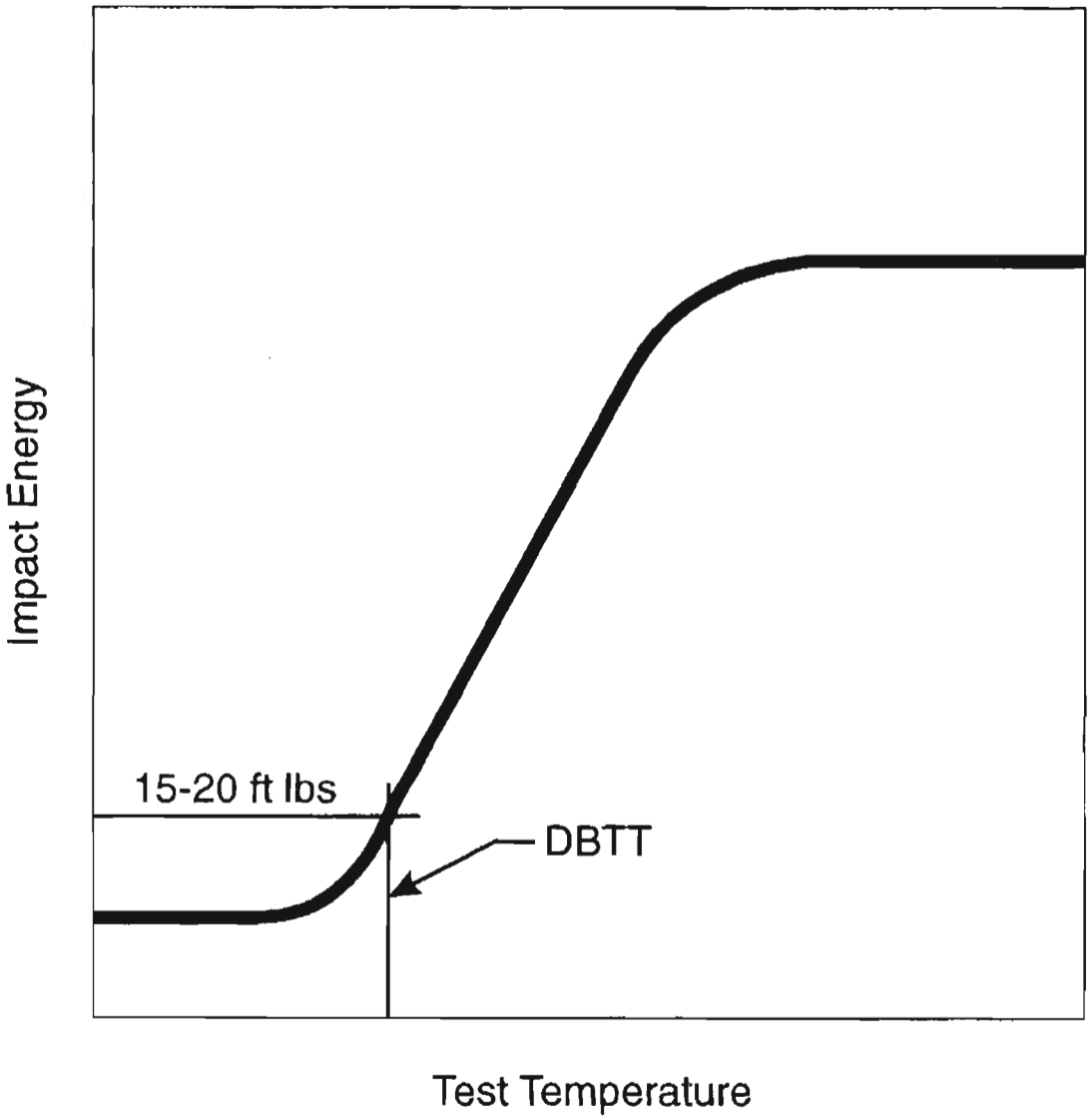

Figure 13. Illustration of the Impact Test, Ductile to Brittle Transition Temperature (DBTT)

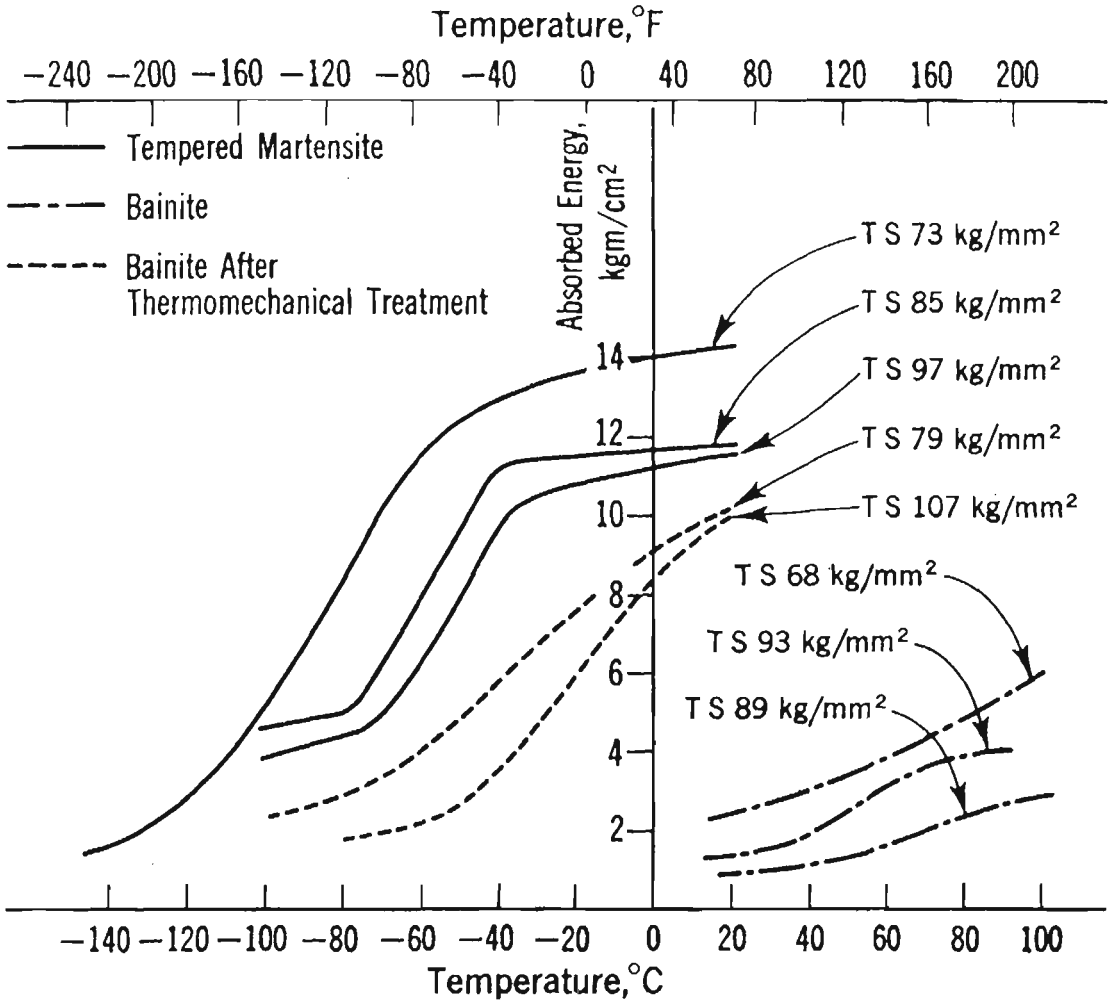

Figure 14. Impact Energy Transition Curves for a Manganese-Molybdenum-Boron Steel (Source: Habraken/Economopoulos, Ref. 11)

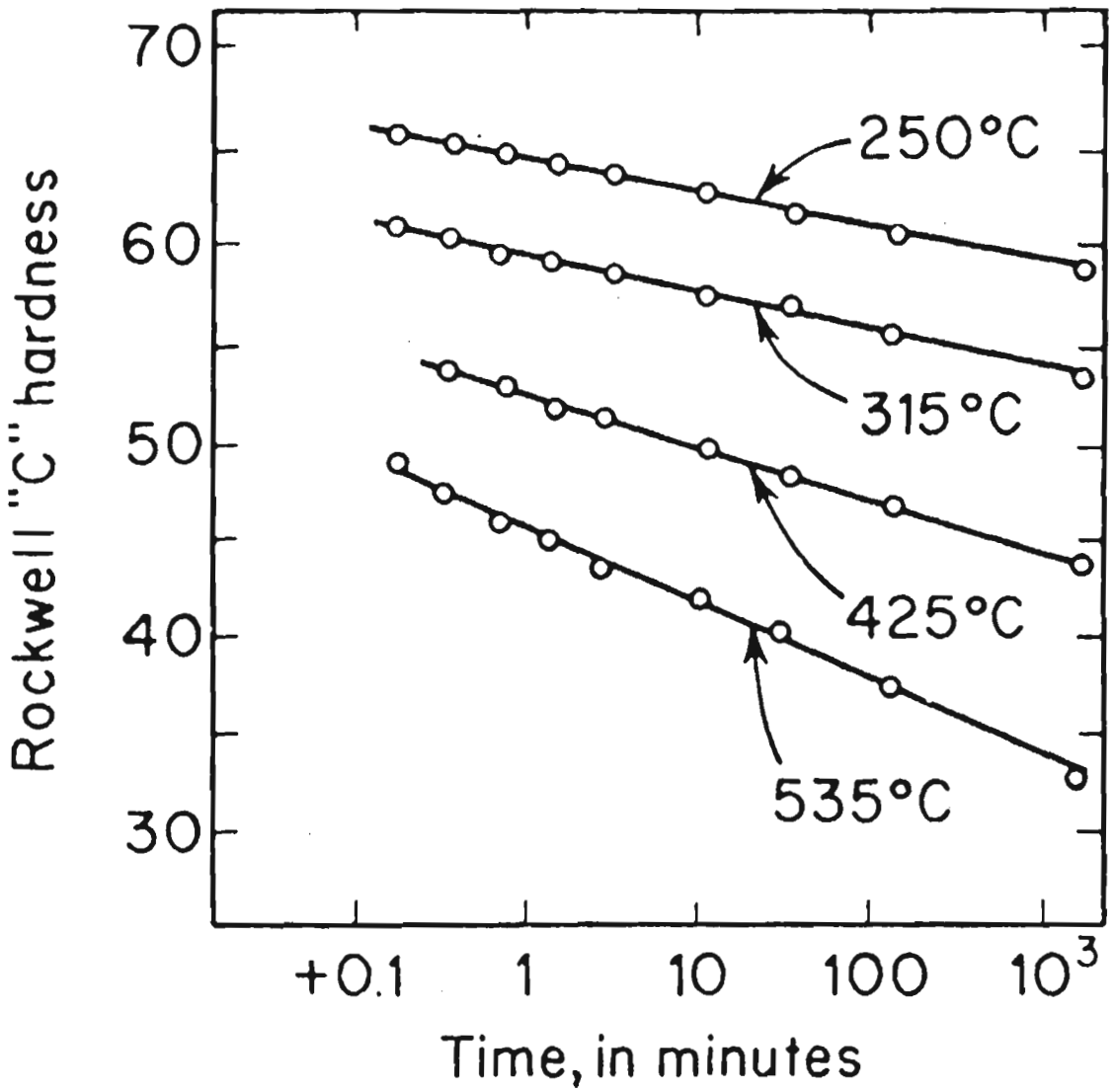

Figure 15. Decrease in Rockwell C Hardness of Eutectoid Steel for Different Tempering Times and Temperatures (Source: Bain, Ref. 12)

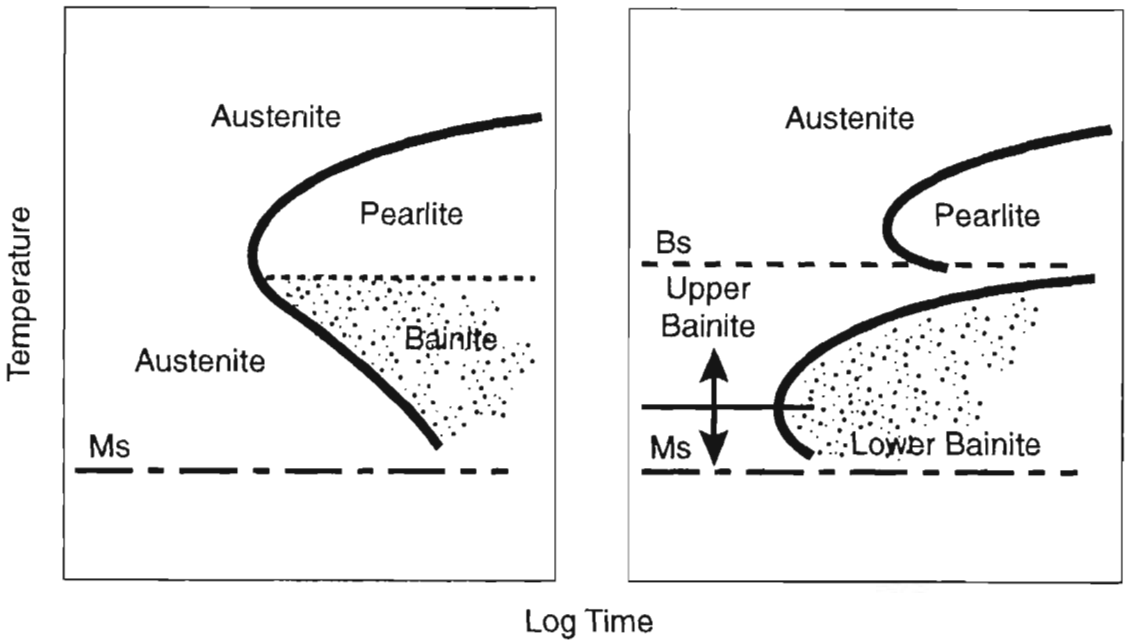

Figure 16. Conceptual Comparison of TTT Curves

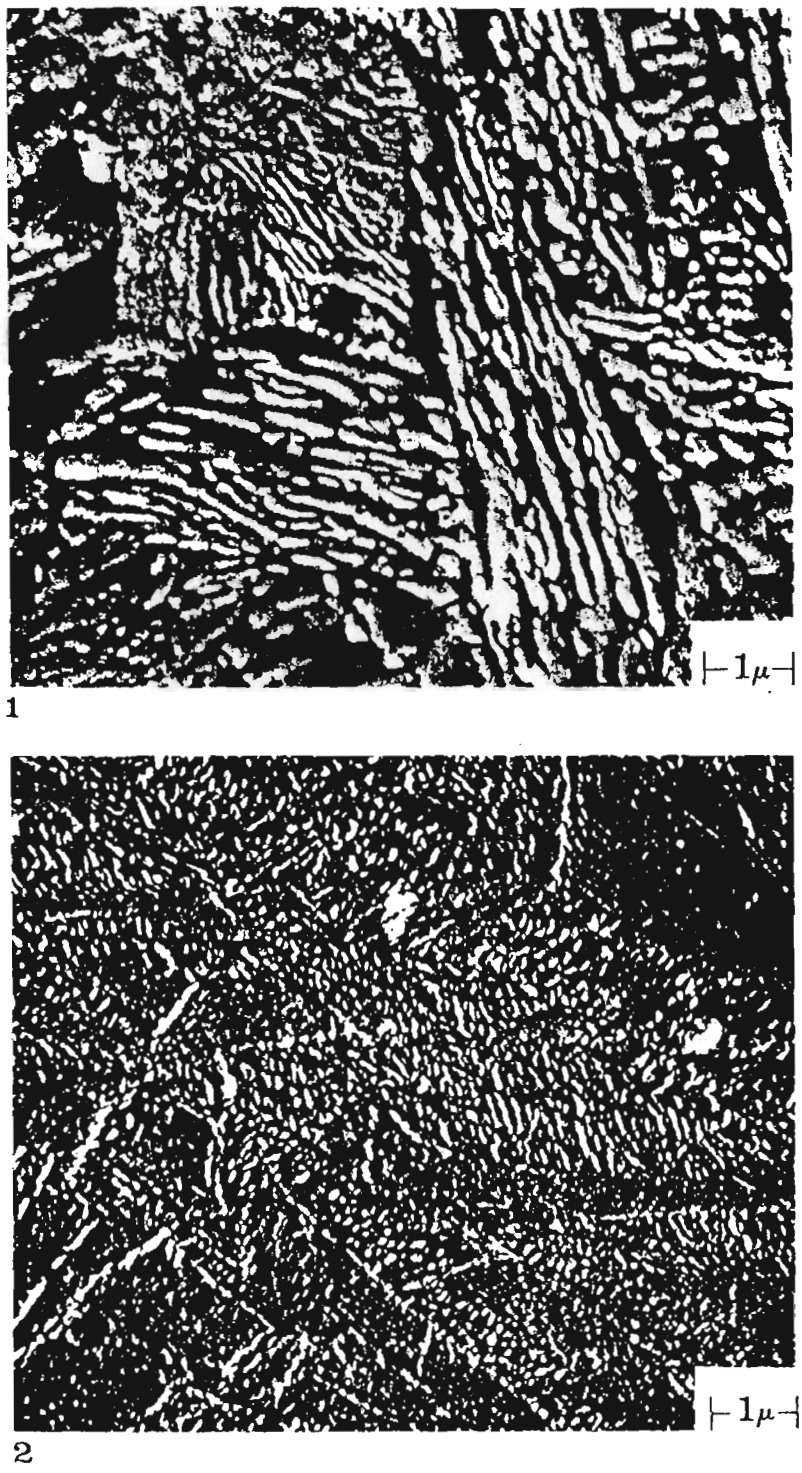

Figure 17. Typical Microstructures for Upper (1) and Lower (2) Bainite in a High-Carbon Steel (Source: Habracken/Economopoulos, Ref. 11)

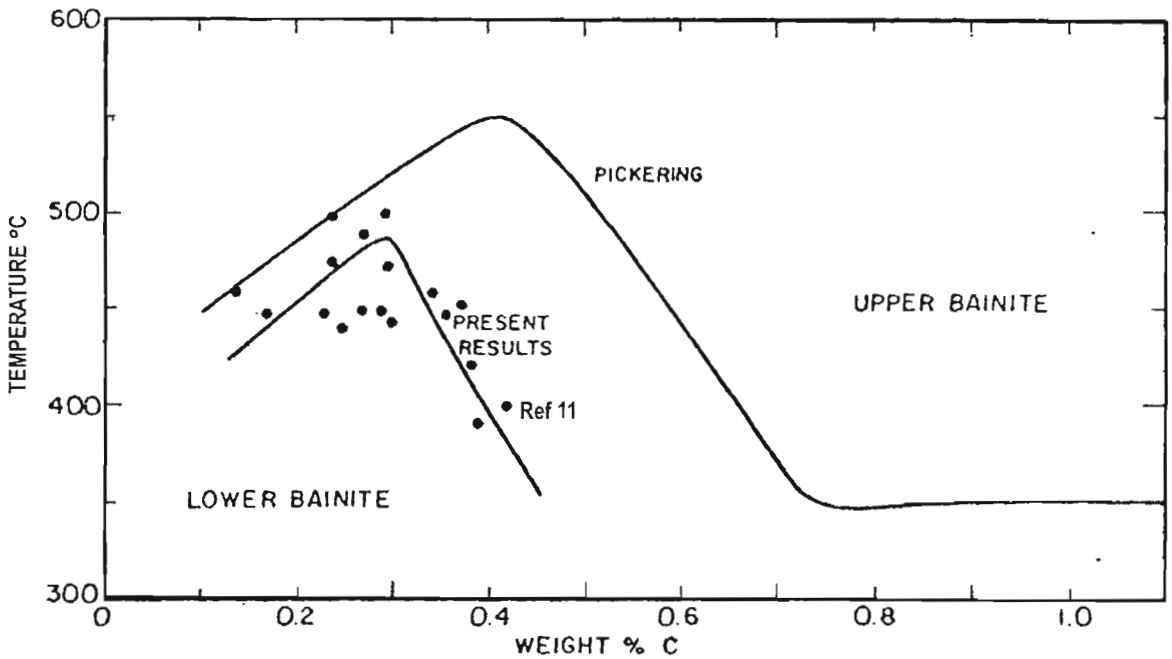

Figure 18. Effect of Carbon on the Temperature Change from Upper to Lower Bainite (Source: Parker, Ref. 15)

The categorization of bainite is not quite so simple as the description given in the preceding paragraphs would suggest [16]. In addition to the carbide-containing bainites, there is a granular, carbide-free bainite. The granular bainite can be comprised of retained austenite and a martensite/austenite aggregate [17]. The granular bainite is the result of slower continuous cooling into the top of the bainite transformation curve (Figure 19). The slower cooling reduces the carbon supersatuation in the austenite with a corresponding reduction in the likelihood of carbide precipitation. In the view of some workers in the field, the picture may be yet more complicated; Reynolds et al. [18] have proposed the identification map shown in Figure 20.

The tensile strength of low carbon (<0.25 w/o) bainite formed by air-cooling, has been related directly to the chemical composition by Pickering [13] as follows:

$$\begin{aligned}\text{Tensile Strength (tons per sq. in.)} = {} & 16 + 125\ (\text{w/o C}) + 15\ (\text{w/o Mn} + \text{w/o Cr}) \\ & + 12\ (\text{w/o Mo}) + 6\ (\text{w/o W}) + 8\ (\text{w/o Ni}) \\ & + 4\ (\text{w/o Cu}) + 25\ (\text{w/o V} + \text{w/o Ti})\end{aligned}$$

No contribution to strength is attributed to silicon. De Boer et al. [10] also have developed an expression relating strength to chemical composition, in this case including the contribution of silicon:

$$\begin{aligned}\text{Tensile Strength (MPa)} = {} & 430 + 688\ (\text{w/o C}) + 81\ (\text{w/o Si}) \\ & + 196\ (\text{w/o Mn}) + 202\ (\text{w/o Cr}) + 80\ (\text{w/o Mo}) \\ & + 400\ (\text{w/o V})\end{aligned}$$

Pickering [13] points out that for lower carbon alloys, the transformation temperature is closely related to the B_{50}[4] temperature, which in turn is related linearly to chemical composition. The transformation temperature dependence of tensile strength is shown in Figure 21. For carbon contents up to 0.25 w/o, Figure 18 indicates that the maximum temperature at which lower bainite will be found ranges from 752° to 887°F (400° to 475°C). Therefore, only the very highest tensile strengths in the temperature range labeled "bainites" (of Figure 21) are likely to be for *lower* bainites.

Figure 22 illustrates that yield strength generally follows tensile strength such that the YS/TS ratio is close to 0.65 to 0.70. The results of the de Boer et al. work are also plotted (+) on the figure; they agree reasonably well with the pattern of behavior for the lower carbon alloys.

Habraken and Economopoulos [11] note that, "the impact strength of lower bainite is generally higher than that of tempered martensite" (presumably at the same strength level). "Formation of upper bainite leads to severe loss of yield strength and appreciable embrittlement." This is, to some extent, consistent with the observation of Pickering [13] that lower bainites of considerably

[4] 50 percent transformation.

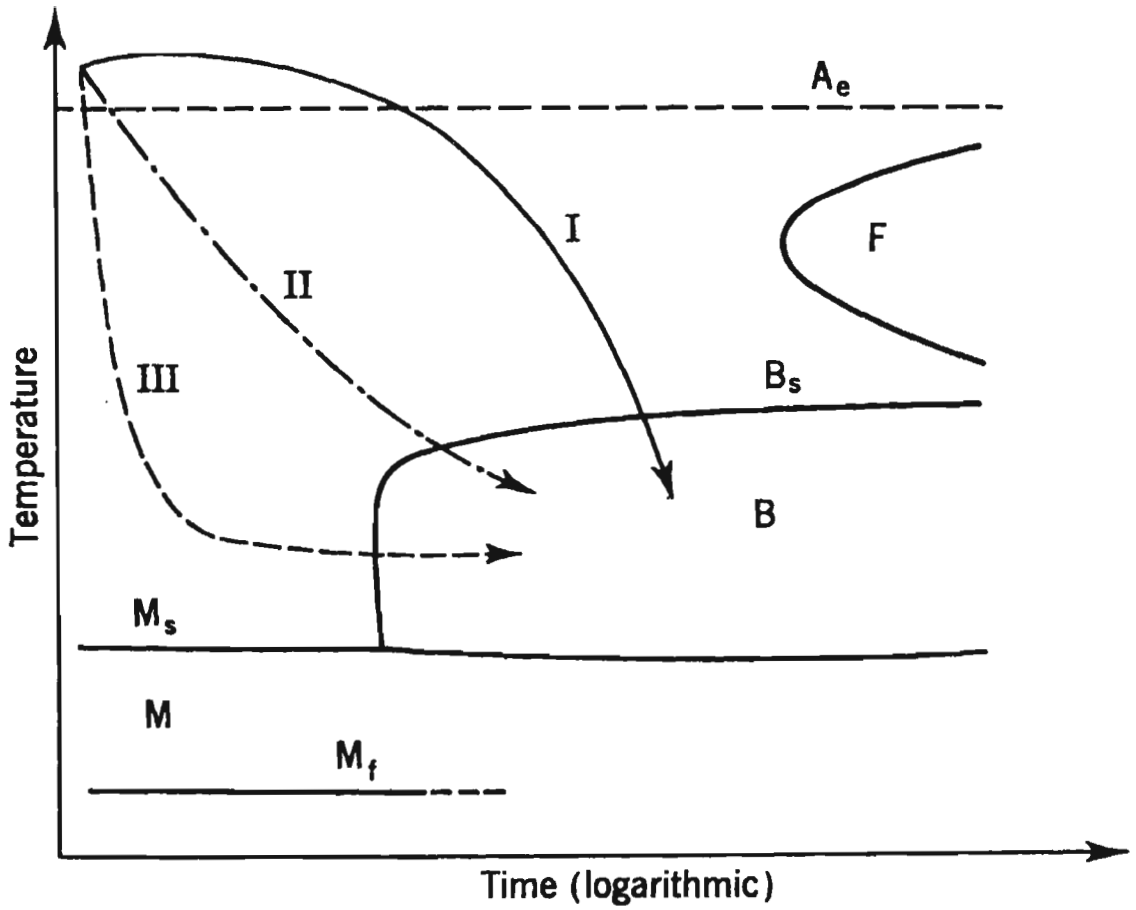

I. produces a structure with ferrite and austenitic-martensitic particles

II. produces a carbide-free acicular structure or conventional upper bainite

III. produces conventional lower bainite

Figure 19. Schematic Representation of Transformation in a Low-Carbon Alloy Steel (Source: Habracken/Economopoulos, Ref. 11)

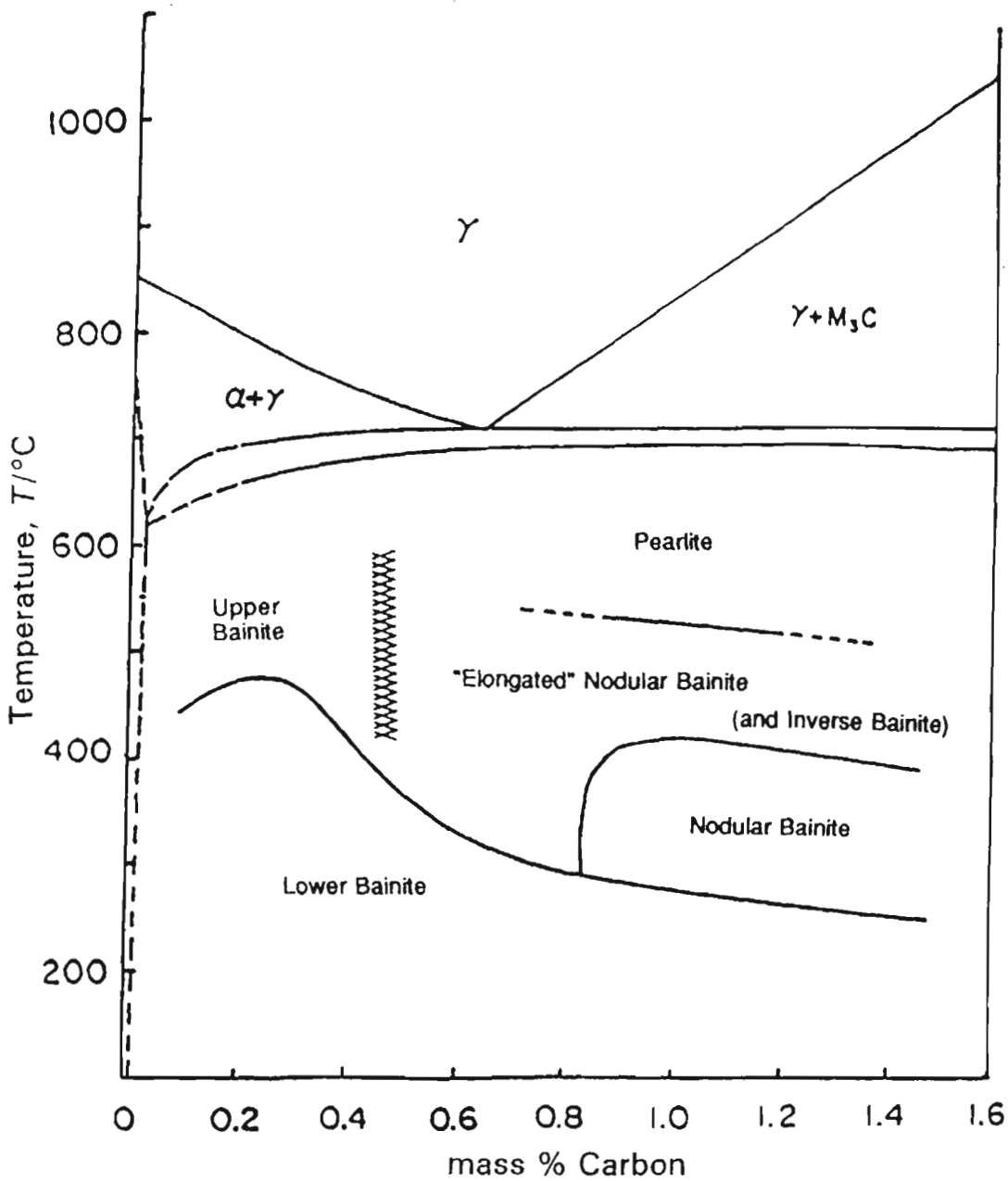

Figure 20. Temperature/Composition Morphology Map (Source: Reynolds, et al., Ref. 18)

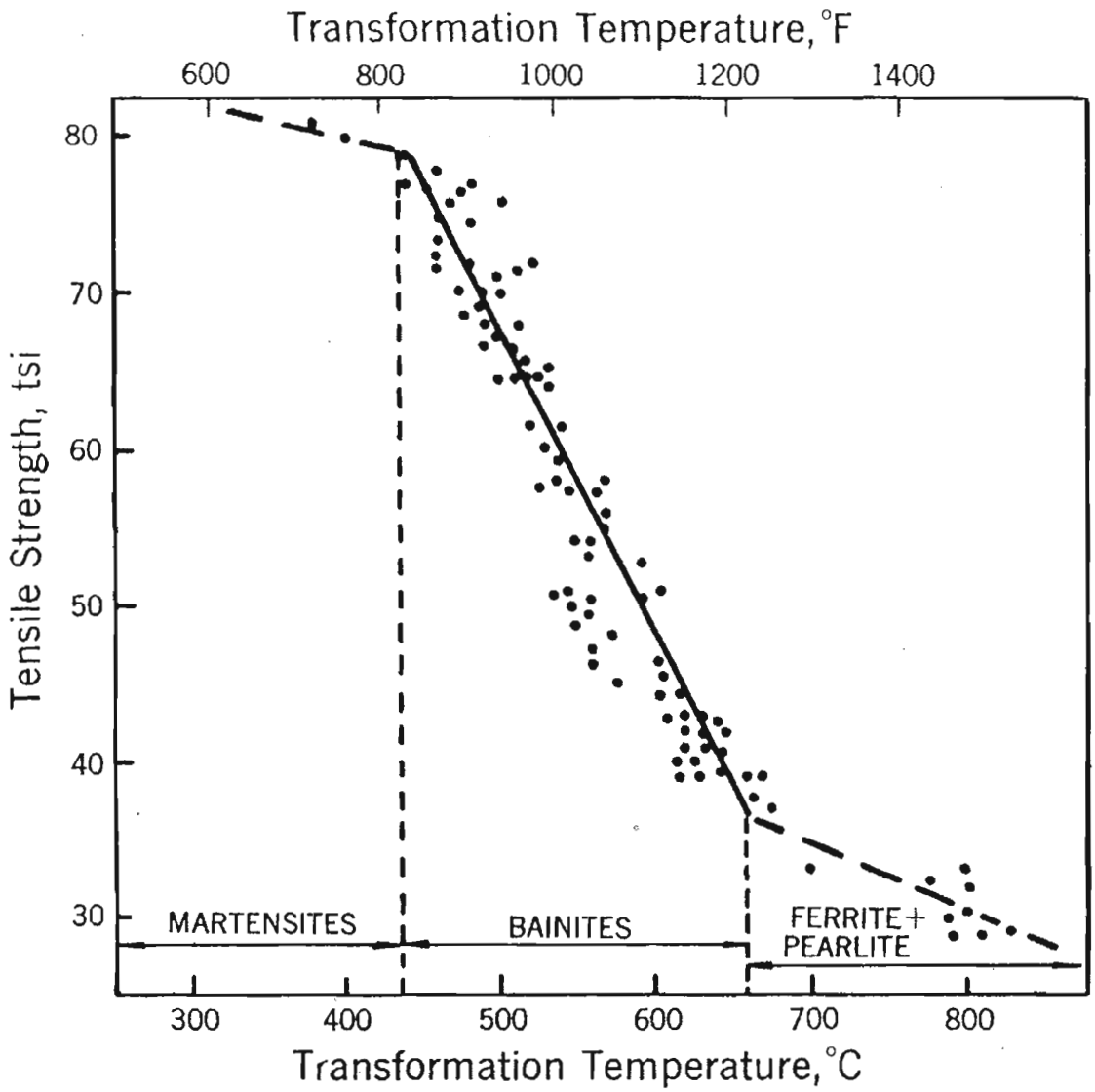

Figure 21. Effect of Transformation Temperature on Tensile Strength (Source: Pickering, Ref. 13)

high strength can have impact transition temperatures lower than those of upper bainites having considerably lower strengths (Figure 23). If the strength of the upper bainite drops low enough, however, the transition temperature may be lower than the best lower bainite transition temperature. Irvine [19] noted that for low-carbon steels containing modestly high Mn and Cr levels (1.5 w/o each), the impact energy dropped as tensile strength increased, except that at very low transformation temperatures (where bainite would form), the impact energy increased modestly as tensile strength increased (Figure 24). The addition of 2 to 4 w/o Ni and 1 to 2 w/o Mo increased overall toughness by about 100 percent but retained the same pattern of behavior.

Alloying elements, which are the essential ingredients of change in the transformation behavior, also achieve significant improvements in strength. Figure 25 illustrates the effects of carbon and substitutional alloying elements on hardness. The tendency for hardness to increase is much less for bainitic structures than for martensitic structures. Of the substitutional alloy additions, chromium is perhaps the most effective strengthening addition with vanadium next (though vanadium is usually added in much more modest amounts). Manganese and molybdenum fall into an intermediate category with nickel having the least effect. Manganese and chromium tend to be used most often because of their modest alloying costs. More will be said of this later.

2.4 HARDENABILITY

Alloying additions - most usually manganese, silicon, chromium, molybdenum, vanadium, and nickel - are made to control the shape and position of the TTT and CCT transformation curves. The alloying additions do not always have the same effect on retarding the pearlite and bainite transformations and in altering the martensite start temperature. Therefore, it is possible to delay the pearlite transformation more than the bainite transformation so that a prominent bainite nose can be created. However, if a lower bainite structure is sought, the bainite nose may need to be moved to longer times to allow the cooling path III to be achieved as shown on Figure 19. Comon et al., [20] have proposed a relationship between the minimum[5] cooling rate (between temperatures of 1,472° and 1,112°F (800° - 600°C)) to achieve complete transformation to bainite in a heavy section and the chemical composition:

$$\text{Log (deg C/hr)} = 3.7 + 0.955 / (0.16 + \text{w/o C}) - 1.96\ (\text{w/o Mo}) - 0.965\ (\text{w/o Mn}) - 0.751\ (\text{w/o Ni}) - 0.54\ (\text{w/o Cr})$$

Table 1 [21] illustrates (in descending order of effect) the effectiveness of a number of alloying additions upon five categories of transformation: austenite to ferrite/pearlite - isothermal and continuous cooling; austenite to bainite - isothermal and continuous cooling; and austenite to martensite - continuous cooling. Molybdenum is the most effective alloy addition to delay the pearlite transformation, followed closely by manganese. Fortunately, if one wants to make the bainite nose more pronounced, molybdenum is about the least effective addition in influencing the bainite transformation isothermally. However, its effect on the continuous cooling bainite transformation and the suppression of the martensite start temperature is just behind that of manganese. Carbon is not listed in the table, but it has about the same effect as manganese in both the pearlite and bainite transformations. Boron also is not listed in the table; very small amounts of boron (0.003 w/o) tend to suppress ferrite formation and therefore, in low carbon alloys, tend to increase the proportion of bainite. Molybdenum and boron together act very strongly to favor bainite formation, especially in low-carbon steels.

[5] This rate would just miss the pearlite or proeutectoid nose.

Table 1. Effect of Alloy Elements, in Decreasing Order of Magnitude, on Delaying Austenite Transformations (Source: Sage et al, Ref. 21)

Transformation to ferrite and pearlite -isothermal	*Transformation to ferrite and pearlite -continuous cooling*	*Transformation to bainite -isothermal*	*Transformation to bainite -continuous cooling*	*Transformation to martensite -continuous cooling*
Mo Mn Cr Ni Si Cu	Mo Mn Ni Cr	Mn Cr Ni Si Mo	Mn Mo Cr Si Ni	Mn Mo Cr Si Ni

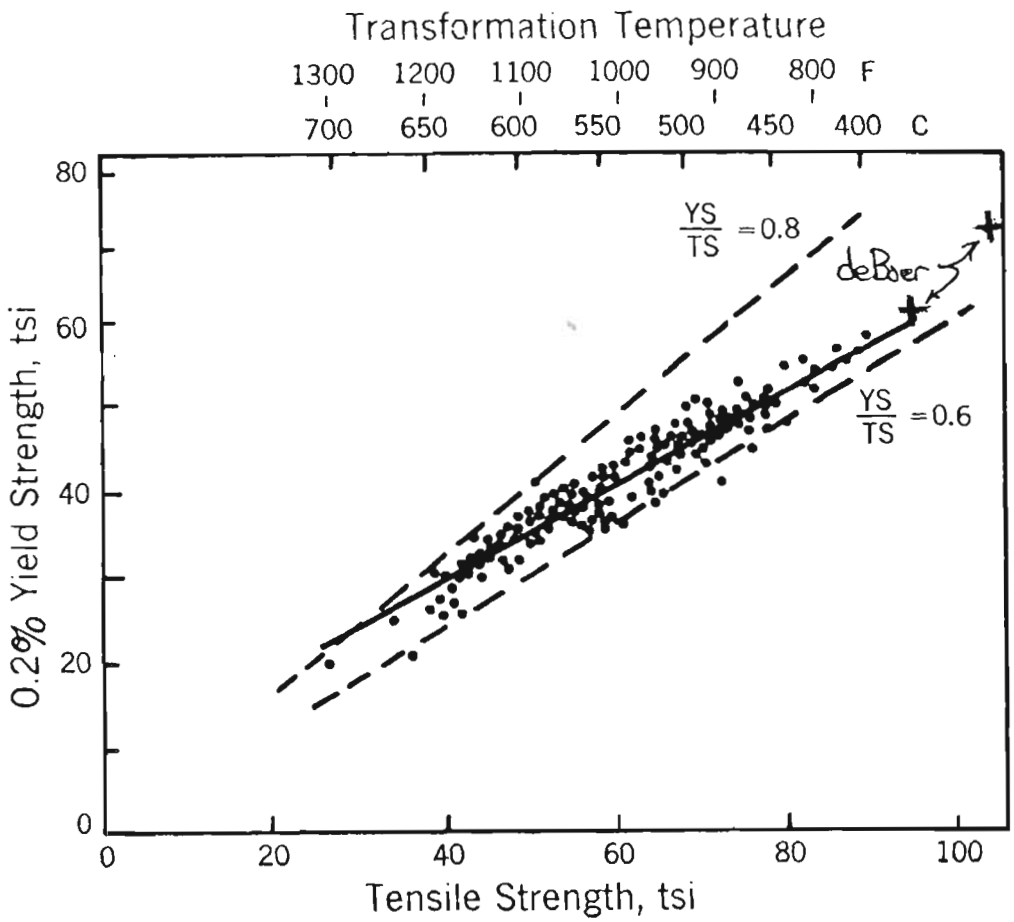

Figure 22. Yield Strength: Tensile Strength: Transformation Temperature Interrelationships (Source: Pickering, Ref. 13)

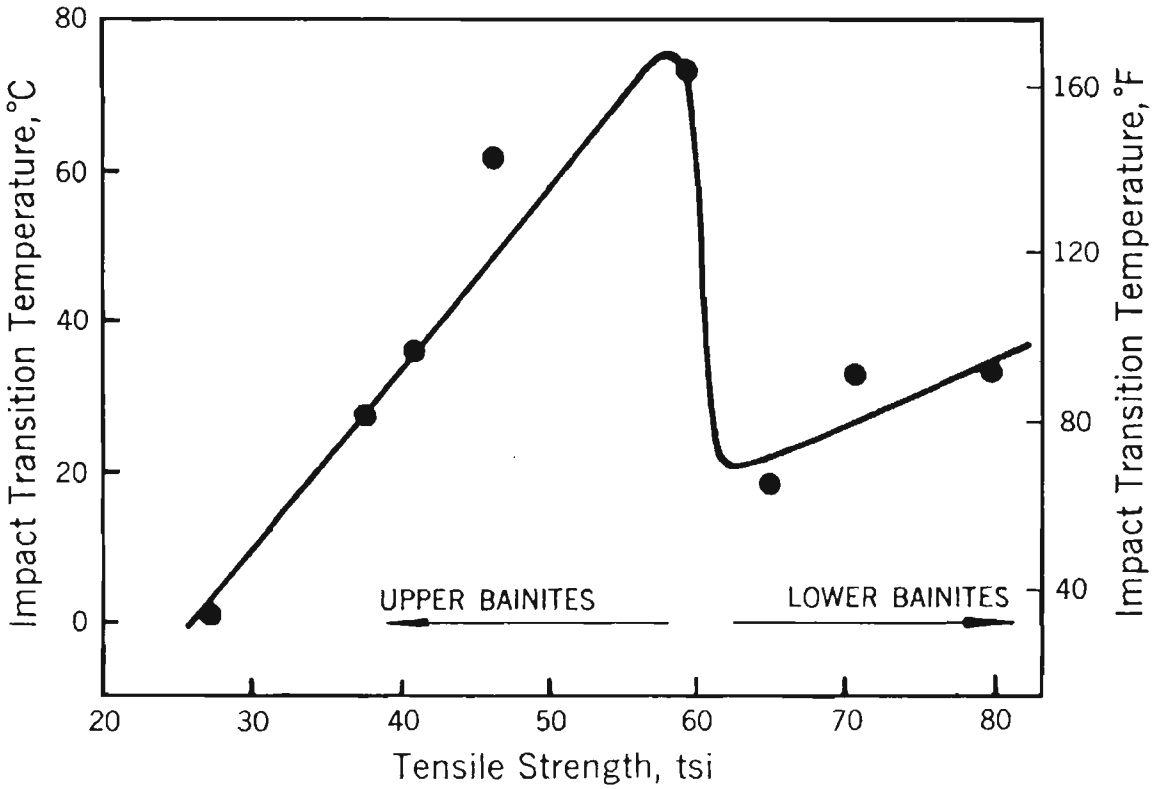

Figure 23. Effect of Tensile Strength on Impact Transition Temperature in Bainitic Steels (Source: Pickering, Ref. 13)

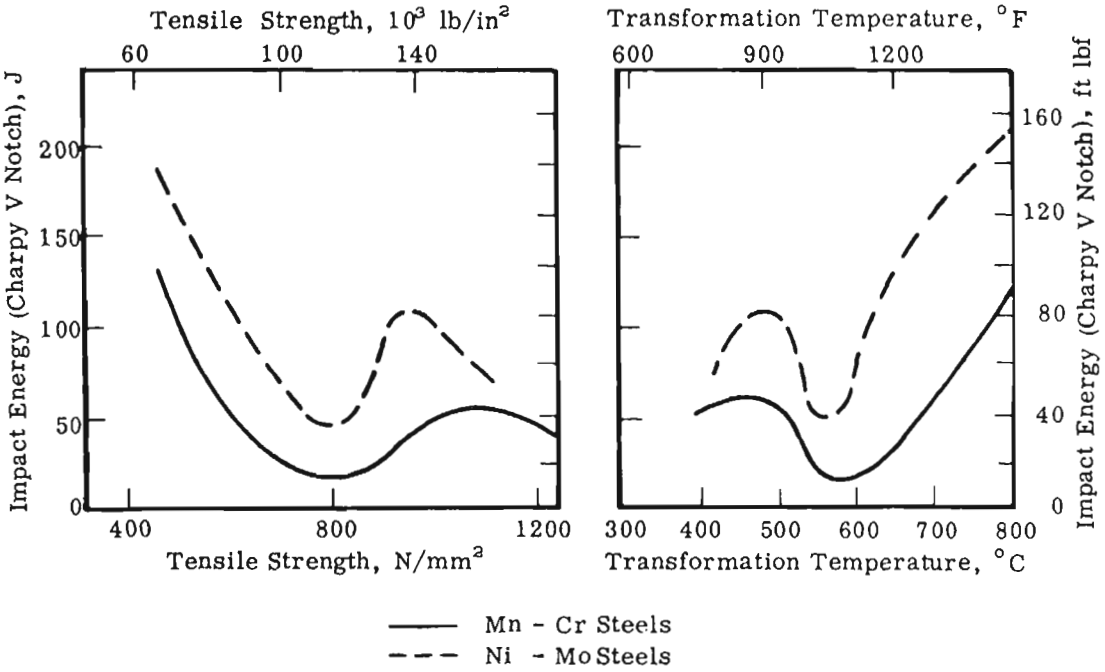

Figure 24. Relationships between Impact Energy, Tensile Strength, and Transformation Temperatures for Mn-Cr and Ni-Mo Steels (Source: Irvine/Pickering, Ref. 19)

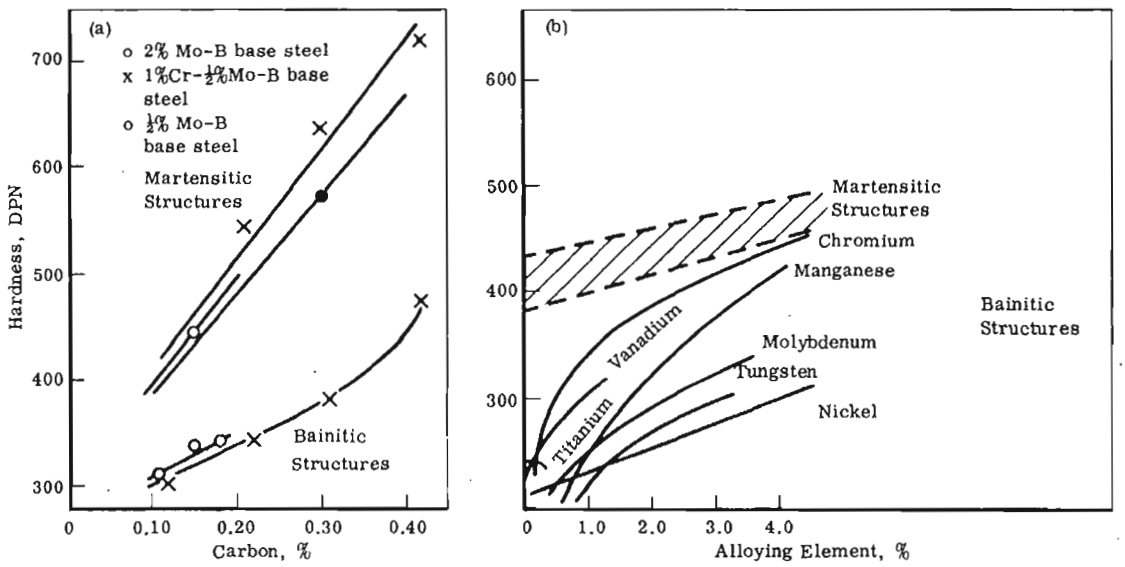

Figure 25. Effects of Carbon and Alloy Additions on Bainite and Martensite Hardness (Source: Irvin/Pickering, Ref. 19)

The information given in the preceding paragraph may be helpful in a qualitative manner, but is not of much help in even a semiquantitative fashion to decide what direction alloy adjustment should take to achieve bainitic microstructures for rails, wheels, and tank car shells. Therefore, in the next section of this report, a semiquantitative computer program, SteCal™ 2.0, will be exercised in a systematic fashion to develop a more rigorous assessment of alloy element content on the times and temperatures for bainite and pearlite transformation.

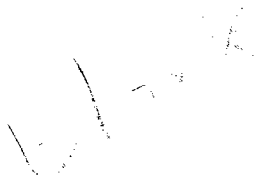

3. COMPUTATIONAL EXERCISE

SteCal™ 2.0 is a computer code authored by Pascual Tarin and is available from ASM International. It calculates a number of transformation parameters upon input of chemical composition[6] and grain size. The allowable limits for the alloying elements are listed in Table 2. The transformation parameters include the A_1, Ac_1, & Ac_3 temperatures, the pearlite nose temperature, and the start time and 50 percent transformation time at the nose, the bainite start, 50 percent and 99 percent transformation temperatures, the bainite nose temperature and times for bainite start at the nose, and for 50 and 99 percent transformation, and the martensite formation temperatures, M_s, M_{10}, M_{50}, M_{90}, and M_{99} . In addition, the code also calculates a stylized version of the isothermal and continuous cooling transformation curves.

Before attempting to use the program systematically to map out the effects of different alloying additions on pearlite and bainite transformation, it will be worthwhile to see how well the program predicts the transformation characteristics for cases where these have been established experimentally. Two such comparisons seem most appropriate. The first is for a modified 1065 steel (Figure 26), which is within the allowable chemical composition range for the computer code and roughly approximates an older intermediate manganese rail steel. The second is for the bainitic rail steel composition described by de Boer et al. [10] (Figure 27).

Figure 26 reveals one of the distinct limitations of the computer code: when the bainite 'nose' trails appreciably behind the pearlite nose, the stylized presentation of the model does not show the merging of the region between the two noses as evident in the experimentally determined transformation. The dashed line connecting the two noses is an estimate of what the actual curve might look like working from the computer-generated curves. Table 3 shows that the computer model makes a good estimate of M_s and M_{50}, but not so good for M_{90}. The estimate of Ac_1 was satisfactory, but the estimate of Ac_3 was less so. With the stylized computer curves, the estimate of the nose temperature is 200°F (93.3°C) too high; also the time estimate for the pearlite nose was a few seconds longer than that observed experimentally (that actually is excellent agreement). Comparing the time-@-bainite-nose-start with the experimental start curve at 744°F (395.6°C), the agreement is seen to be quite good. Overall, the agreement is qualitatively useful, especially if one blends the region between the pearlite and bainite noses on the computer-stylized plot.

[6] C, Mn, Si, P, S, Cr, Ni, Mo, B.

Table 2. SteCal™ Allowable Composition Limits

	w/o
Carbon	0.05 to 0.7
Manganese	< 2.7
Silicon	< 2.0
Chromium	< 2.5
Nickel	< 5.0
Molybdenum	< 1.0

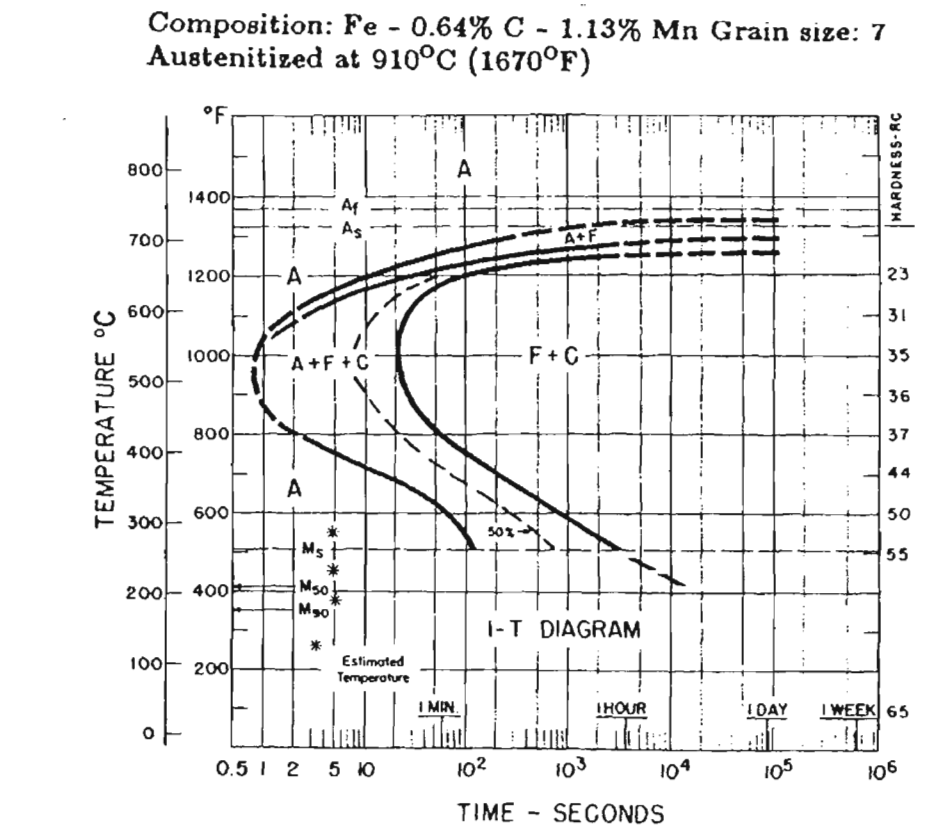

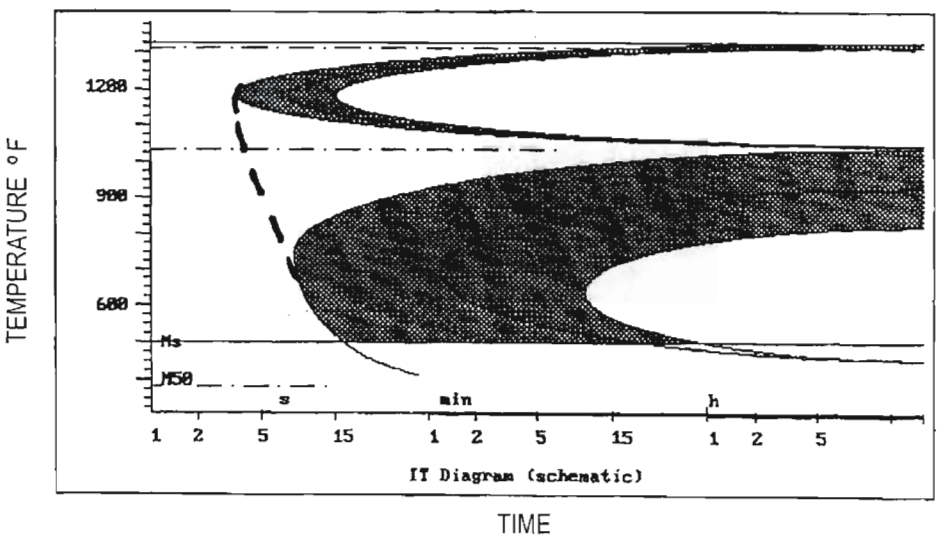

Figure 26. Experimentally Determined and Calculated TTT Diagrams for AISI 1065 Modified Steel (Source: ASM Atlas of TTT Diagrams)

Observed

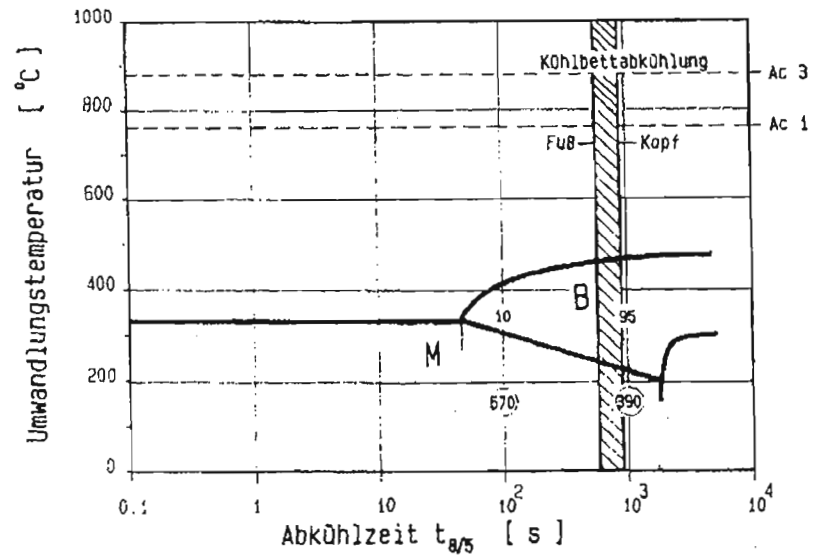

Calculated TTT

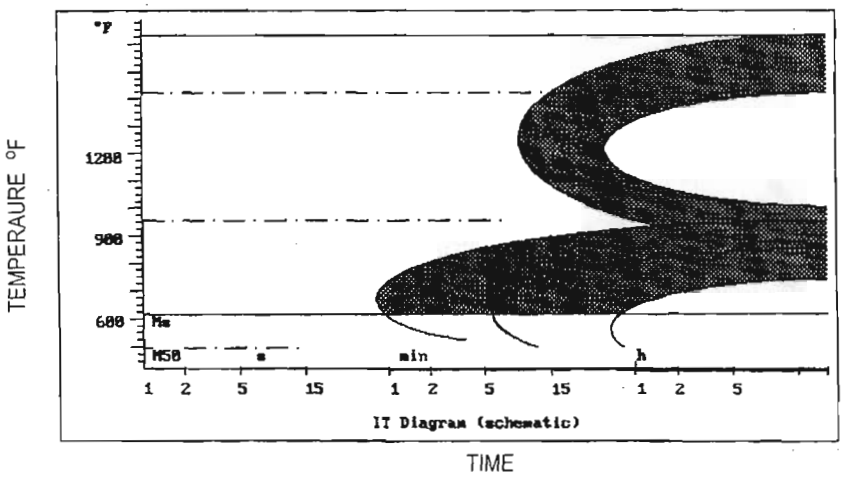

Calculated CCT

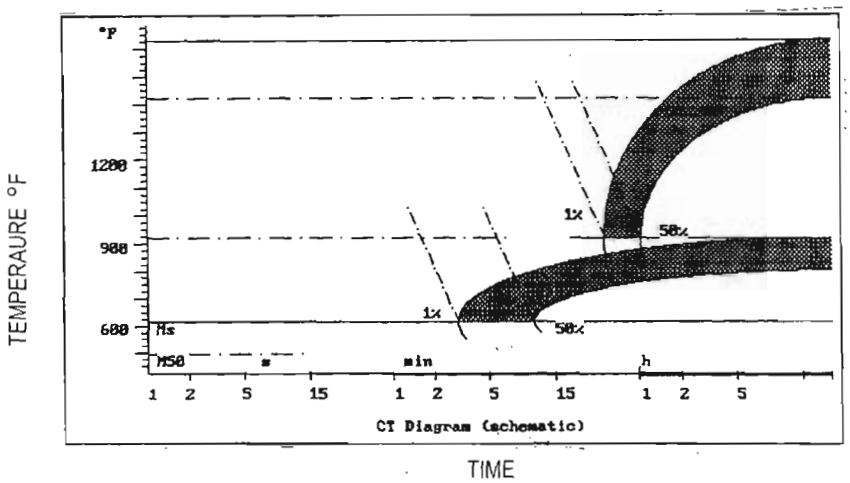

Figure 27. Reported and Calculated TTT/CCT Diagrams for Bainitic Rail Steel

Figure 27 is both encouraging and discouraging. Table 4 summarizes the transformation parameters where comparisons can be made. There is fair agreement on the Ac_1 and Ac_3 temperatures. Agreement on M_s, B_s, and the bainite nose temperature also is good. However, the start time for the bainite nose (SteCal™ isothermal prediction) is very sensitive to whether the vanadium is considered to be in solid solution and is effective in influencing hardenability. For isothermal transformation, the time to the start of the bainite nose is about twice as large as that shown experimentally (120 seconds vs 60 seconds), if vanadium is considered to be fully in solution and effective in increasing hardenability. If the vanadium is not considered to have an effect on hardenability, the predicted time-@-bainite-nose is 50 seconds – in close agreement with the experimental observations. However, it is not clear from the de Boer et al. paper whether the transformation diagram shown is a continuous cooling diagram or an isothermal diagram. The practice described in the text would suggest that it is a continuous cooling diagram. Were a comparison to be made with the predicted continuous cooling diagram, the agreement for the time-@-bainite-nose would be 1-minute experimental vs 6 minutes predicted, with vanadium fully solutionized, and 3 minutes with no hardenability contribution from the vanadium. This suggests that SteCal™ can over-predict the transformation times significantly.

The major difference between the predicted isothermal and the reported experimental diagrams is the predicted presence of a pearlite nose at about 1,292°F (700°C) and 25 minutes (1500 seconds) for full vanadium effectiveness, and 9 minutes (540 seconds) for no vanadium contribution. The experimental diagram does not show the presence of such a nose. However, the continuous cooling pearlite transformation predicted by SteCal™ is about 3 hours (10,800 seconds) for full vanadium effectiveness and about 30 – 40 minutes (1800 to 2400 seconds) for no vanadium contribution. The 3-hour time is well beyond the time range of the de Boer et al. transformation diagram.

It should not be assumed automatically that the computer calculation is in error. Krauss [22] has noted that the method by which the transformation behavior is measured may lead to some variation in key times and temperatures. Keeping these observations in mind, it is recommended that the following exercise be considered semiquantitative, intended solely for trend prediction.

The computer program has been exercised to show the effect of changing levels of individual alloying elements on the following parameters:

Pearlite and Bainite nose temperatures
Bainite and Bainite nose start times
Martensite start temperature

The pearlite and bainite start times at the nose will yield an idea of whether the alloy addition has more effect on delaying the pearlite or bainite transformations. The exercise has been undertaken for two steel compositions to measure any interaction with carbon content. These are a eutectoid composition comparable to a 250 BHN rail steel and the de Boer bainitic steel with 0.4 w/o carbon.

Table 3. Comparison of Calculated and Observed Transformation Parameters of AISI 1065 Modified Steel

	Observed[a]	Calculated (SteCal™)
Pearlite Nose Temp (°F)	970	1185
Pearlite Nose Time (sec)	0.8	3
50% Transformation at Nose Temp (sec)	8	8
Bainite Nose Temp (°F)	(no nose)	744
Bainite Nose Time (sec)	6-7[b]	8
Martensite Start Temp (°F)	505	499
Martensite 50% Temp (°F)	410	382
Martensite 90% Temp (°F)	350	121

[a] ASM, Atlas of Time-Temperature Diagrams for Irons and Steels, 1991

[b] Start time at 744°F

Table 4. Comparison of Calculated and Reported Transformation Parameters for Bainitic Rail Steel[10]

		Calculated (SteCal™)			
		A		B	
	Observed[10]	TTT	CCT	TTT	CCT
Ac_1	770	772	770	778	781
Ac_3	880	888	880	908	906
B_s	480	514	495	499	483
Bainite Nose Temp	330	354	320	339	319
Bainite Nose Time	60	50	180	120	360
M_s	330	323	320	323	319

All temperatures are °C; all times are in seconds.

(A) no vanadium contribution to hardenability

(B) full vanadium contribution to hardenability

The concept of hardenability is based on the multiplicability of the alloy contributions [23]. This means that the effect (most especially on time to transformation) of a particular alloying addition can depend upon the levels of other alloy additions. To test this concept, several different ratios of levels of key alloying elements (Cr, Mn, and Mo) have been fixed and the content levels of other elements in the alloy have been varied; this analysis is particularly useful in identifying the conditions under which the bainite nose emerges from under the pearlite nose.

Figures 28 through 34 portray the influence of individual element variation on the pearlite and bainite nose starting times for carbon, manganese, silicon, chromium, nickel, and molybdenum, without and with boron respectively in a basic carbon steel[7] and the de Boer et al. bainitic steel.[8] Increases in the carbon and alloy element contents retard both the bainite and pearlite transformations. However, there are some differences in behavior among the elements. The influence of carbon rises quickly as carbon is first added, and then drops off rapidly as carbon content approaches 0.7 w/o. In contrast, the other alloying additions cause the transformation start times to increase much more nearly linearly (on a semilog scale) as the content increases. Silicon seems to have relatively little effect on transformation start times, whereas carbon and molybdenum have the greatest effect. With the exception of molybdenum (with and without boron), in the basic carbon steel, the times to the pearlite nose are less than or equal to the bainite nose times. This tells us that a distinct bainite nose, which protrudes out to the left (shorter times) under the pearlite nose, is not likely to exist in the basic carbon steel composition to which manganese, silicon, chromium, or nickel is added. However, molybdenum makes the difference. Figures 33 and 34 show that molybdenum additions[9] over 0.2 w/o cause the pearlite nose transformation start time to lag behind the bainite nose transformation start time; thus, here a distinct bainite nose develops. The time separation of the bainite and pearlite noses increases rapidly as the amount of molybdenum increases. The effect of boron in conjunction with molybdenum is to somewhat further retard both the pearlite and bainite transformations. The de Boer et al. bainitic rail steel exhibits a different relationship of the pearlite and bainite nose transformation start times; here, the pearlite times are always longer than the bainite times, typically by a factor of nearly 10. This factor is perhaps just a bit larger than the relative pearlite/bainite nose times for the basic rail steel. Although the presence of molybdenum has caused the pearlite nose time to significantly exceed the bainite nose time, the overall increase in both transformations has been caused by the other alloy additions (increased silicon, chromium, and molybdenum) made to the de Boer et al., steel.

This tells us that a candidate alloy is likely to contain molybdenum (to produce the distinct bainite nose) plus some other alloy additions to delay both pearlite and bainite transformations sufficiently to allow interrupted spray quenching to bring the surface, and then the interior temperatures, down close to the bainite nose temperature (or slightly thereunder). But this must be done without dropping metastable austenite below the martensite start temperature.

[7] 0.7 w/o C, 0.8 w/o Mn, and 0.25 w/o Si.
[8] 0.4 w/o C, 0.8 w/o Mn, 1.4 w/o Si, 1.0 w/o Cr, 0.7 w/o Mo, and 0.1 w/o V.
[9] Perhaps vanadium as well; in SteCal™ one unit of V = 2 units of Mo if V is fully in solution.

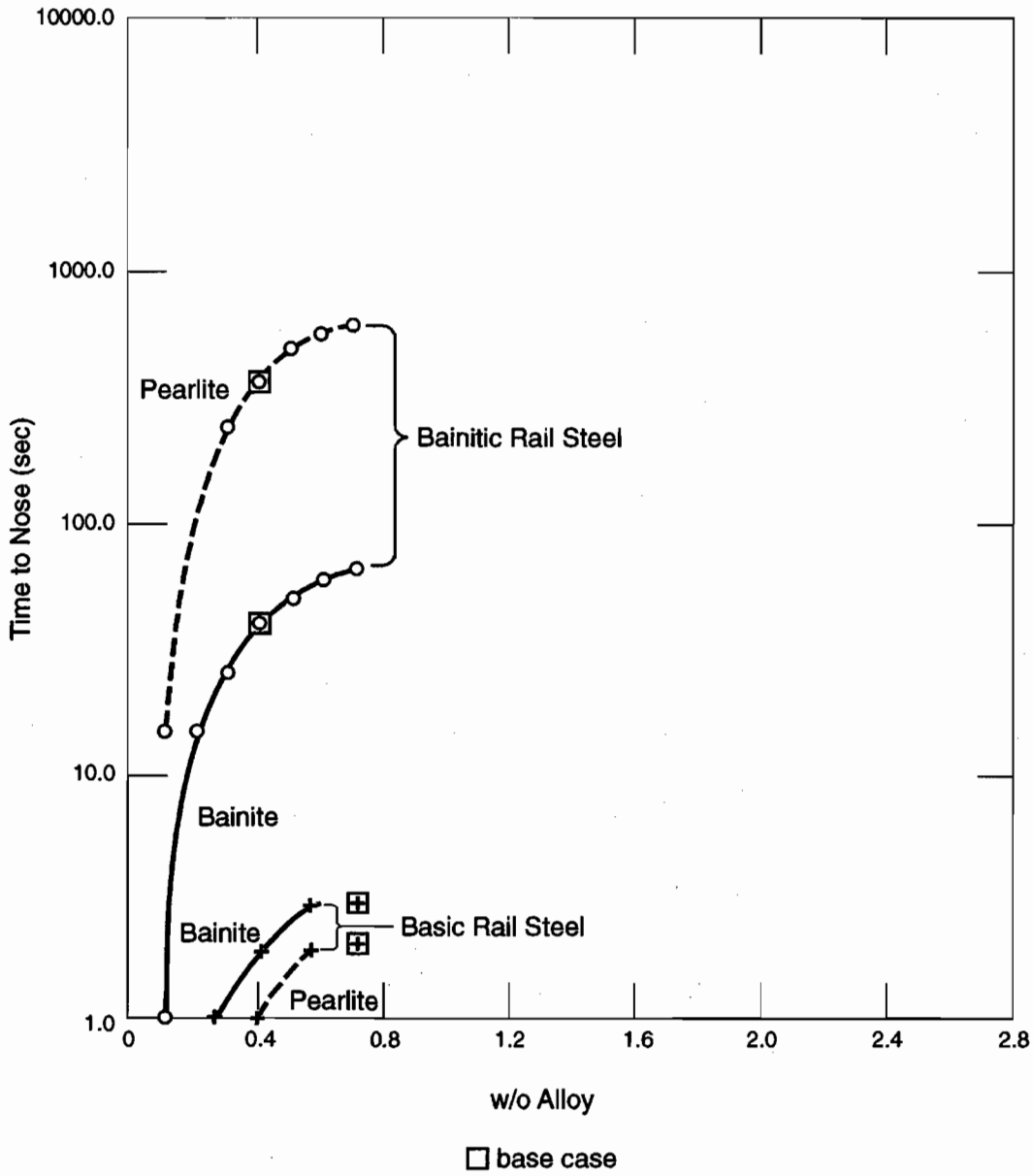

Figure 28. Effect of Carbon on the Times to Pearlite and Bainite Noses

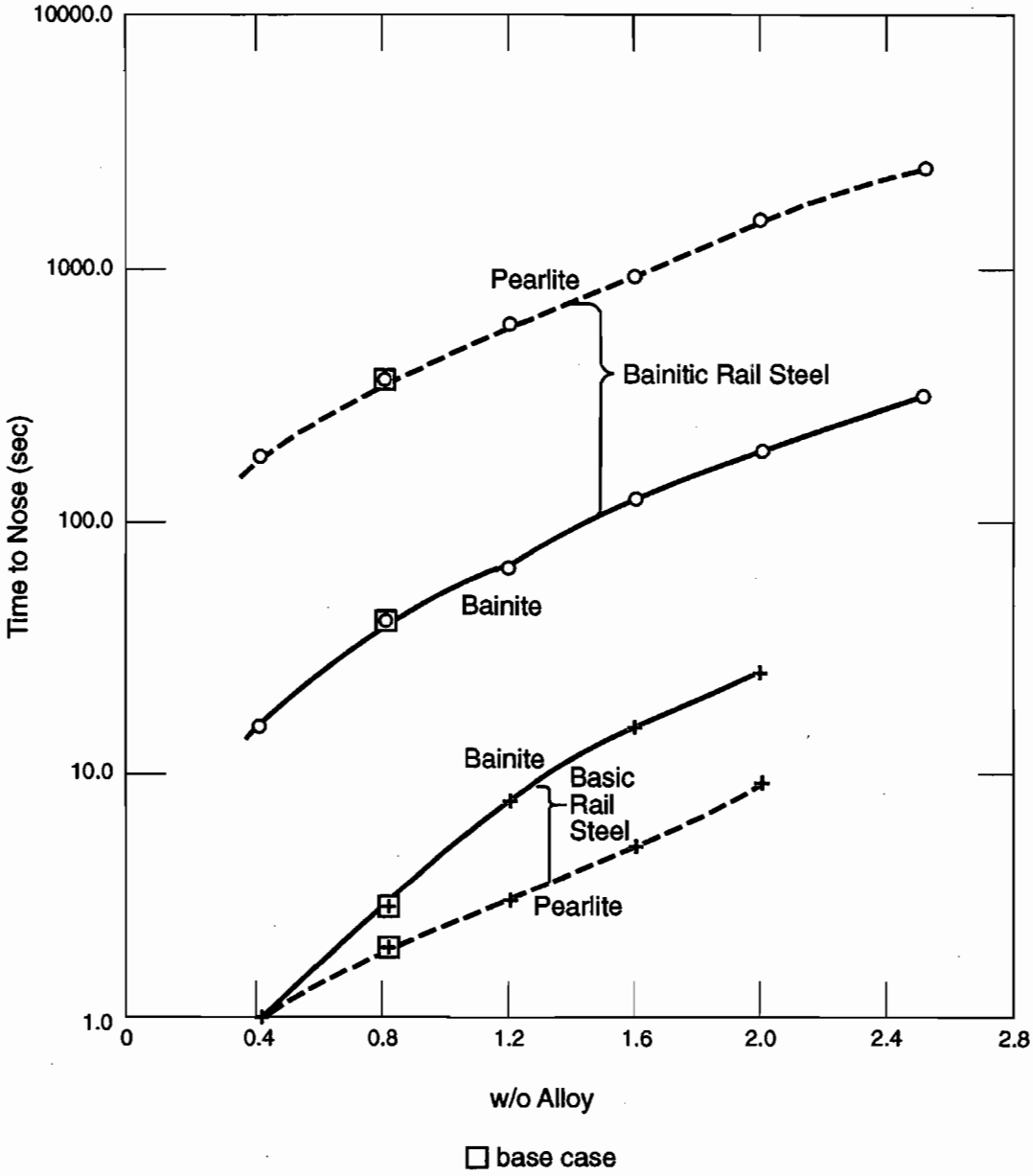

Figure 29. Effect of Manganese on the Times to Pearlite and Bainite Noses

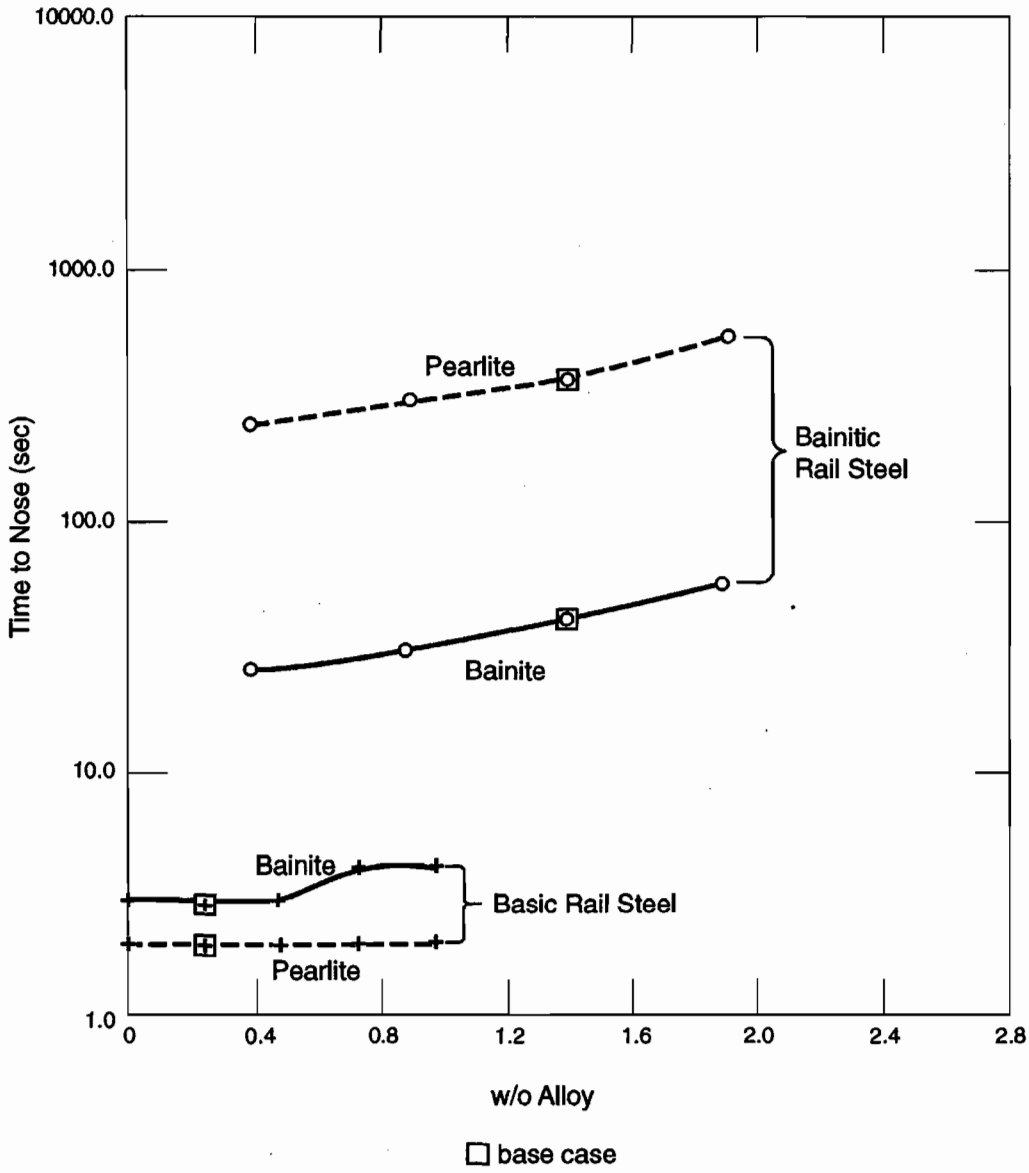

Figure 30. Effect of Silicon on the Times to Pearlite and Bainite Noses

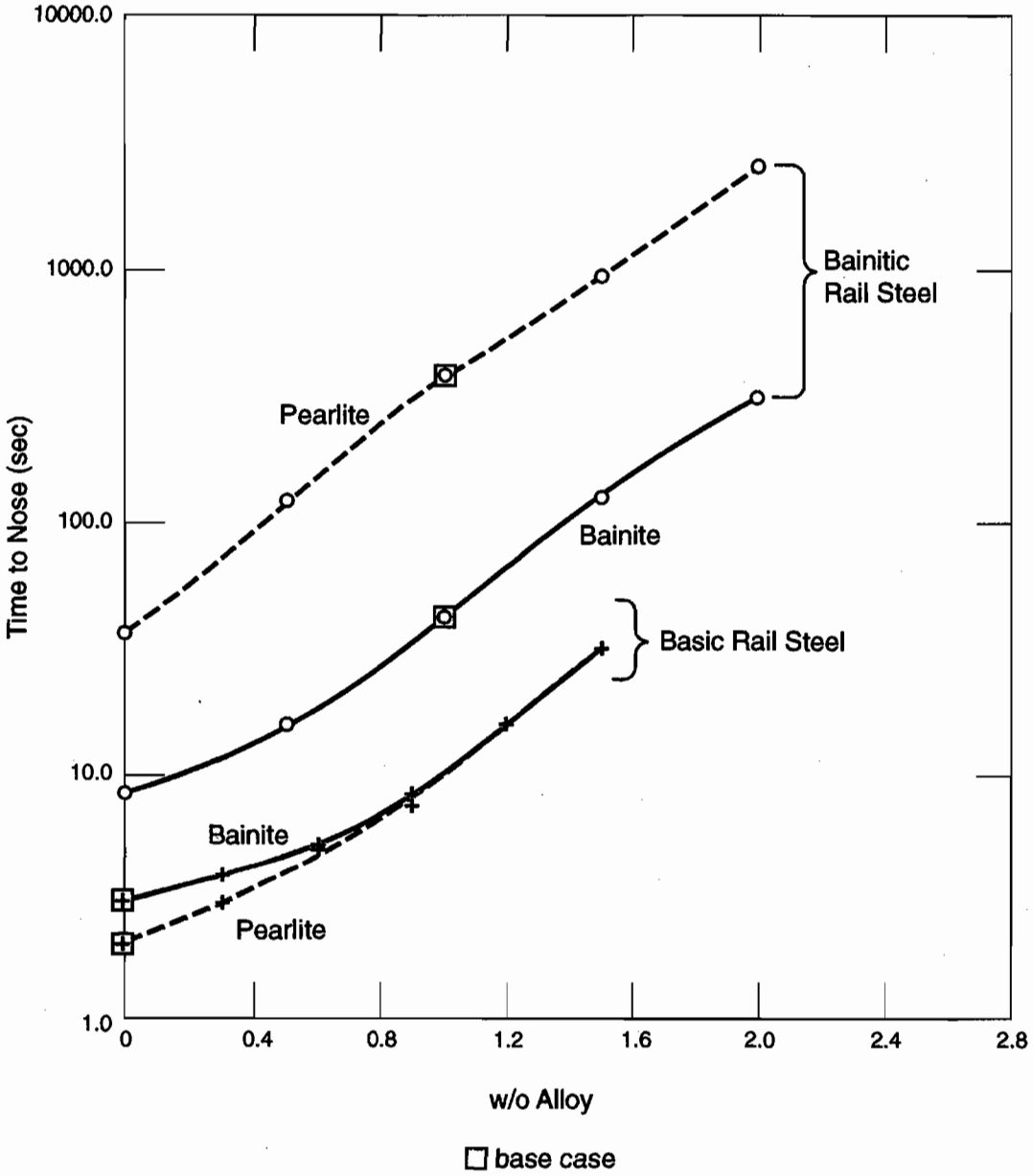

Figure 31. Effect of Chromium on the Times to Pearlite and Bainite Noses

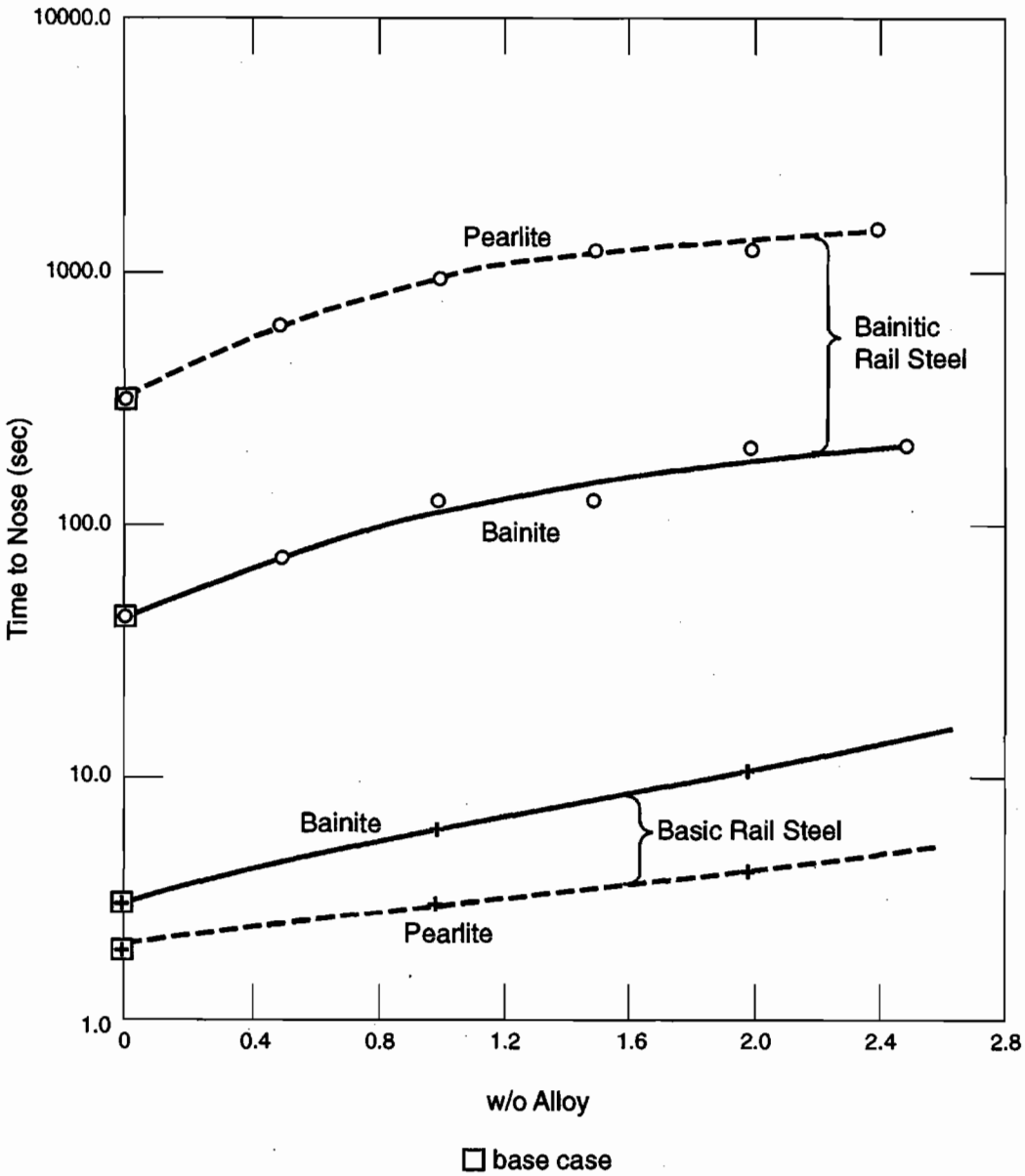

Figure 32. Effect of Nickel on the Times to Pearlite and Bainite Noses

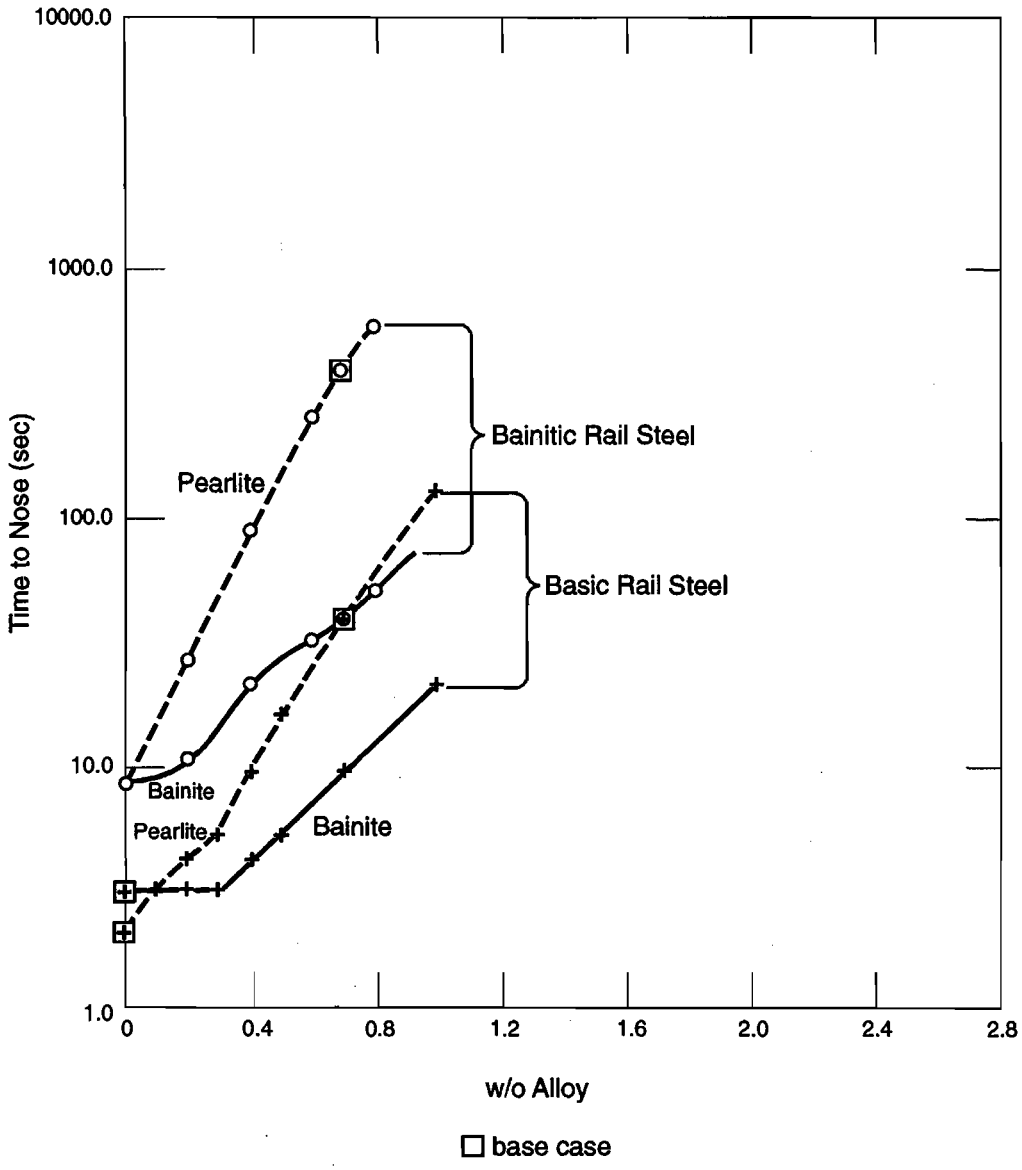

Figure 33. Effect of Molybdenum without Boron on the Times to Pearlite and Bainite Noses

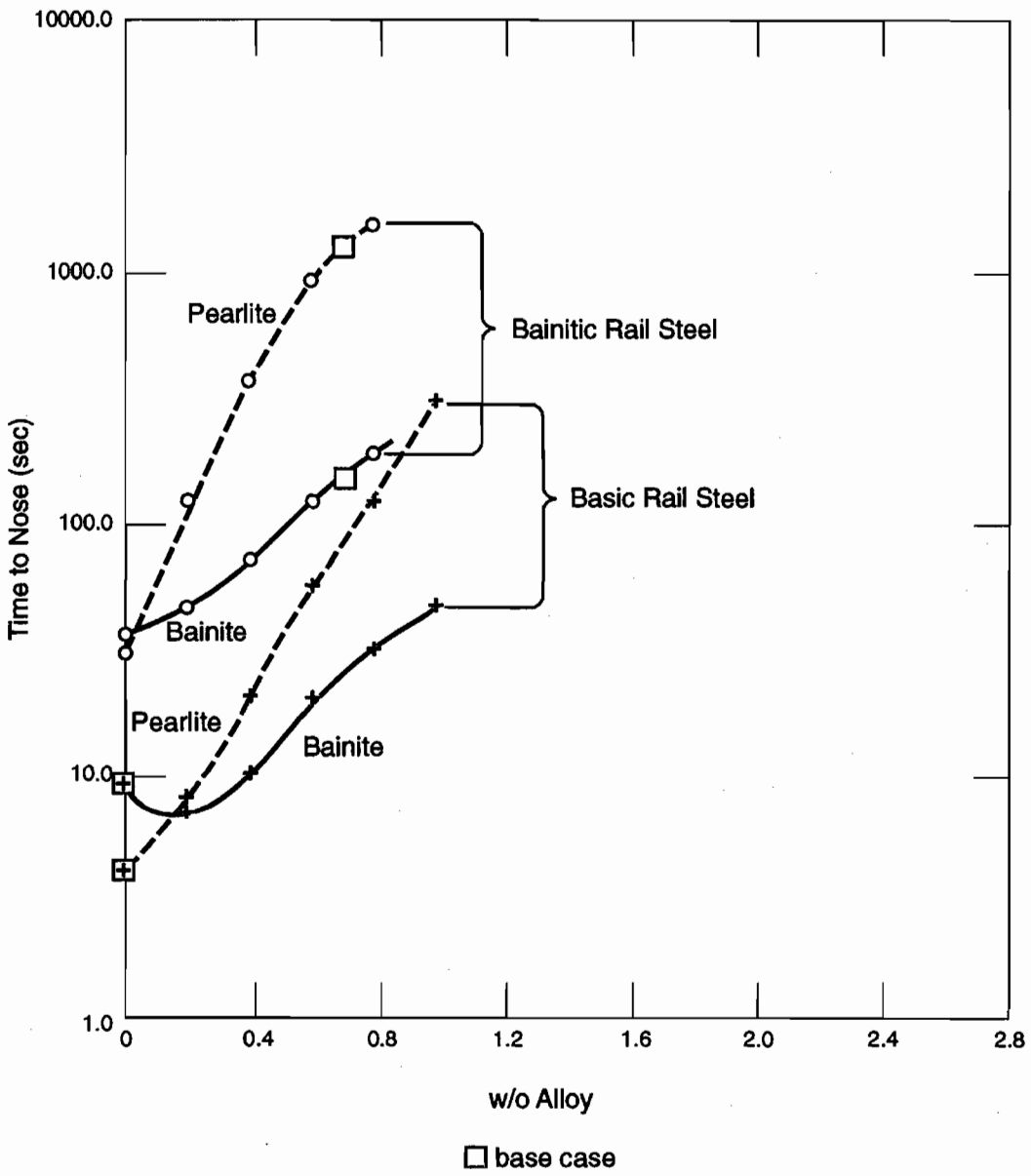

Figure 34. Effect of Molybdenum with Boron on the Times to Pearlite and Bainite Noses

Figures 35 through 41 illustrate how increasing carbon and alloying element content serves to lower both the bainite nose temperature and the martensite start temperature. In some cases, the predicted bainite nose temperature falls below the martensite start temperature – a condition suggesting that lower bainite cannot form. Carbon has the most pronounced effect on depressing both the martensite start and the bainite nose temperatures. Silicon has no predicted effect on either temperature. The effect of substantial alloying (as is the case with the de Boer et al. alloy) is to bring the martensite start temperature curves closer to the bainite nose temperature curves. In the case of manganese and chromium additions, the closer proximity causes the two curves to cross – at 1.4 w/o Mn and at 1.65 w/o Cr. Thus, for a heavily alloyed steel, the bainite nose would drop beneath the martensite start temperature at these concentrations of manganese and chromium and achievement of lower bainite would not be possible; martensite would more likely be formed if one tried to accomplish such a transformation. Alloys having smaller amounts of alloy additions would likely be able to tolerate higher levels of manganese and chromium and still have the bainite nose safely above the martensite start temperature.

Therefore, there are three fundamental requirements necessary to design an alloy for in-line quenching to achieve a lower bainitic microstructure:

(1) produce a bainitic nose sufficiently pronounced (in advance of the pearlite nose) to assure that pearlite transformation will not occur;

(2) delay the bainite transformation long enough so that austenite can be in-line quenched to the temperature at or just under the bainite nose temperature before any transformation occurs; the delay needed will depend upon the heat removal capacity of the quenchant and the temperature of the bainite nose; and

(3) have the bainite nose temperature sufficiently above the martensite start temperature so that there is little danger of accidentally forming martensite and that it will be possible to transform slightly under the bainite nose to produce lower bainite.

The question is how to go about achieving these requirements. The work of de Boer et al., provides a place to start. Indeed the de Boer et al. alloy does meet the first two requirements. And it is possible that isothermally, the bainite nose is at least somewhat above the martensite start temperature even though SteCal™ predicts both to be close together (M_s = 320 - 323°C and bainite nose temp = 339 - 354°C).

One of the major drawbacks of the de Boer et al. alloy is likely to be high cost because of the high molybdenum content. Therefore, it will be fruitful to use SteCal™ to vary the alloy content from that of the de Boer et al. alloy in a systematic fashion to predict the changes in the transformation characteristics and, in the process, lower the amount of molybdenum needed.

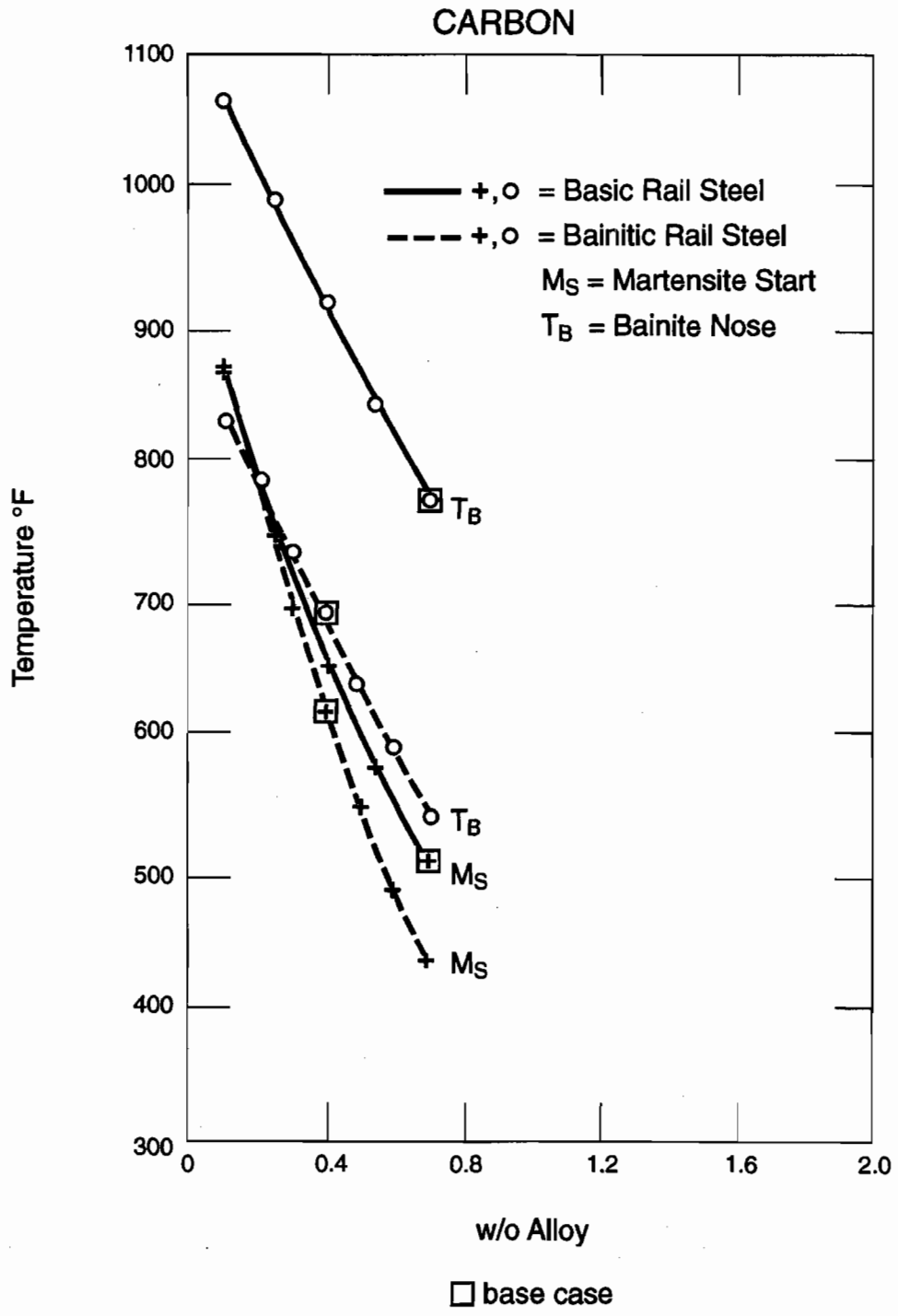

Figure 35. Effect of Carbon on the Martensite Start and Bainite Nose Temperatures

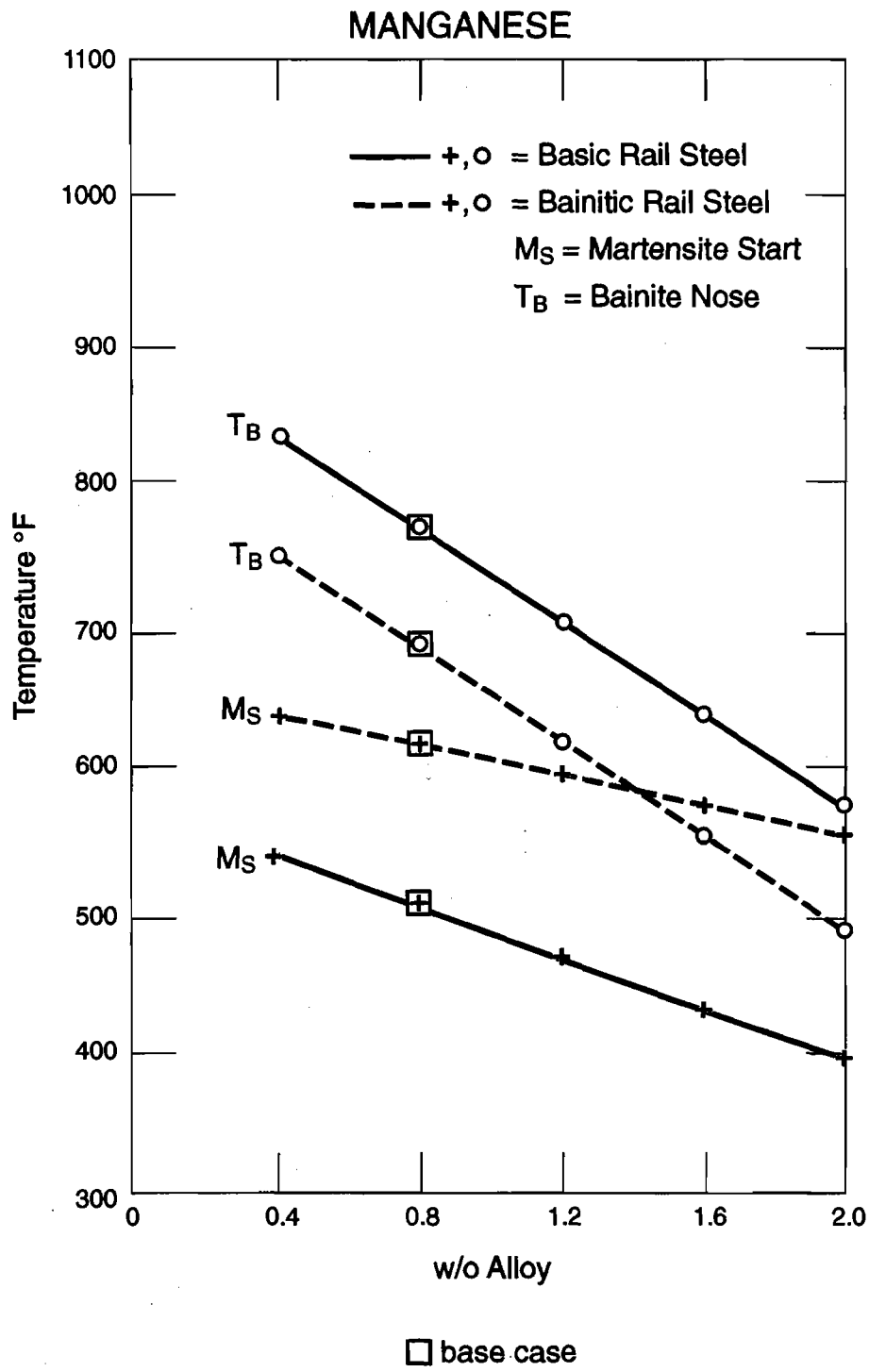

Figure 36. Effect of Manganese on the Martensite Start and Bainite Nose Temperatures

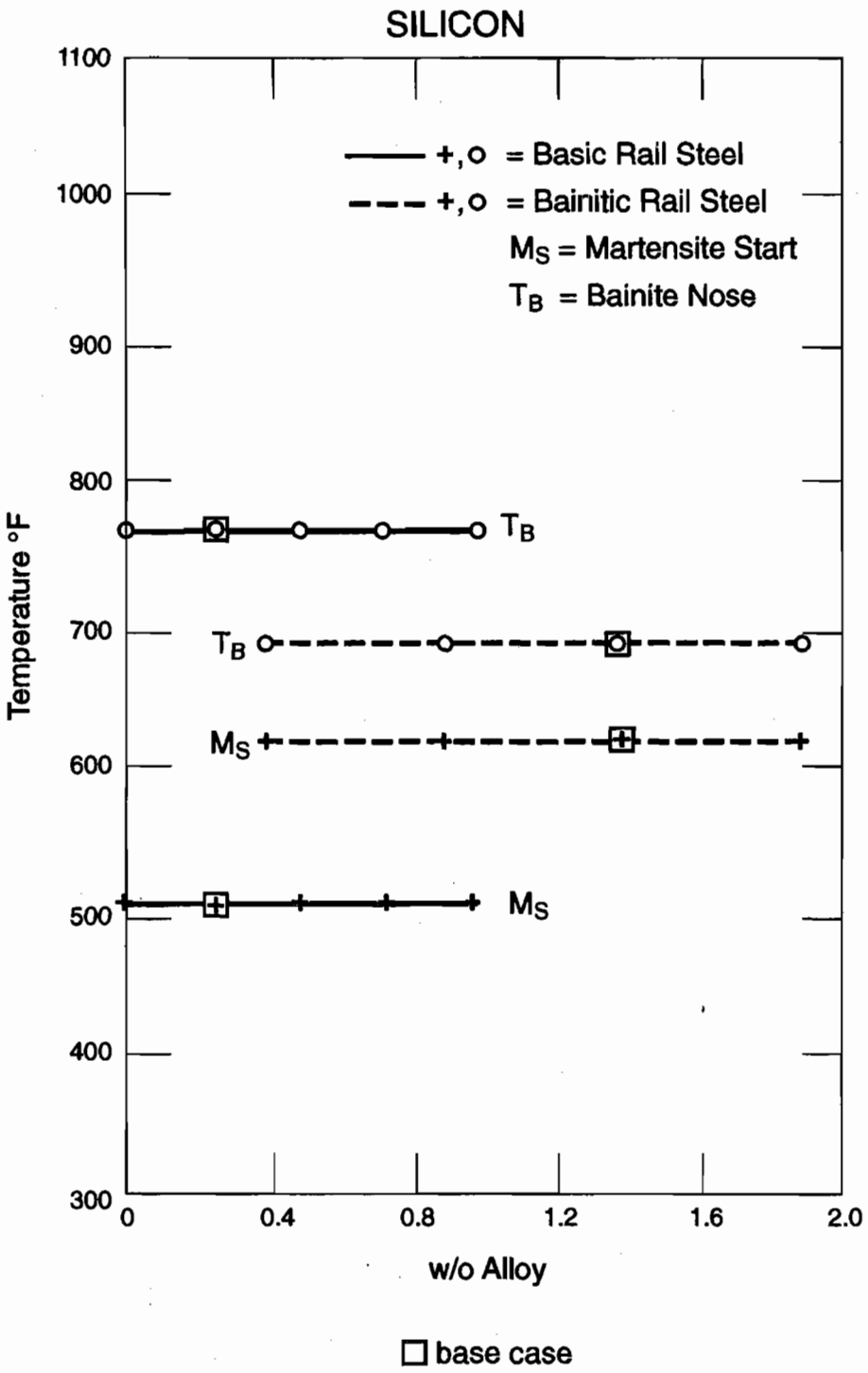

Figure 37. Effect of Silicon on the Martensite Start and Bainite Nose Temperatures

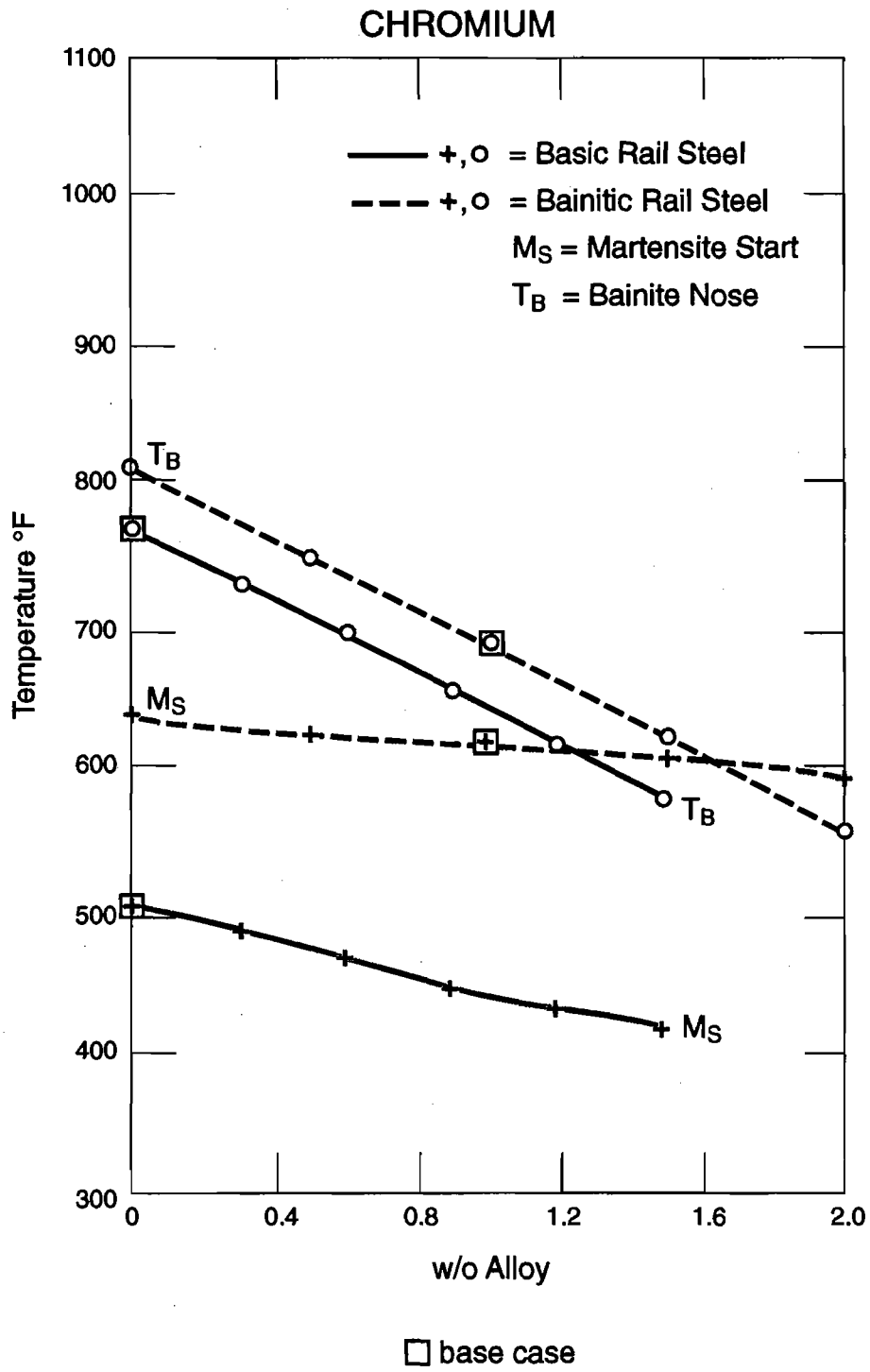

Figure 38. Effect of Chromium on the Martensite Start and Bainite Nose Temperatures

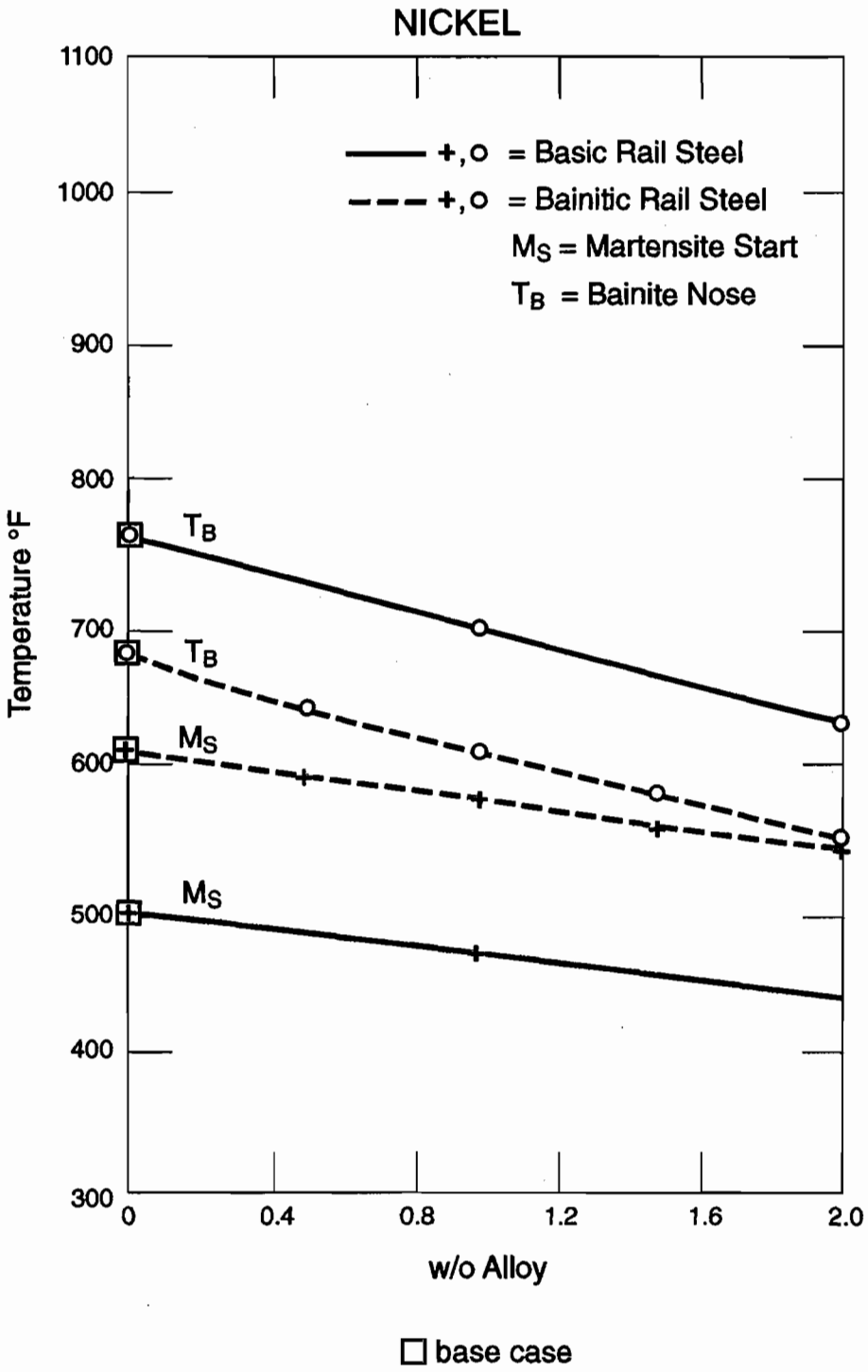

Figure 39. Effect of Nickel on the Martensite Start and Bainite Nose Temperatures

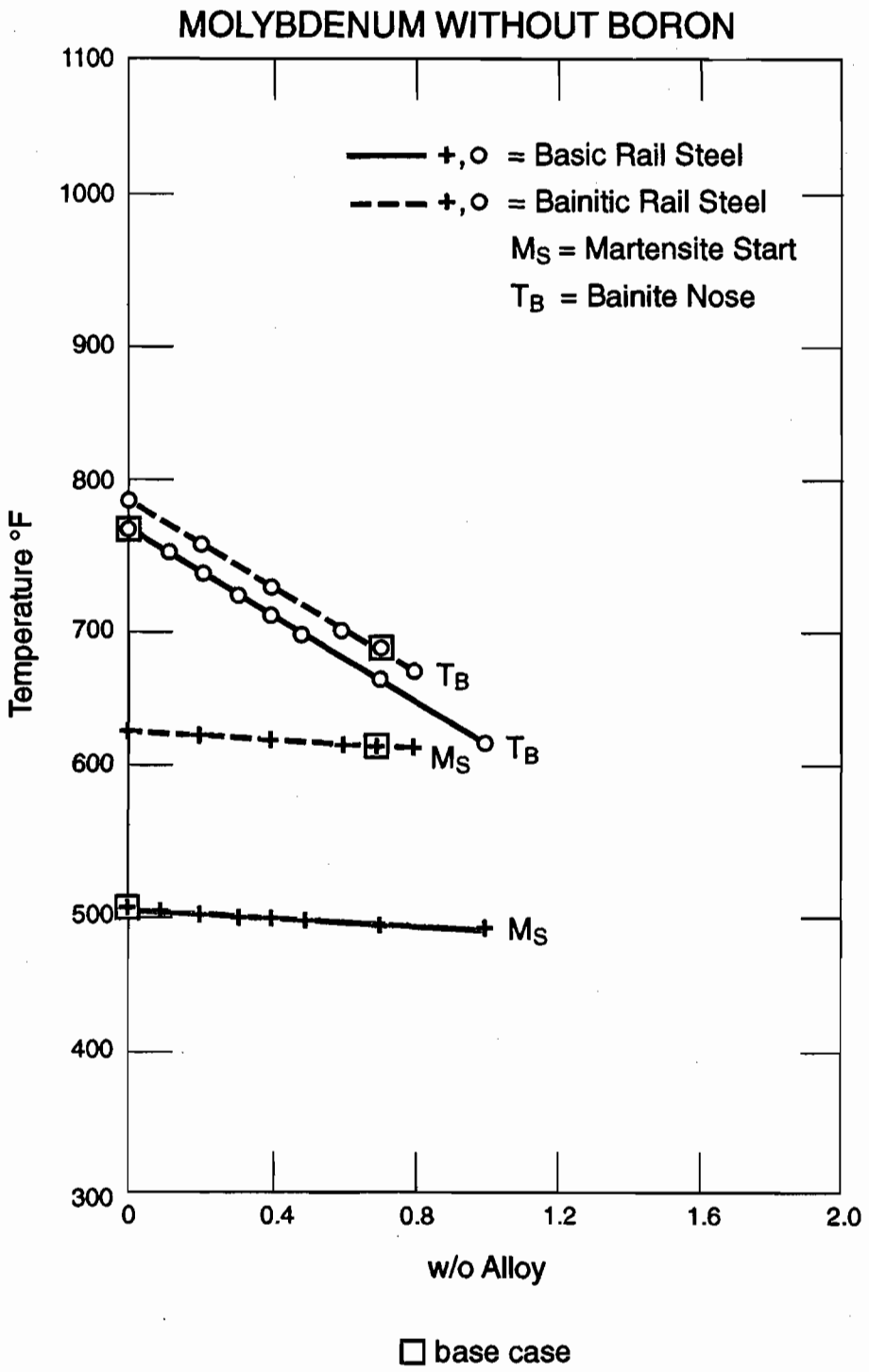

Figure 40. Effect of Molybdenum without Boron on the Martensite Start and Bainite Nose Temperatures

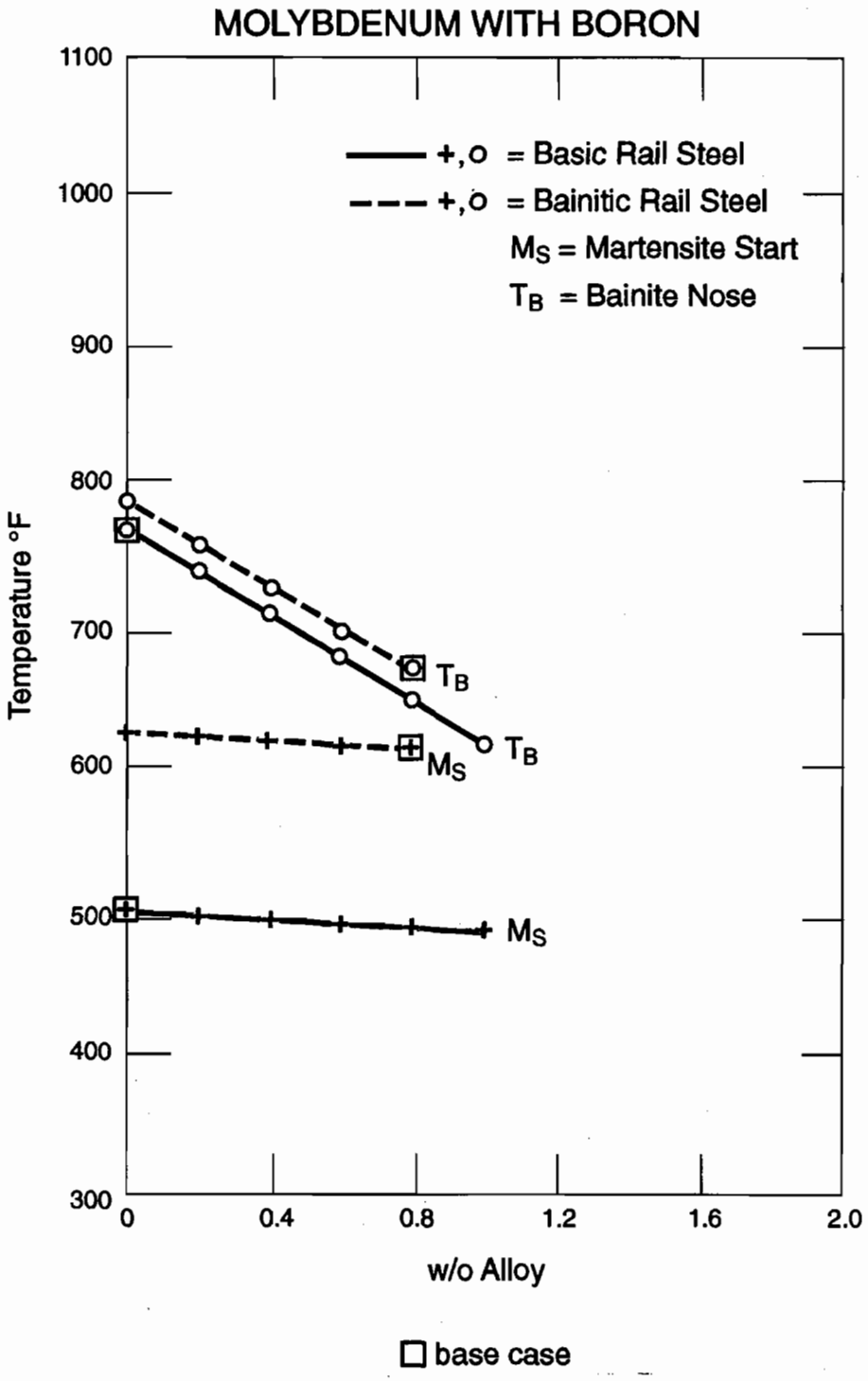

Figure 41. Effect of Molybdenum with Boron on the Martensite Start and Bainite Nose Temperatures

The de Boer et al., bainitic alloy differs from basic carbon rail steel in that it has lower carbon content and higher silicon, chromium, and molybdenum levels. Figures 30 and 37 suggest that the silicon level is not likely to have much effect on transformation characteristics. It would appear that molybdenum is present to cause a distinct bainite nose and the chromium is present to delay transformation of both pearlite and bainite. Increased silicon would be expected to stabilize untransformed austenite, delaying the precipitation of iron carbide from bainite containing regions of metastable austenite. Figure 42 illustrates how the transformation times and temperatures approach those of basic carbon rail steel as the amounts of chromium and molybdenum are reduced. The figure also shows the influence of boron in combination with molybdenum on the times to the pearlite and bainite noses. Boron has no effect upon the transformation temperatures – only the times. Figure 43 portrays the change in position and shape of the transformation diagrams. This exercise suggests that one could reduce the chromium and molybdenum by 25 percent, add boron[10] and still delay the pearlite reaction to the same degree that SteCal™ predicts for the de Boer et al. alloy; indeed the bainite nose time would be further retarded from 50 seconds to 75 seconds while the temperature difference between the bainite nose and the martensite start temperature would be increased from 87.8°F to 140°F (31°C to 60°C).

It is not necessary to decrease the chromium content with the molybdenum. This was done only to illustrate how the addition of those two elements (plus the reduction in carbon content) led from the basic rail steel alloy to the bainitic alloy. Further reductions in molybdenum content to 0.4 w/o are possible if the chromium is kept at 1.0 w/o. Indeed, if the manganese level is raised slightly (Cr held at 1.0 w/o), the pearlite and bainite transformations can be retarded further, albeit at the price of reduced temperature difference between the bainite nose temperature and the martensite start temperature. Some compensation for this can be achieved by reducing the chromium content. Table 5 contains some of these results.

This effort shows that the temperature difference between the bainite nose and the martensite start temperature can be increased to over 100°F (37.8°C) with the time at the bainite nose well over 1 minute, while the molybdenum content can be reduced to 0.4 w/o. To a large extent this has resulted from the use of boron in conjunction with the molybdenum. Probably further reductions in the molybdenum are possible, albeit with some sacrifice in the time at the bainite nose and nose-to-martensite start temperature difference.

Before moving on to discuss application of these concepts, it will be fruitful to take note that the de Boer et al., alloy is very close in composition to one of a series reported by Cias [24]. Copies of the CCT curves for this alloy series, taken from the ASM Atlas of Time-Temperature Diagrams for Irons and Steels[11] are portrayed on Figure 44. The primary composition difference with the de Boer et al., composition is the somewhat lower chromium content (0.72 w/o vs 1.1 w/o). The figures illustrate the effect of varying the molybdenum content. The effects are that as

[10] 0.003 w/o boron is considered to be a typical amount.
[11] G. F. VanderVoort, Editor, ASM International 1991.

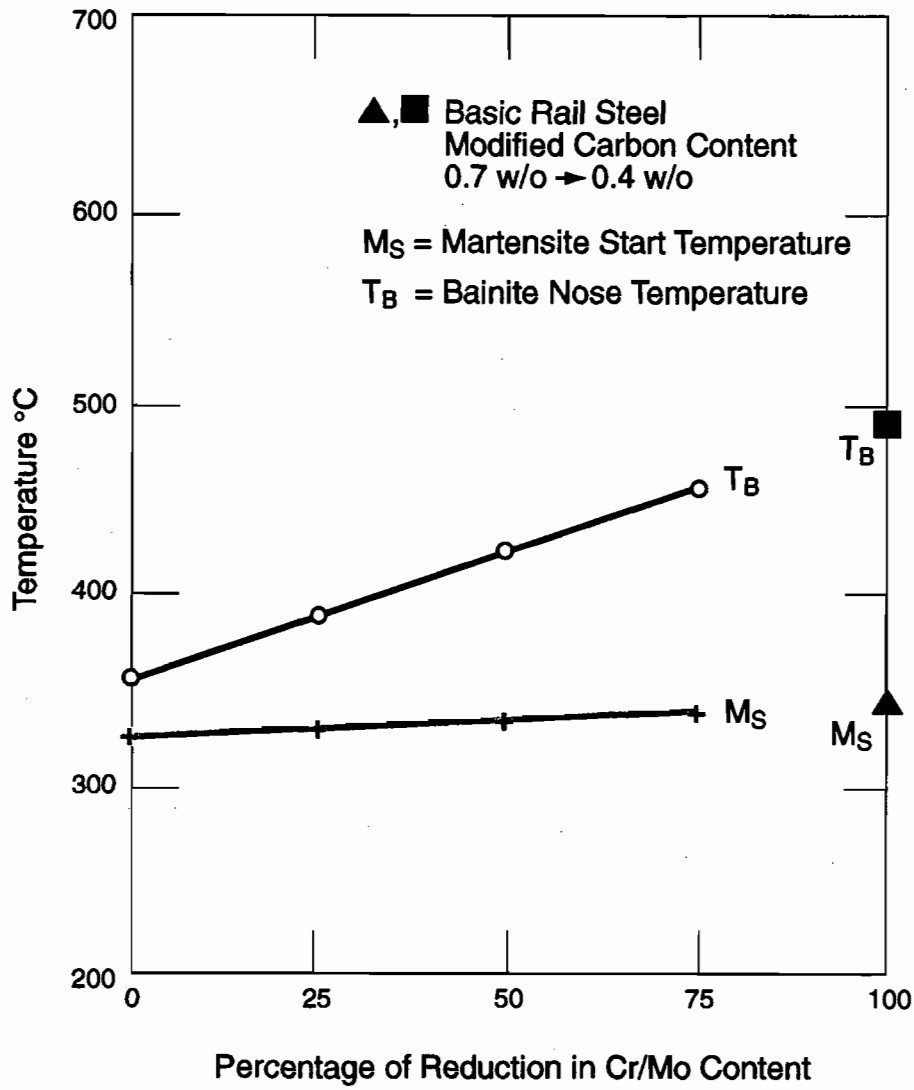

Figure 42a. Effect of Cr and Mo Reduction on the Martensite Start and Bainite Nose Temperatures

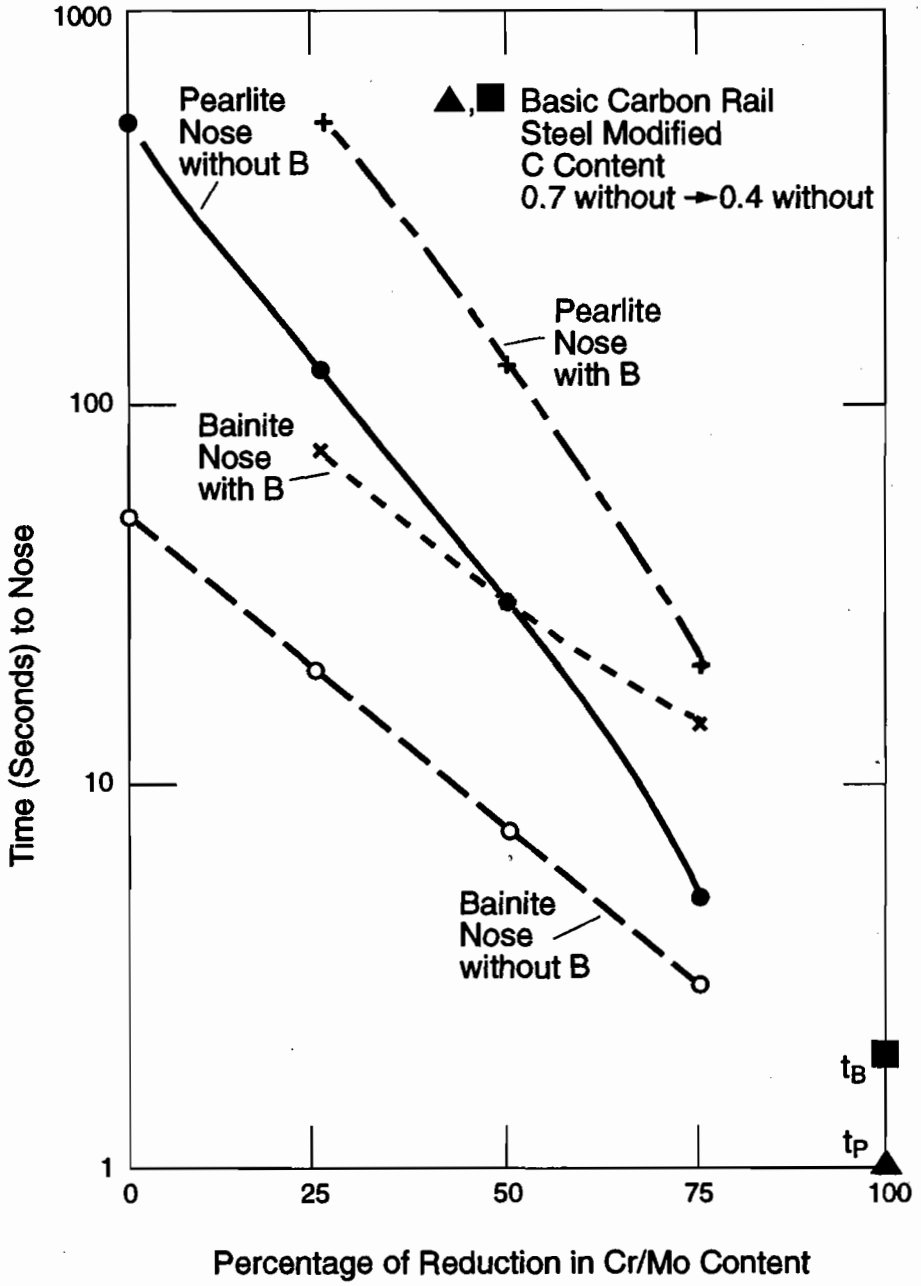

Figure 42b. Effect of Cr and Mo Reduction on the Times to the Pearlite and Bainite Noses

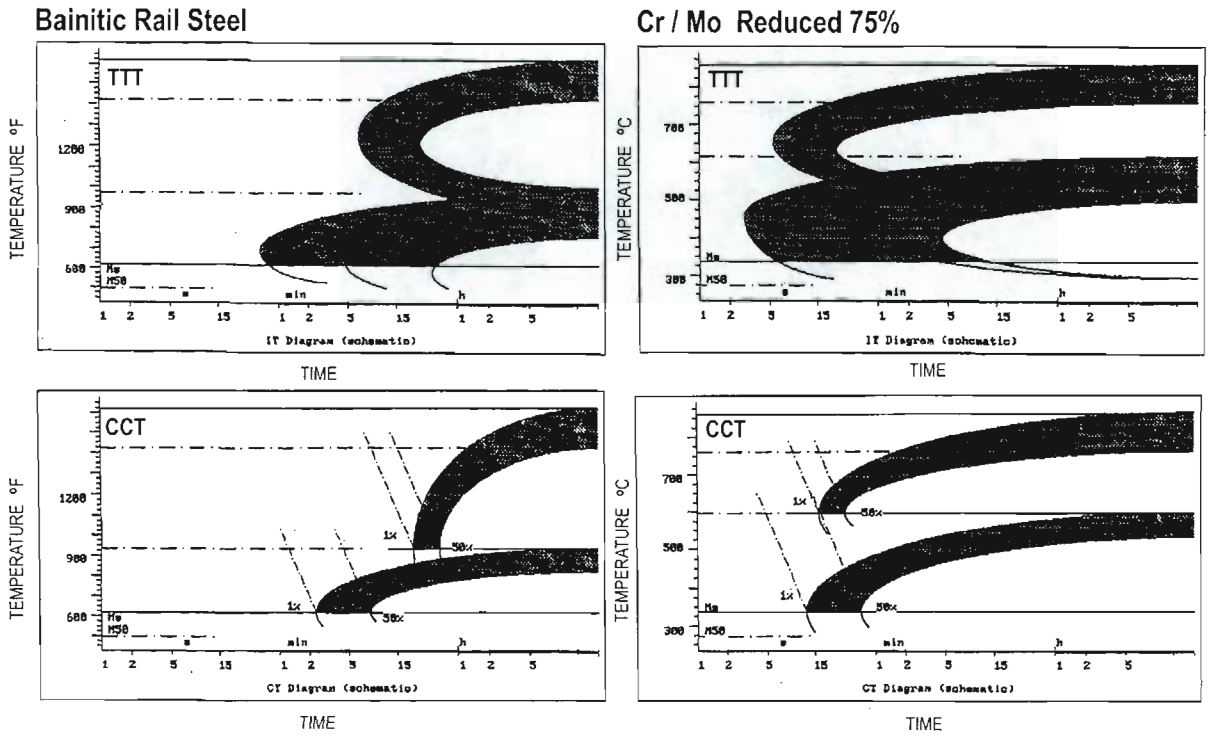

Figure 43. Changes in the TTT and CCT Curves with Cr and Mo Reduction

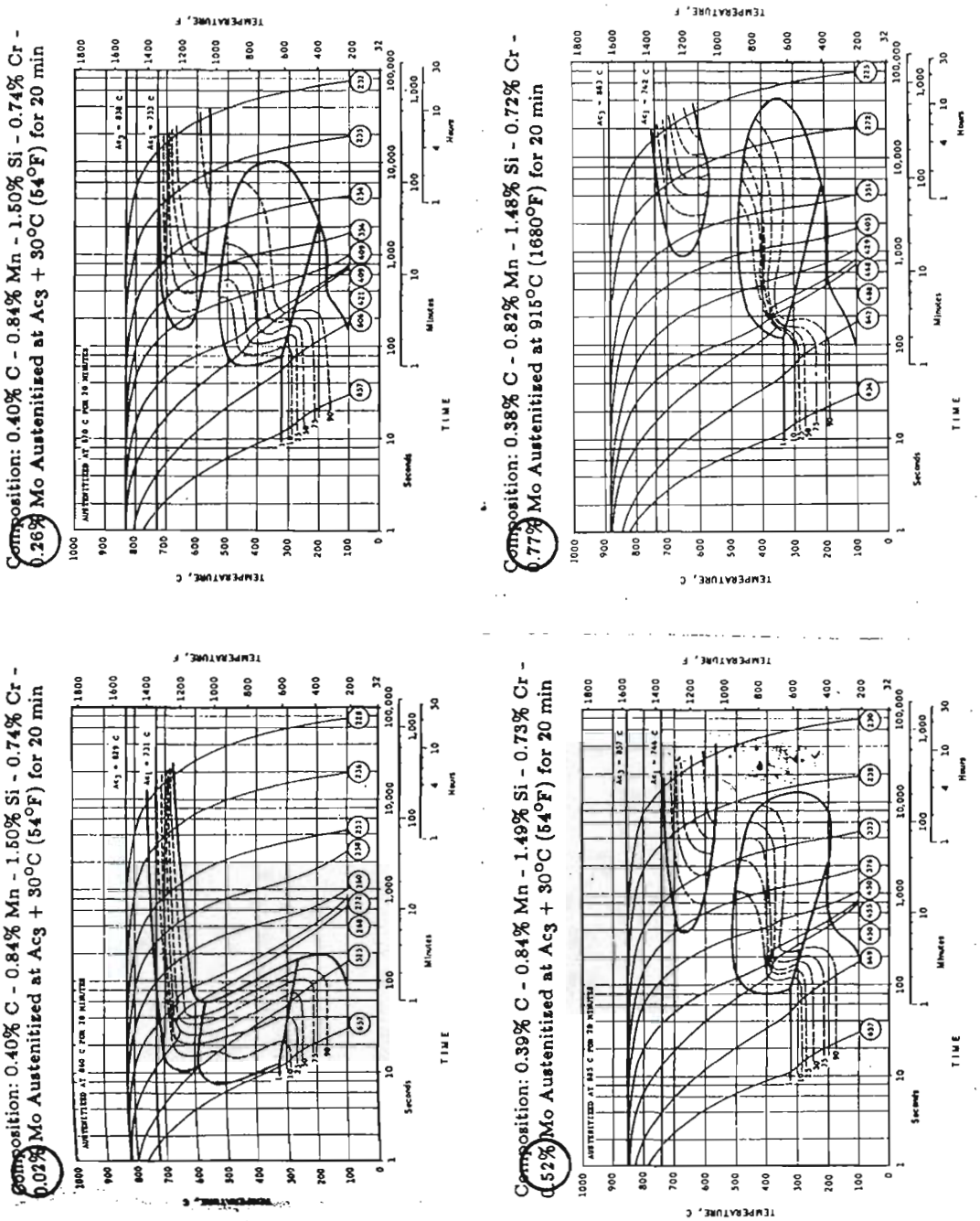

Figure 44. Experimentally Determined CCT Diagrams for Alloy Similar in Composition to de Boer et al. Alloy (Source: Cias, Ref. 24)

the molybdenum content decreases, (a) the bainite nose temperature increases (especially relative to the M_s temperature), (b) the time-to-start of bainite transformation decreases, and (c) the degree to which the pearlite nose lags behind the bainite nose diminishes. This behavior is in excellent qualitative agreement with the SteCal™ predictions. It also may be worth noting that the additional 0.4 w/o Cr in the de Boer et al. alloy would be expected to shift the pearlite nose back by about 150 percent (refer to Figure 31), which would put the nose at about 2,250 seconds. This suggests that perhaps there is a pearlite nose that could appear on Figure 9 above and back from the bainite transformation boundary. The figures show that lowering the molybdenum content from 0.77 w/o to 0.52 w/o could reduce the time-to-start of transformation at the bainite nose from about 120 seconds to 80 seconds (a factor of 33 percent) in good qualitative agreement with the SteCal™ prediction.

Table 5. Effects of Manganese and Chromium Variations on Key Transformation Parameters

Composition, w/o							Transformation Parameters						
C	**Mn**	**Si**	**Cr**	**Mo**	**B**		**M_s(°C)**	**T_P(°C)**	**T_B(°C)**	**Δ(°C)**	**t_P(s)**	**t_B(s)**	**t_P/t_B**
0.4	0.8	1.4	1.0	0.4	yes		327	670	387	60	360	70	5.14
0.4	0.9	1.4	1.0	0.4	yes		324	668	378	54	420	85	4.94
0.4	1.0	1.4	1.0	0.4	yes		321	667	369	48	480	120	4.0
0.4	1.0	1.4	0.8	0.4	yes		323	663	383	60	300	70	4.29
0.4	1.0	1.4	0.9	0.4	yes		322	665	376	54	420	85	4.94

T_P = Pearlite nose temperature; t_P = Pearlite nose time

T_B = Bainite nose temperature; t_B = Bainite nose time

$$\Delta = T_B - M_S$$

t_P/t_B = a measure of the effectiveness in suppressing the pearlite transformation relative to the bainite transformation

4. APPLICATIONS

In-line hardening to produce bainitic, most desirably lower bainitic microstructures, appears to be applicable to railroad rail, wheels, and tank car plate. To the extent that turnout and crossing frogs are manufactured from rail, they too may be able to benefit from this technological innovation. However, rails, wheels, and tank car plate have use limitations placed upon them that may limit the application of the in-line hardening process. For instance, rails and tank car plate must be welded after hardening whereas this is not a requirement for wheels. Rails may need to be roller straightened after rolling, and tank car plate must be formed into cylinders and end shells after hardening. Wheels, though not formed or welded after hardening, are subject in service to high rim temperatures resulting from braking action. These requirements do not directly limit the applicability of in-line hardening, but they do influence the suitability of alloys that might be selected to meet the need to have a bainitic or lower bainitic microstructure. This issue, as well as those of strength, toughness, and cost, will be discussed in the following sections.

4.1 RAIL

The exercise of SteCal™ has demonstrated that compositional modifications of a commercially available bainitic rail steel are theoretically possible to permit in-line heat treatment to achieve a lower bainitic microstructure. This is possible with reduced molybdenum content through the use of boron in small concentrations in the alloy. Nevertheless, the use of molybdenum is required to suppress the pearlite transformation and produce a distinct bainite nose on the transformation diagram. The cooling path for one of the potential alloys is portrayed in Figure 45. To just miss the bainite nose, the cooling rate[12] would need to be about 752°F (400°C) per minute. Lower cooling rates (down to 104°F (40°C) per minute) would yield bainite but not lower bainite. Below 104°F (40°C) per minute, the microstructure would be expected to be pearlitic in an isothermal transformation. Faster rates (than 752°F (400°C) per minute) would result in the formation of untempered martensite if the quench were not halted before 620.6°F (327°C), the martensite start temperature. Therefore, the in-line hardening process would need to be able to cool reproducibly at the indicated rate down to 716°F (380°C) (just below the bainite nose temperature), where after quench interruption would allow the surface temperature to rise sufficiently so that the metastable austenite would not immediately transform to bainite. The continuous cooling curve predicted for this alloy (also Figure 45) indicates that 50 percent of the transformation would be complete in about 10 minutes. The next 50 percent might take another 40 minutes, which suggests that in order to avoid martensite formation, the cooling rate should not exceed about 140°F (60°C) in 50 minutes, i.e., 34.2°F (1.2°C) per minute. It is not clear that this would be a natural cooling rate in air at this temperature (near 608°F (320°C)); Bramfitt [2] noted that the pearlite producing in-line method had a cooling rate during "isothermal" transformation of 113°F (45°C) per minute at temperatures near 1,112°F (600°C). Fortunately, the martensite start temperature usually drops during continuous cooling as illustrated in the de Boer et al., paper, which would suggest that cooling rates of 38.7°F (3.7°C) per minute would avoid martensite formation. One of the potential difficulties of attempting transformation so close to the martensite start temperature is the possibility that one may encounter martensite toward the end of the transformation if the temperature is not kept truly constant.

[12] All cooling rates referred to will be the average cooling rates in the temperature range from 800 to 500°C.

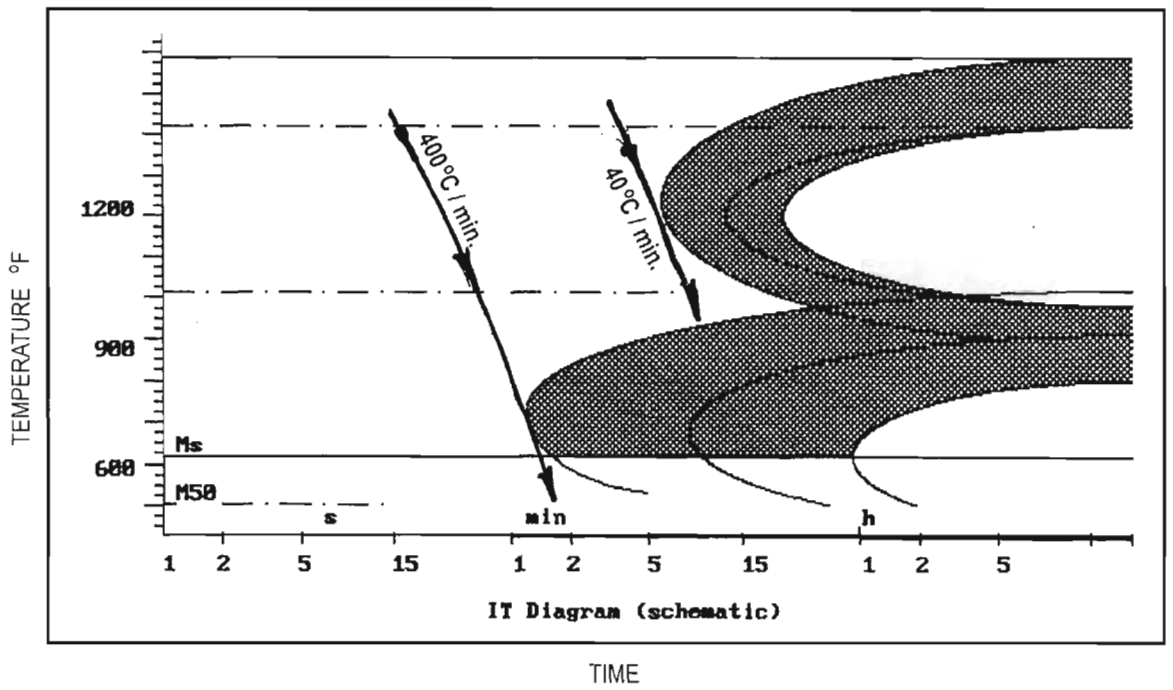

Figure 45. Critical Cooling Paths in the Modified Bainitic Rail Steel Composition

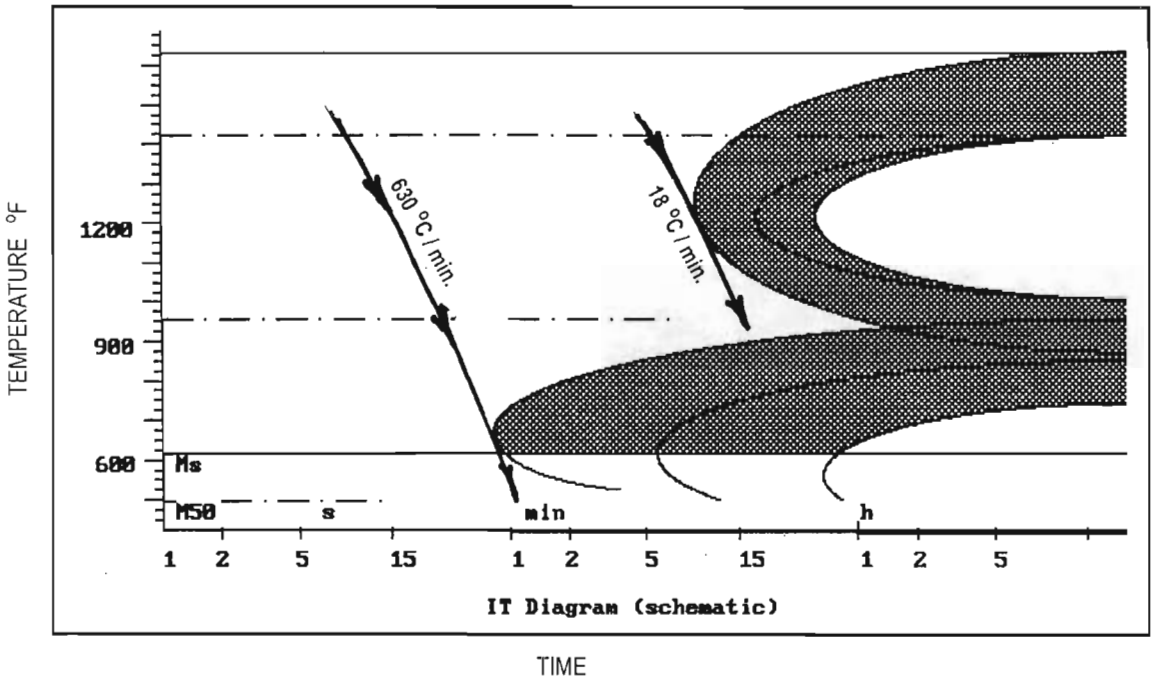

Figure 46. Critical Cooling Paths in the Unmodified Bainitic Rail Steel Composition

The situation for the de Boer et al. alloy with much higher molybdenum content is much the same (see Figure 46). The bainite nose is somewhat to the left (shorter time) of that on Figure 45 for the lower molybdenum alloy, so the cooling rate to just miss the bainite nose is greater, i.e., about 1,166°F (630°C) per minute. But the predicted pearlite nose is somewhat more to the right (longer times) so the minimum cooling rate to achieve a fully bainitic microstructure also is lower, i.e., about 64.4°F (18°C) per minute. This figure can be compared to that calculated from the expression developed by Comon et al. [20] given earlier in the text. The calculated minimum cooling rate for the de Boer et al. alloy (0.4 w/o C, 0.8 w/o Mn, 1.4 w/o Si, 1.0 w/o Cr, 0.8 w/o Mo.) works out to be about 42.8°F (6°C) per minute, which represents good agreement.

There is a large difference in the times for complete transformation between the bainitic alloys and the more conventional pearlitic rail steel composition. The transformation diagram of the de Boer et al. paper (Figure 9) shows that to complete the bainite transformation, without martensite occurrence, requires about 35 minutes. The SteCal™ prediction (isothermal diagram, Figure 45) for the same composition suggests about the same time. But, Bramfitt's paper [2] shows that the pearlite transformation takes only a few minutes for completion. The difference between a few minutes and 30 - 40 minutes could make a very large difference in the economics of the process. If the overall bainite transformation time (start to finish), needed to be shortened, the nose of the bainite transformation probably would need to be shifted to shorter times, i.e., lower alloy additions. But doing so would increase the quenching rate needed, probably to well over

1,112°F (600°C) per minute. In addition, the chance of forming pearlite or a mixed pearlitic/bainitic microstructure upon welding would increase.

At this point it is appropriate to take brief note of the possible effects of rail welding. Typically, the average cooling rate (in the range of 1,472°F to 932°F (800°C to 500°C)) following electric flash butt welding is 33.8-35.6°F (1-2°C) per second (140°-248°F (60°-120°C per minute)). Reference to Figure 45 indicates that normal cooling should avoid a pearlitic microstructure; the microstructure in the heat-affected zones will not be lower bainite, but rather, it will be upper bainite. Thermite welding can involve slower cooling rates than 33.8°-35.6°F per second. It seems that partially pearlitic microstructures might be possible. The de Boer et al. reference [10] indicates that thermite welds have been made satisfactorily with a short preheat (1 minute) practice, using the high molybdenum alloy. Longitudinal hardness traverses made on both electric flash butt and thermite welds are shown on Figure 47. The boundaries of the heat-affected zones have hardnesses of about 340 HV (320 BHN), which suggests the possibility of a tempered bainitic structure. It is not entirely clear what the microstructure would be between 340 HV and 450 HV.

The potential tensile strength of the modified lower molybdenum alloy can be calculated from the expression suggested by Irvine and Pickering [19] and by the expression derived by de Boer et al. [10]. By the expression of Irvine and Pickering, the ultimate tensile strength of the lower molybdenum alloy is predicted to be 196 ksi, which is equivalent to a hardness of 393 BHN. By the de Boer et al. expression, the predicted ultimate tensile strength is 175 ksi, which is the equivalent of only 362 BHN. The low molybdenum alloy could be strengthened somewhat by increasing the carbon level to 0.5 w/o and adding 0.1 w/o vanadium. The Irvine/Pickering expression then would predict an ultimate tensile strength of 226 ksi (435 BHN). The additional carbon and vanadium content will somewhat modify the transformation characteristics by delaying the start of the bainite transformation to 2 minutes and lowering the bainite nose temperature to 649°F (343°C) and the martensite start temperature to 548.6°F (287°C). This reduces the temperature range in which lower bainite can be formed to 132.8°F (56°C), as opposed to 140°F (60°C) for the original lower molybdenum alloy.

This author suspects that the Irvine/Pickering and de Boer et al. expressions do not correctly assess the strength if lower bainite is the transformation product. This is reflected in the work of Clayton and Devanathan [9] where, for a commercially available chromium-molybdenum rail steel, they produced upper and lower bainitic microstructures of significantly different hardnesses (472 and 535 BHN respectively). The calculated ultimate tensile strengths and hardnesses for the commercially available chromium-molybdenum alloy are as follows:

de Boer et al.	182 ksi	(372 BHN)
Irvine/Pickering	259 ksi	(484 BHN)

The Irvine/Pickering expression comes very close to predicting the observed hardness (by conversion from the ultimate tensile strength) for upper bainite. Apparently no transformation diagrams are available for this commercially available chromium-molybdenum rail steel; SteCal™ predicts the diagrams shown on Figure 48. The Clayton/Devanathan work found that the maximum hardnesses occurred at transformation temperatures near 500°F (260°C). Figure

48 suggests that this is entirely reasonable; the bainite nose temperature is predicted to be 647°F (341.7°C).

With in-line hardening, the intent is to produce a stronger, tougher microstructure in the head of the rail. An issue that has not been addressed is what should be the microstructure of the web and base of the rail. It is not clear whether the web and base should be bainitic or pearlitic. A bainitic web and base would strengthen the rail as a whole, perhaps to the extent that it would be difficult to roller straighten (this may be a problem with the de Boer et al. rail). But, it is unlikely that alloy compositions that separate (timewise) the bainite and pearlite noses as much as the de Boer et al. alloy will allow pearlite to form in the web and base. Yet, if the timewise separation is caused to be less (reduce the molybdenum content and/or eliminate the boron), then normal cooling during conventional electric flash butt welding and thermite welding could yield pearlitic or mixed pearlitic/bainitic microstructures in the rail-head. This probably is not desirable. Welding techniques could be modified to allow shorter preheats which would increase cooling rates (less chance of pearlite formation). In any event, depending upon what microstructure is required in the web and base, the alloy composition may have to be more fully tailored than has been done in this exercise in order to balance the conflicting needs of head vs web/base vs weld microstructure. If a pearlitic web/base were desired, a composite rail having different head and web/base chemical compositions would presumably meet that need.

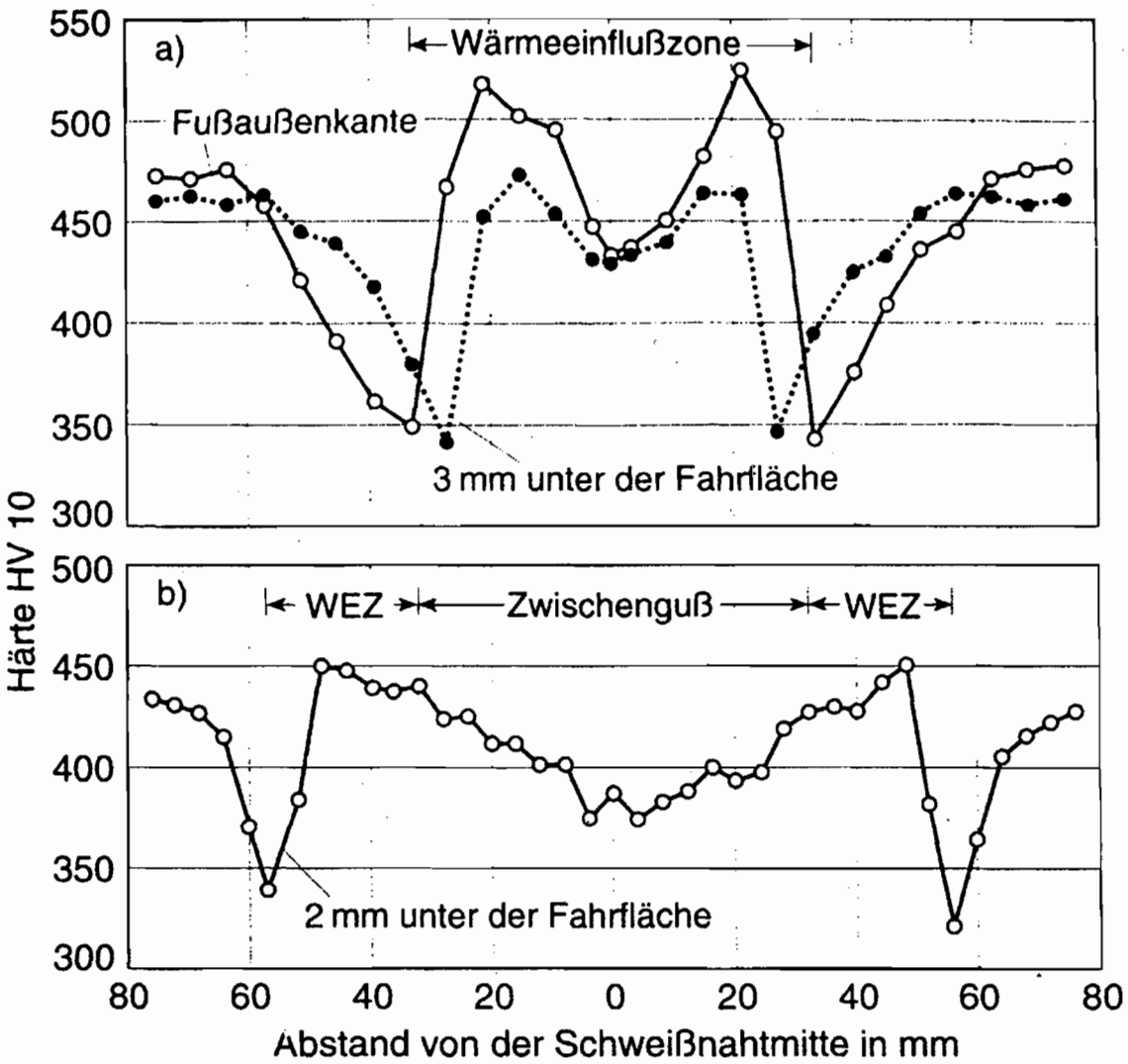

Figure 47. Hardness Traverses of Electric Flash Butt and Thermite Welds (Source: de Boer et al., Ref. 10)

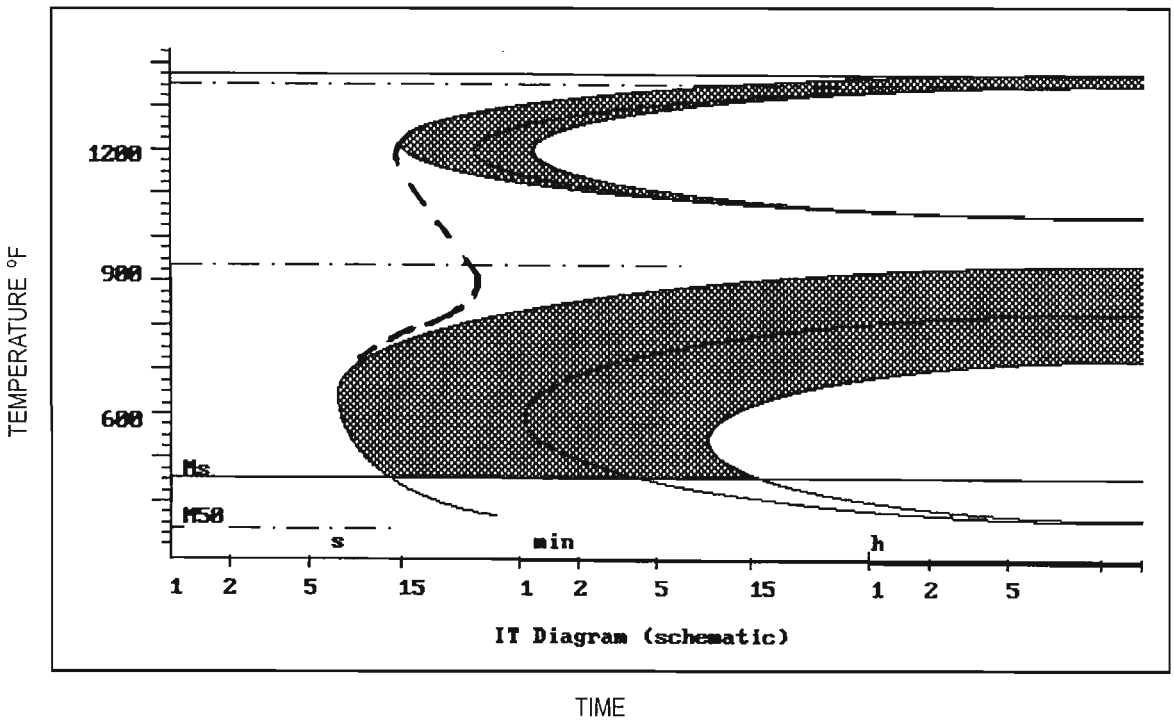

Figure 48. SteCal™ Prediction of the TTT Diagram for a Commercial CrMo Rail Steel

4.2 WHEELS

Wheels generally have chemical compositions and mechanical properties very similar to those of rail steels. However, there is one significant difference in their performance requirements: wheels are expected to experience very elevated tread surface temperatures due to emergency and drag tread brake application. To the extent that tread temperatures exceed 1,292°F (700°C),[13] there is the possibility that the tread surface could be resolutionized to austenite. Except in very long drag braking periods where the rim and outer portion of the plate may be heated enough to slow rim cooling, there appears to be the possibility that the resolutionized rim surface might be chilled rapidly enough to avoid any bainite nose and form martensite upon cooling. Alloy compositions that promote bainite nose occurrence and shift the pearlite nose to much longer times will be especially prone to martensite formation upon chill cooling to room temperature. It may well be that any composition that allows lower baintite to be formed (under a pearlite nose) by in-line hardening processes cannot be used in wheels that could undergo sufficient tread heating to resolutionize the metal.

However, perhaps an upper bainite rim could be produced by a modified in-line quenching practice, which sought to continuously cool the wheel rim. The alloy needed to work with such a process most probably would still need to have molybdenum (and boron) present. This would allow (upper) bainite to be the preferred transformation product. However, the bainite nose would need to extend (leftward on the transformation diagram) to such short times that even under chill quenching conditions the bainite nose would act to shield the alloy from the martensite transformation. This implies rather low carbon contents with sufficient alloying additions to achieve the needed strength. This author thinks that alloys to meet these requirements currently are under development for turnout and crossing frog applications at the Oregon Graduate Institute under the direction of P. Clayton [25]. These alloys can contain substantial manganese (2 w/o), silicon (1.8 w/o), chromium (1.9 w/o), and nickel (up to 2 w/o) as well as 0.5 w/o molybdenum with boron. The carbon content is near 0.25 w/o. B_s values in the range of 824° to 1,013°F (440° to 545°C) have been reported for cooling rates as high as 77°F (25°C) per second (2,732°F (1500°C per minute)).

Some of the alloy additions are costly. Perhaps leaner concentrations of the expensive alloy additions could be found that would still allow improved wheel hardness and toughness (the low carbon alloys tend to be tougher than the high carbon alloys), yet still allow the bainite nose to shield against transformation to martensite under chill quenching conditions. Indeed, a low carbon, 1.4 w/o nickel molybdenum-boron alloy of more modest silicon, manganese, and chromium has been reported by Cias [24]. The CCT diagram is shown on Figure 49. It exhibits a very extended bainite shelf (10 seconds to 18,000 seconds) at almost constant temperature (500°C ± 5°C) over a range of cooling rates from 1100°C/minute to 1°C/minute.

[13] 1,022°F (550°C) is more likely to be a maximum temperature in severe brake application situations, but 1,292°F (700°C) might be encountered under conditions where the brakes could be locked up.

4.3 TANK CAR PLATE

TC - 128 is a steel, the mechanical properties of which are considered desirable for tank car shell usage. It is a low-carbon, modest manganese steel having some small additions of molybdenum and vanadium along with a bit of chromium and nickel. Its yield and tensile strengths are about 50 - 60 ksi and 80 - 100 ksi respectively in the normalized condition. The impact toughnesses and energies and transition temperature [26] are listed below.

Charpy energy, lower shelf	3 ft lb
Charpy energy, upper shelf	55 ft lb
Lower shelf toughness, K_{Id}	21 ksi$\sqrt{in}$
Upper shelf toughness, K_{Id}	91 ksi$\sqrt{in}$
Transition temperature	- 30°F

The Irvine/Pickering expression estimates the ultimate tensile strength of the upper bound chemical composition to be 156 ksi, were the microstructure to be bainitic rather than normalized (pearlitic). This value is considerably above the maximum of 100 ksi in the normalized condition and suggests that were it possible to achieve a bainitic structure with this alloy, considerable improvements in strength could result.

SteCal™ has been used to estimate the transformation diagrams at the upper compositional limits (see Figure 50). The presence of a small amount of molybdenum and vanadium have produced a distinct bainite nose, but it does not extend very far to the left of the pearlite nose and the time to the isothermal nose is very short, i.e., 3 seconds. Exercise of SteCal™ suggests that one need only double the effective molybdenum content (w/o Mo + 2 x w/o V) and add boron (0.003 w/o) to move the bainite nose back to about 50 seconds (Figure 51). However, doing so decreases the temperature difference between the bainite nose and the martensite start temperature from 94°F down to 61°F. This makes the achievement of a lower bainite transformation more problematic.

However, by some adjustment of the manganese content downward from 1.35 w/o to 1 w/o, the bainite nose/martensite start temperature difference can be increased to 107°F (41.7°C), albeit with the bainite nose time reduced to 20-25 seconds. This is illustrated in Figure 52. Considering that the thickness of tank car plate is likely to be much less than the height of a rail-head (or a wheel rim thickness), perhaps shorter times to the bainite nose may be entirely acceptable. Indeed, some further small reductions in manganese, chromium, and nickel might be allowable.

A question that needs to be answered before an alloy design analysis proceeds further is whether a lower bainitic tank car plate can be formed readily without problems due to its potentially greater strength. Similarly, the welding cooling rates need to be well defined in order to establish to what extent the pearlite transformation needs to be delayed.

Composition: 0.11% C - 0.85% Mn - 0.38% Si - 1.42% Ni - 0.76% Cr - 0.005% B - 0.54% Mo Austenitized at Ac_3 + 30°C (54°F) for 12 min

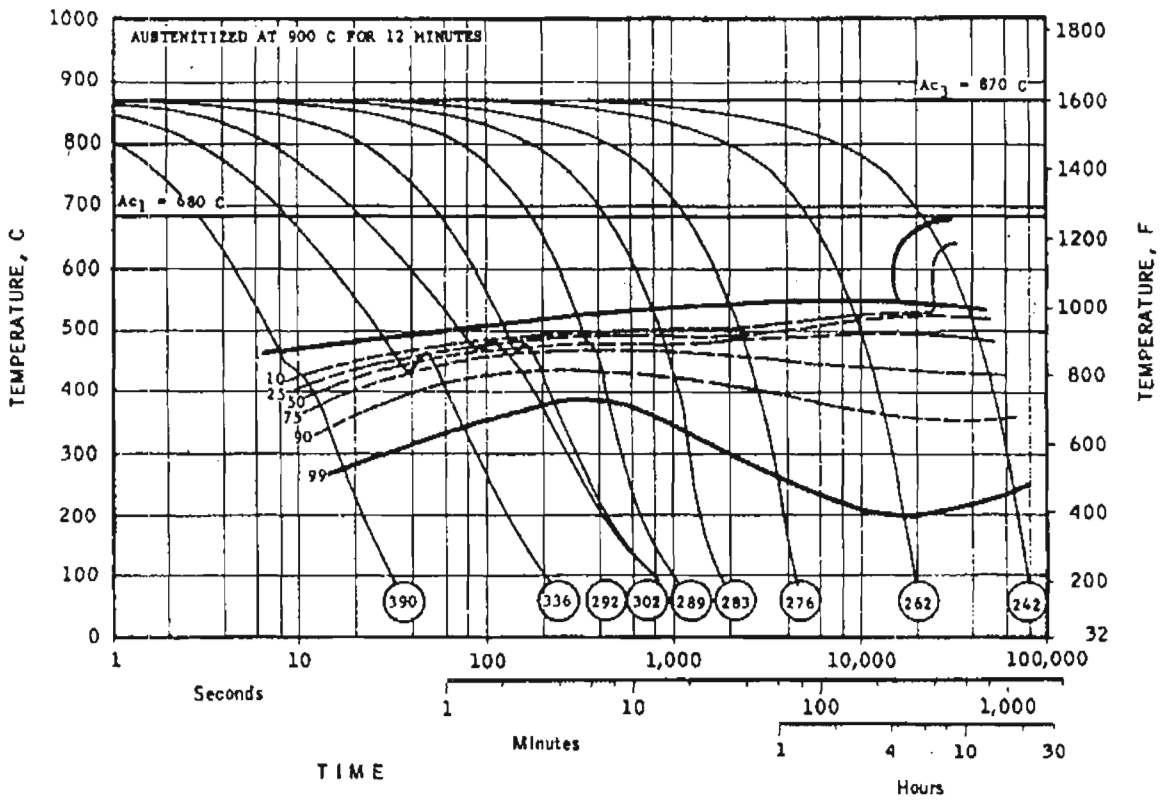

Figure 49. Experimentally Determined CCT Diagram for a Low Carbon, 1.4 w/o Nickel Alloy Similar to Those Studied at OGI (Source: Cias, Ref. 24)

5. CONCLUSIONS

The analysis described in the previous sections shows that there are measures that can be taken to make it possible to produce in-line hardened rails, wheels, and tank car plate that have lower bainitic microstructures. These measures rely strongly on control of the molybdenum and boron contents of the steels. Some questions remain to be answered such as what should the web microstructure of rails be (and perhaps by inference, the plate microstructure of wheels), and whether fully (lower) bainitic hot-formed products can be subsequently roll-formed (plate) and roller-straightened (rail).

The challenge for a lower bainite in-line hardening process is to cool rapidly and reproducibly to temperatures well below those needed for pearlite transformation. In doing so the process must avoid martensite formation during the initial interrupted quench and during the subsequent quasi-isothermal bainite transformation. This is likely to present a challenge for welding practices. Steels having such high alloy contents as those described above are likely to retain small amounts of austenite after transformation. Under high rolling contact pressures, it is possible that cyclic plastic deformation may induce some of this retained austenite to transform at room temperature to untempered martensite. This has been observed to occur in roller bearing steels (52100) with possible beneficial effects on residual stresses (by encouraging the development of compressive residual stresses). The fact that many of the alloy additions lower the martensite start temperature is a disadvantage, in that quench cracking would be promoted were some martensite transformation to occur. However, quench cracking can be minimized by ensuring that the transformation is to bainite rather than to martensite, most especially under conditions approaching isothermal transformation.

The issue of alloying costs has not thus far been considered. So, before ending this work, some idea of relative cost of alloying[14] can be obtained from the somewhat outdated (1968) costs [27] shown in Figure 53. Though the dollar figures are no longer realistic, the relative rankings for different alloy additions would still be expected to be appropriate. If comparisons are made to manganese, which is about the least expensive addition, nickel, molybdenum, and zirconium can be seen to be the most expensive - up to four to eight times for molybdenum and up to sixteen to twenty times for nickel - for a unit of hardenability. Boron is comparable to manganese. Silicon and chromium are perhaps two to three times more expensive. Therefore, while considerable variation in the transformation characteristics of steels can be had by alloy addition, the cost can be high. It is for this reason that modestly low molybdenum additions with boron have become attractive.

Finally, words of caution need to be repeated with regard to the use of SteCal™ in this work. It is this author's view that SteCal™ provides a fair semiquantitative assessment of the effects of alloying additions on transformation behavior, and therefore, helps point in the direction that any alloy development effort should take. But, it does not necessarily define key temperatures and times with sufficient accuracy to establish alloy compositions with the certainty needed to step directly into a production development program.

[14] The costs are given as $ per Grossman unit. The Grossman unit cost is the $ per cwt divided by the value of the hardenability multiplier of the alloy addition.

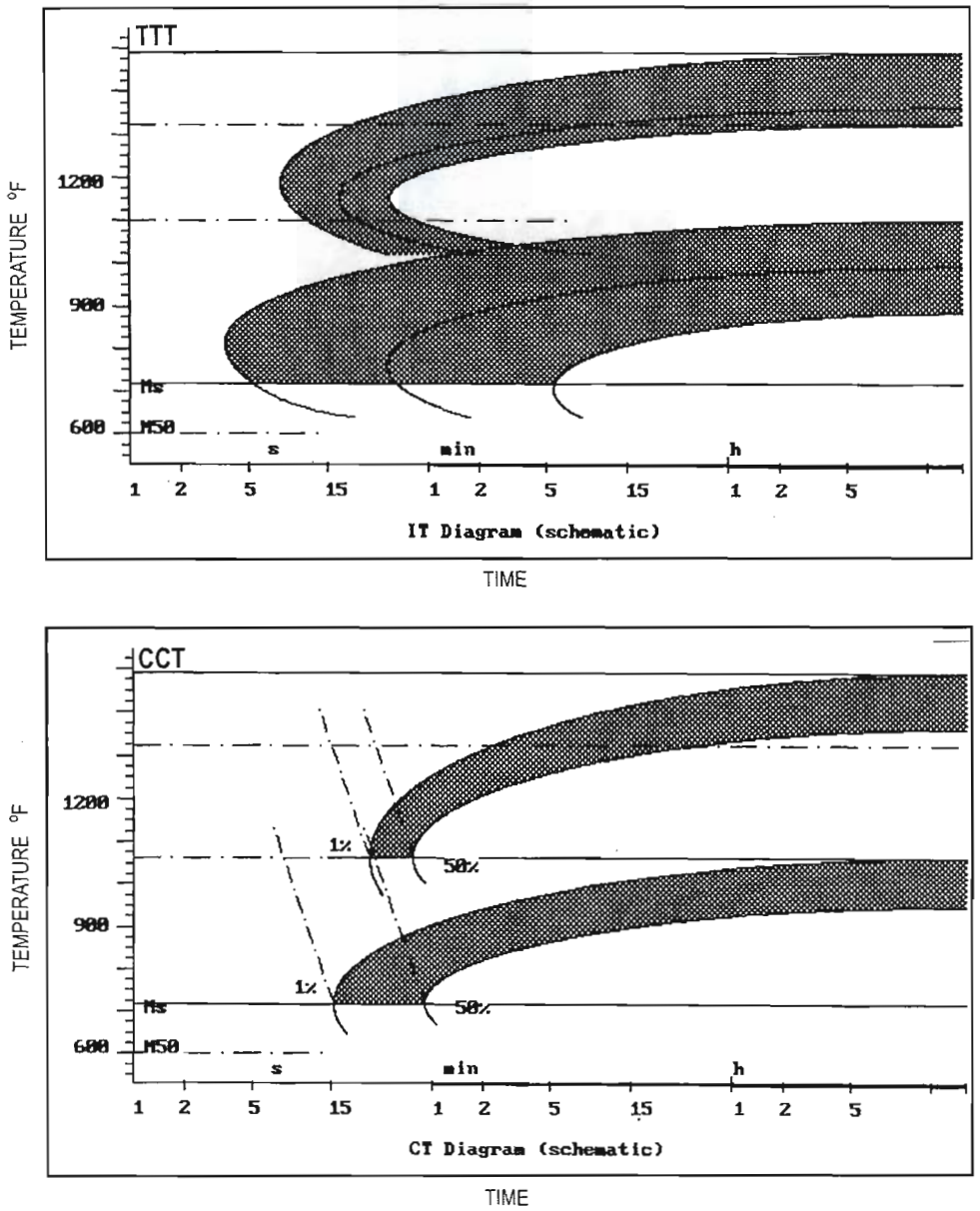

Figure 50. SteCal™ Prediction of the TC 128 TTT and CCT Diagrams

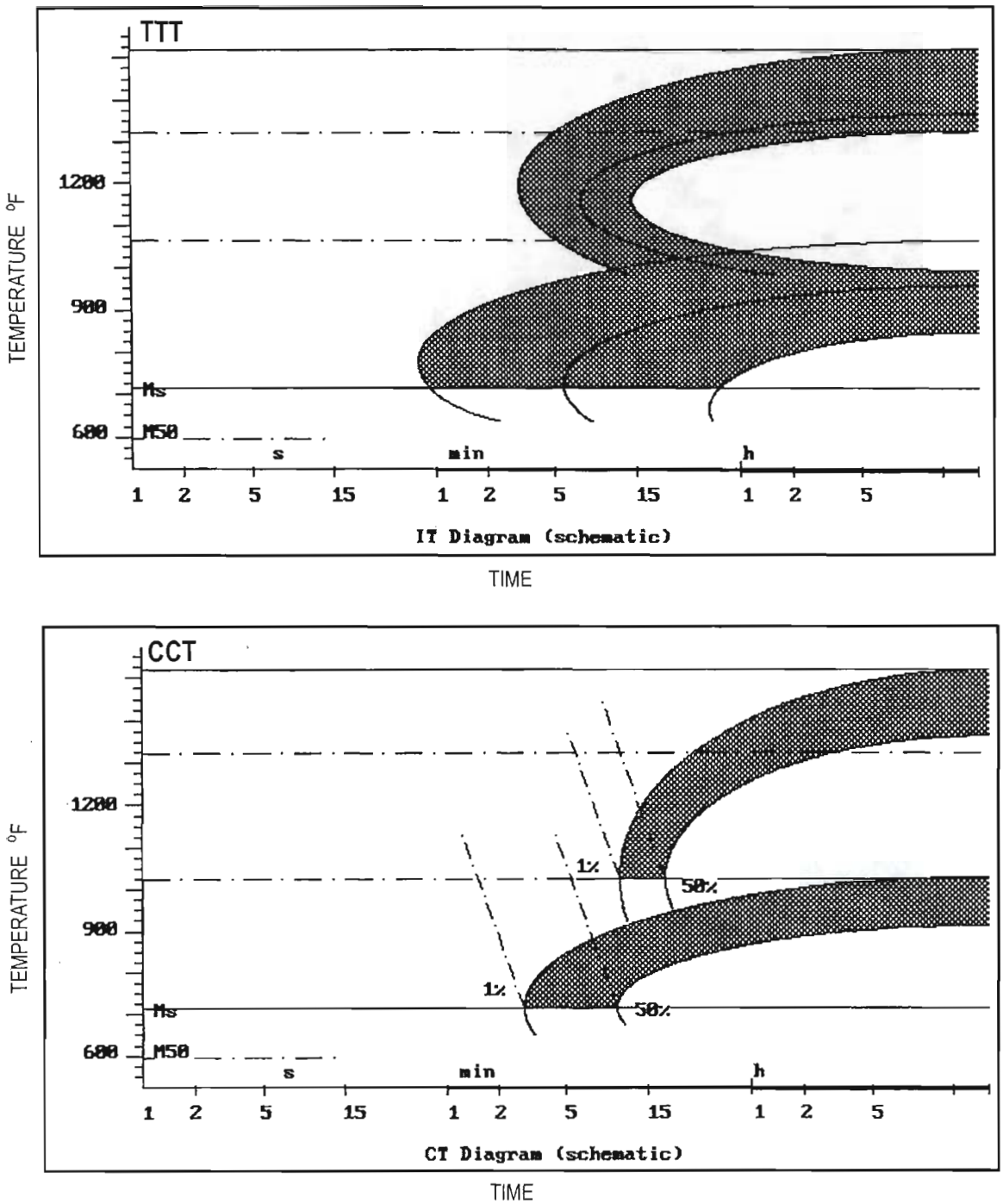

Figure 51. SteCal™ Prediction of the TTT and CCT Diagrams for TC 128 having increased Mo with B

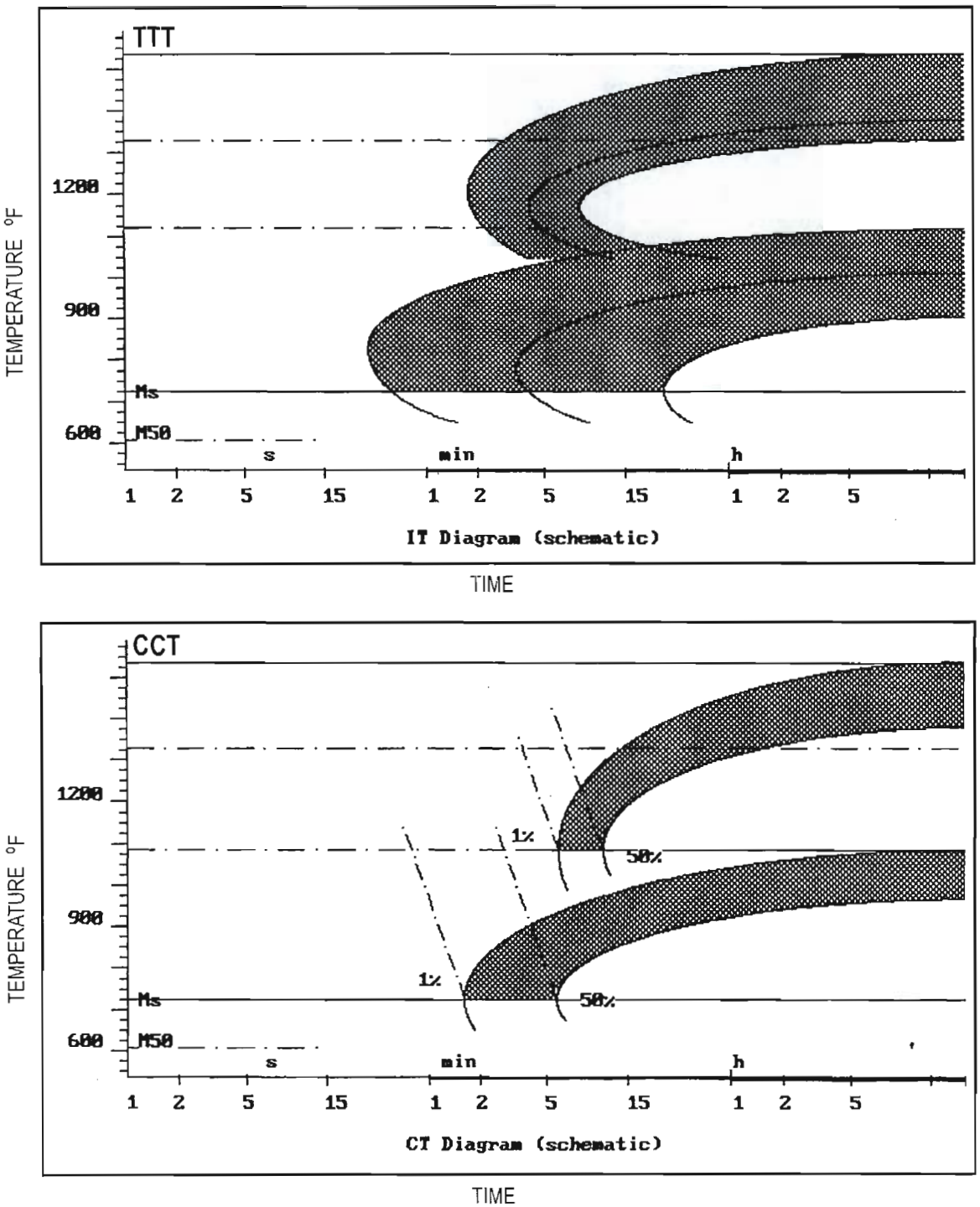

Figure 52. SteCal™ Prediction of the Effect of Lowering Manganese Content in the Modified TC 128 Alloy

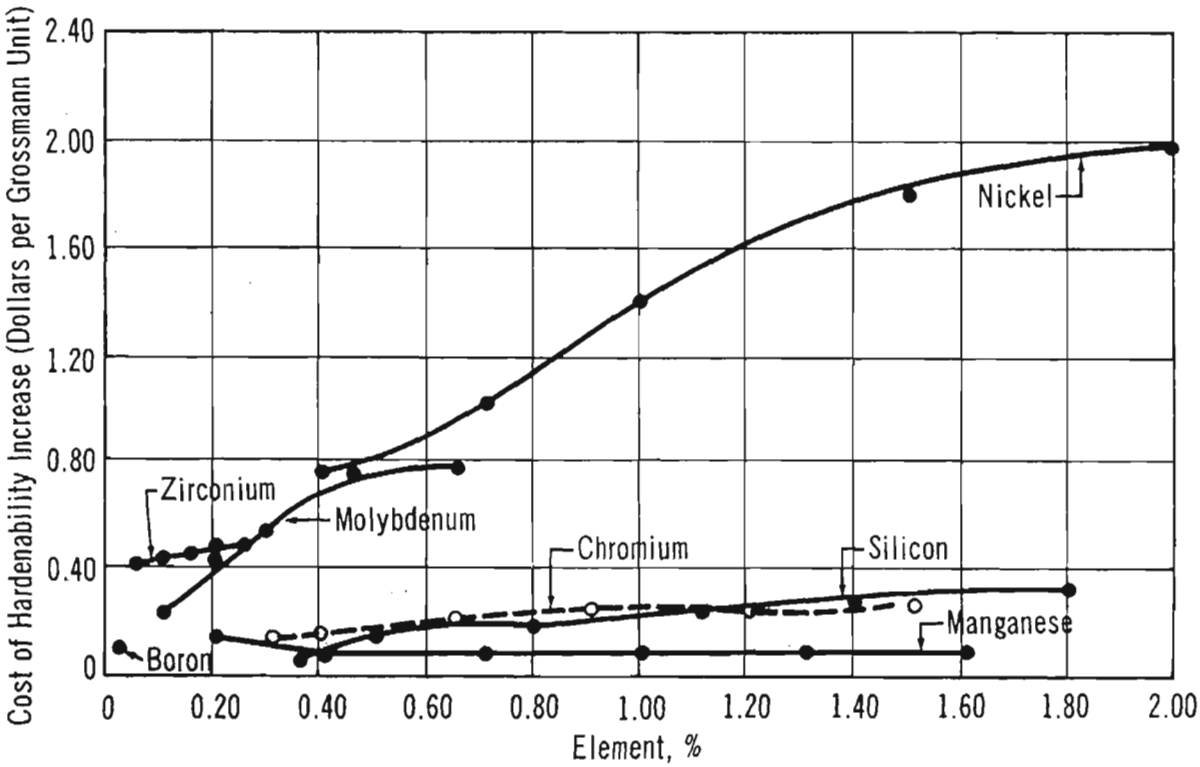

Figure 53. Cost of Hardenability Increases (Source: Kern, Ref. 26)

REFERENCES

1. U.S. Patent 3,846,183, "Method of Treating Steel Rail", 5 November 1974.

2. Bramfitt, B.L., I&SM, June 1991, pp 33-41.

3. Bramfitt, B.L., R.L. Cross, and D.P. Wirick, I&SM, January 1995, pp 17-21.

4. Bramfitt, B.L., D.P. Wirick,, and R.O. Cross, Steel Engineer, June 1996.

5. Economopoulos, M., N. Lambert, P. Simon, and R. Conti, ISS, vol 28, 1990, pp 143-152.

6. Conti, R., J. Dahm, R. Paring, and E. Trausch, ISS, Vol. 28, 1990, pp 153-168.

7. Kennon, N.F., Met Trans, Vol. 9A, 1978, pp 57-66.

8. Kalousek, J., D.M. Fegredo, and E.E. Laufer, Proc Int'l Conf on Wear of Materials, pp 212-231, K.C. Ludema (Ed), Vancouver, 14-18 April 1985, ASME, NY 1985.

9. Clayton, P. and R. Devanathan, Wear, 1992, v 156, pp 121 – 131.

10. de Boer, Harold,, Satya R. Datta, Hans-Jurgen Kaiser, Stein Olav Lundgren, Bruno Musgen, Herbert Schmedders, und Klaus Wick, Stahl und Eisen, 115 (1995) Nr 2, 16 Feb 1995, pp 93-98.

11. Habraken, L.J., and M. Economopoulos, Transformation and Hardenability in Steels Symposium, 27-28 February 1967, Climax Molybdenum Co. of Michigan/University of Michigan, pp 69-108.

12. Bain, E.C., Functions of Alloying Elements in Steel, ASM, 1939.

13. Pickering, F.B., ibid (11) pp 109-132.

14. Oblak, J.M., and R.F. Hehemann, ibid (11) pp 15-38.

15. Parker, E.R., Met Trans A, Vol. 8A, July 1977, pp 1025-1042.

16. Bramfitt, B.L., and J.G. Speer, Met Trans A, Vol. 21A, April 1990, pp 817-829.

17. Biss, V., & R.L. Cryderman, Met Trans, 1971, Vol. 2, pp 2267-2276.

18. Reynolds, W.T., H.I. Aaronson, and G. Spanos, Material Trans, JIM, Vol. 32, No. 8 (1991) pp 737-746.

19. Irvine, K.J., and F.B Pickering, J.I.S.I. 1960, Vol. 194, Feb, pp 137-153.

20. Comon, J., P.F. Martin, and P. Barien, Rev Met., 1967, Vol. 64, pp 361-370.

21. Sage, A.M., J.H. Woodhead, and D.W. Evans, Vanedium Structural Steels - A Review of Published Papers - quenched and tempered, Highveld Steel & Vanadium Corporation, Ltd., Sept. 1971.

22. Krauss, G., Steel: Heat Treatment and Processing Principles, ASM 1995, p 92.

23. Grossman, M.A., Trans AIME, Vol. 150, p 242 (1942)(24).

24. Cias, W.W., Phase Transformation Kinetics and Hardenability of Medium-Carbon Steels, Climax Molybdenum Co., Greenwich, CT.

25. Clayton, P., "Advanced Steels for Railroad Frog Applications" AAR Report, in press.

26. DOT 105/111/112/114 Tank Car Shell Cracking and Structural Integrity Assessment.

27. Kern, R.F., Metal Progress, November 1968, pp 61 - 73.